5.1 Introduction

The primary purpose of the present study is to find out a suitable electrolyte for practical applications. And for this, knowledge of electrical transport properties of these glass compositions is a must.

To investigate the transport properties of prepared glass compositions, DC methods are not suitable as polarization effects take place at electrode-specimen (electrolyte) interface due to piling up of mobile cations. And hence, AC impedance spectroscopy method has been adopted in the present study to understand transport properties of PbI_2 doped Ag_2O-V_2O_5-B_2O_3 glasses. Four main formalisms of AC impedance spectroscopy namely, Complex impedance, AC conductivity, dielectric permittivity and modulus have been utilized to understand various phenomena related to ion transport in these glass compositions at different temperatures from room temperature to below their glass transition.

A systematic study of complex impedance on silver based super ion conducting glasses was first made by Grant *et al.* [1, 2] for $Ag_7I_4AsO_4$. After that ac conductivity studies on many silver iodide doped systems AgI-$Ag_2B_4O_7$ [3], AgI-Ag_2MoO_4 [4], AgI-$AgPO_3$ [5], AgI-Ag_2O-B_2O_3 [6], AgI-Ag_2O-V_2O_5 [7], AgI-Ag_2O-P_2O_5-MoO_3 [8], AgI-Ag_2O-B_2O_3-V_2O_5 [9] etc. have been studied widely and the experimental results support the AgI introduced in the glassy network which is responsible for the high ionic conductivity. The relaxation effect in these systems is due to the motion of the mobile species, Ag^+ ions, rather than by the rotation of the dipoles and is termed as conductivity relaxation. The studies on PbI_2-$AgPO_3$ [10], CuI-Ag_2O-V_2O_5 [11], CuI-Ag_2O-B_2O_3 [12], PbI_2-Ag_2O-V_2O_5 [13] and CdI_2-Ag_2O-

V_2O5-B_2O_3 [14] explain the feasibility of obtaining the Ag^+ ion conducting systems with appreciably high conductivity.

In the present study, it was confirmed by the characterization studies that doping of PbI_2 in the host glass Ag_2O-V_2O_5-B_2O_3 system, results in the formation of AgI clusters that are formed due to the exchange reaction between PbI_2 and Ag_2O and the mobile Ag^+ ions available from these AgI clusters will act as the main electrical charge conducting species. Hence, this system will behave essentially as an AgI doped glass. In this chapter, the results obtained from the AC impedance measurements of the PbI_2-Ag_2O-V_2O_5-B_2O_3 glass systems over a wide range of frequency, composition and temperature have been discussed.

The following three Ag^+ ion conducting glass systems were prepared and their electrical transport properties are discussed.

1. **Glass series (a):** $x\ PbI_2$ - $(100-x)$ $[Ag_2O$ - $2(0.7V_2O_5 – 0.3B_2O_3)]$

   where, $5 \leq x \leq 25$ in steps of 5.

2. **Glass series (b):** $y\ (PbI_2.\ 2Ag_2O)$ - $(100-y)$ $[0.7V_2O_5$ - $0.3B_2O_3]$

   where, $30 \leq y \leq 55$ in steps of 5.

3. **Glass series (c):** $z\ (PbI_2.\ Ag_2O)$ - $(90-z)$ V_2O_5 - $10B_2O_3$

   where, $30 \leq z \leq 50$ in steps of 5.

In the first glass series, the amount of PbI_2 has been varied against the host glass composition Ag_2O-$2(0.7V_2O_5$-$0.3B_2O_3)$. Machida *et al.* [15], Deshpande *et al.* [16] and others [17-21] have reported that instead of taking a single glass former, a combination of two glass formers results into higher electrical conductivity. From previous studies [22-23], it has been established that the glass former composition $0.7V_2O_5$-$0.3B_2O_3$ is a good mixed glass former to attain high ionic conductivity in

various glass systems investigated e.g. when CdI_2 is doped in the Ag_2O-V_2O_5-B_2O_3 host glass system, a higher ionic conductivity is achieved than doping AgI alone, as reported by Padmasree *et al.* [24]. And hence this optimized glass former composition $0.7V_2O_5$-$0.3B_2O_3$, of the two mixed glass formers was tested initially in glass series (a) and series (b).

In the glass forming melt, PbI_2 reacts with Ag_2O and forms PbO and two molecules of AgI in the glass forming melt. Now, it is well established that induction of AgI in the host glass network is favorable for ionic motion in the host glass network. Here, AgI helps in increasing conductivity by providing free Ag^+ cations which are easily mobile in ambient conditions like room temperature. The composition x = 25 mole% PbI_2 is found to be the highest conducting composition. However its conductivity is not as high as other conventional AgI containing glasses like $(AgI)_{1-x}$ $(Ag_2MoO_4)_x$ reported by Cutroni *et al.*[25] or AgI-Ag_2O-P_2O_5 glasses reported by Takahashi *et al.*[26]. Moreover, it has been shown by Doi [27] in xAgI-$(1-x)Ag_4P_2O_7$ glasses that with increasing concentration of AgI, the free volume available in this host glass increases. Also to be noted that, ions conduct via available free volume to them, and hence an increase in free volume will enhance ionic conductivity; i.e. it is implied that one may increase the ionic conductivity by having a higher amount of AgI in the host glass which not only provides mobile Ag^+ cations but also adds additional free volume to the host glass structure.

And hence in order to understand the transport properties of these Lead Iodide doped Silver-Boro-Vanadate glasses, another glass series, namely series (b) was prepared. In which, the ratio of PbI_2 to Ag_2O was kept as 1:2, so as to allow all PbI_2 molecules to react with Ag_2O and form AgI in the end glass composition. Here, it should be noted that amount of MI_n (M = Cu, Cd, Pb, Cs, etc., and n = 1, 2, 3 etc.)

type doping salt has been kept lower than $Ag_2O/AgPO_3$, so that chances of exchange reaction between dopant salt and silver oxide are maximized and as a result maximum amount of AgI is created in the end glass product which may help to have higher ionic conductivity.

In the third and last glass series, the glass former B_2O_3 was fixed at 10 mole% and the amount of the second glass former V_2O_5 was varied against *z* mole% of (PbI_2:Ag_2O). In this glass series, one of the glass formers, B_2O_3 has been fixed at 10 mole% and the other glass former V_2O_5, is being varied at the expense of the constant ratio of (PbI_2:Ag_2O). However, as the concentration of only one glassformers of the two is being changed, the well known mixed glass former effect is likely to be observed. Moreover, the ratio of PbI_2 to Ag_2O was kept at 1:1, so that assuming that all PbI_2 is converted to AgI and PbO and no excess PbI_2 or Ag_2O is left in the final product.

For electrical measurements, as quenched glass pieces were used. The glass pieces were polished on both faces by a silicon carbide lapping paper to ensure uniform surface and thickness across the sample. Conducting silver paint was applied on the opposite faces of the polished glass pieces to make contact electrodes. The impedance spectroscopy studies were carried out using Agilent e4980A LCR meter in the frequency range 20 Hz to 2 MHz and the temperature range 30-120˚C.

5.2 Complex Impedance Analysis

The measured impedance data were analyzed using Z^*, σ^*, ε^* and M^* formalisms to obtain various parameters related to transport properties of the glass samples like bulk resistance, DC conductivity, dielectric strength, relaxation time,

hopping frequency of ions. Hence at first, the analysis of Impedance formalism is given as follows.

Series (a): The effect of increasing amount of PbI_2 on the impedance response of the host glass system Ag_2O - $2(0.7V_2O_5$ - $0.3B_2O_3)$ is shown in Fig. 5.1. It shows impedance plots for all compositions of series (a) at different temperatures from 30 ˚C to 100 ˚C in steps of 5 ˚C in the high frequency regime, a small semicircular arc is observed which is followed by a comparatively a larger semicircular arc in lower frequency side. The smaller semicircular arc in high frequency region is believed to be occurring due to relaxation of mobile ions and is considered to be occurring due to long range migration of mobile ions, before they pile up at the electrode-electrolyte interface [28]. Its intercept with the real axis (Z') is taken as the bulk resistance, R_b, of the specimen. By knowledge of the dimensions of the specimen one may calculate the conductivity of the specimen, using the following equation.

$$\sigma = \frac{1}{R_b} \cdot \frac{t}{a} \qquad \text{……. (5.1)}$$

where, σ = conductivity, t = thickness of the specimen *and*

a = cross sectional area of the specimen.

The second semicircular arc/spur that is observed in lower frequency region is a result of polarization of mobile ions at the electrode–electrolyte interface. What happens here, is, that at higher frequencies the mobile ions see no electric field and are virtually immobile due to their inertia and the electric field is changing very rapidly, while in case of lower frequencies (usually less than 10 kHz) the net displacement of ions takes place. At lower frequencies, accumulation of mobile ions takes place at the interface. This pile up of mobile ions results into a net separation of charge carriers in the specimen, which polarizes it.

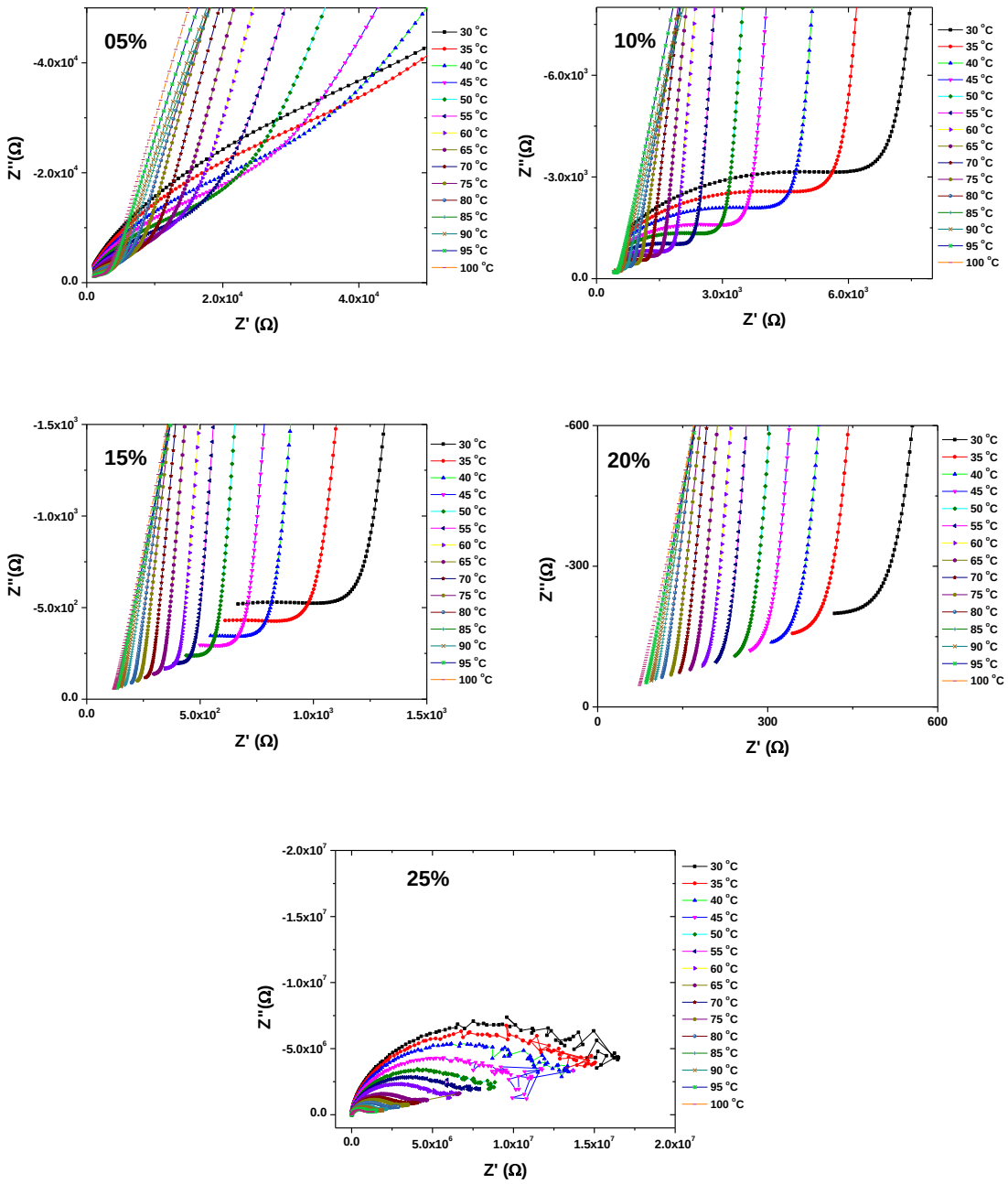

Fig. 5.1. complex impedance (Nyquist) plots for all compositions of series (a) at various temperatures

The larger semicircular arc or a spur in the lower frequency region when compared to the higher frequency side arc. As can be observed from the Fig. 5.1, with increasing temperature the impedance plots shrink in diameter and tend to shift towards origin, indicating a reduction in overall impedance values with increasing

temperature. Such variations with temperature are observed for other compositions also. One may note that there is generally only one incomplete semicircular arc present in most cases. For compositions x = 5 mole% and x = 25 mole%, a polarization spur starts to appear at higher temperatures.

Equivalent circuit approach to model/understand the impedance response of the superionic conductors under study

The impedance response of superionic conducting materials is reproduced by very simple electrical circuits having some basic circuit elements like resistance, capacitance, inductor, CPE (Constant phase element), Warburg and Gerischer elements etc. [29]. The electrical circuit used to re-generate such impedance response is called an "*equivalent circuit*". The complex impedance plots, in general, are modeled using equivalent circuit approach to understand various electrochemical reactions, electrode processes, or ion dynamic processes etc.[30,31]. However, choice of the equivalent circuit remains in question and sometimes is tricky, because a lot of different combinations of Resistances, Capacitance and other key components like Warburg element, Gerischer element etc. produce the similar impedance plot. By and large, an equivalent circuit with minimum number of components should be considered to be the ultimate one, moreover its interpretation should be realistic and practicable.

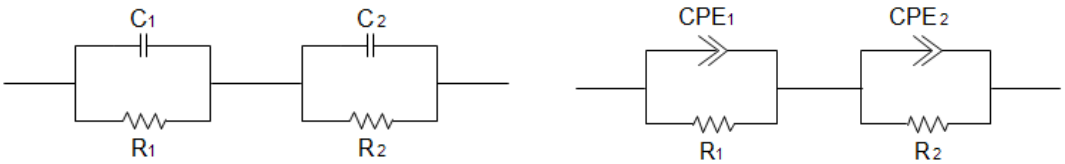

(a) Series combination of two parallel R-C loops **(b) Series combination of two parallel R-CPE loops**

Fig. 5.2. Different Equivalent circuits used to model the impedance response of occurrence of two semicircular arcs in complex impedance plots.

Occurrence of two semicircular arcs in impedance plots can best be fitted to the series combination of two lumped parallel combinations of a Resistance and a Capacitance as shown in Fig. 5.2 (b).

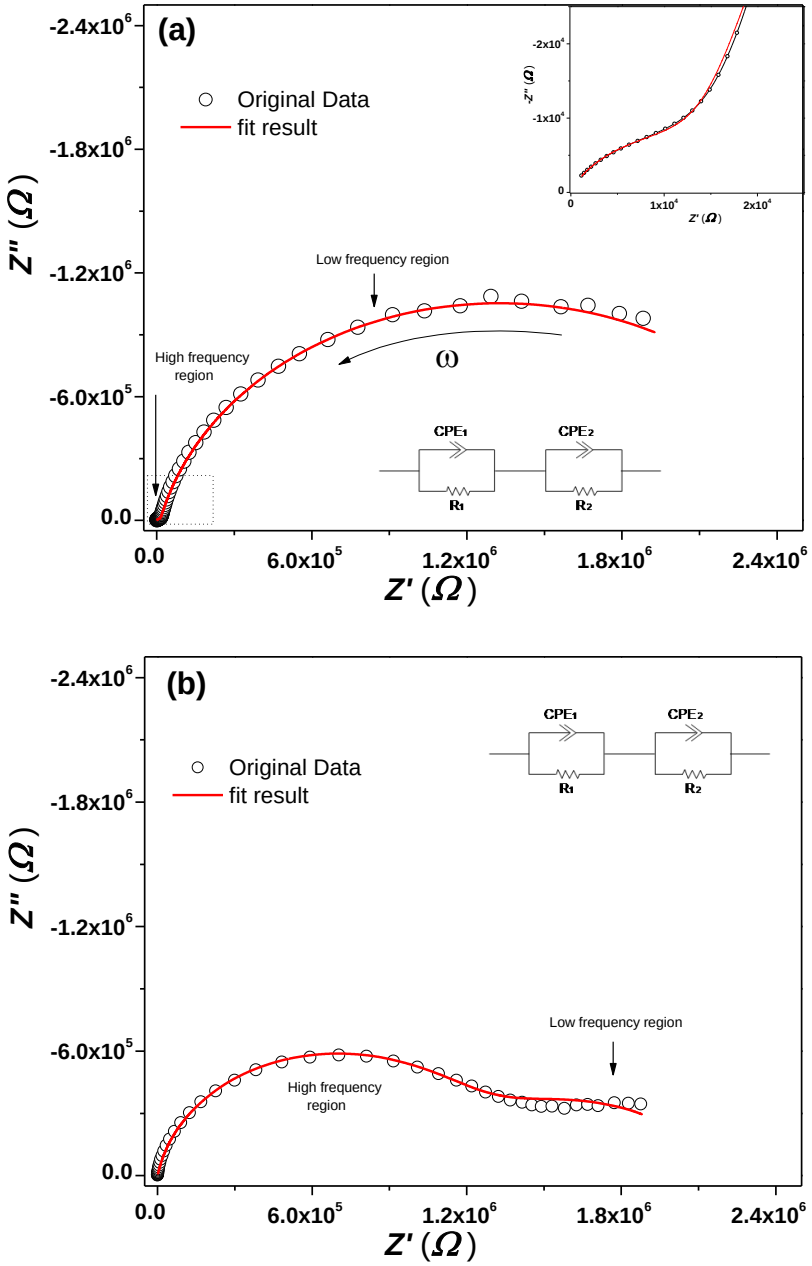

Fig. 5.3. Equivalent circuit fitting of impedance plots using equivalent Circuit of Fig. 5.2 (b) for (a) *x* = 05 mole% (60 ˚C) and (b) *x* = 25 mole% (90 ˚C)
(*Inset: the high frequency portion in enlarged condition*)

No Satisfactory fitting of the impedance plots could be achieved by using the circuit in Fig. 5.2(a). The reason for this disagreement is that if we closely observe

the impedance plots from experiment, we find that the semicircular arcs in high frequency as well as low frequency regions are depressed, i.e. their centers lie below the real axis. This suggests that the specimen might not be a perfect resistor; rather it is having some capacitive component also associated with it. And hence instead of using a pure capacitor, it is replaced by a *Constant Phase Element* (CPE) having impedance $Z_{CPE} = Z_o/(j\omega)^n$ in circuit in Fig. 5.2 (b).

To model the nature of the impedance response, the equivalent circuit of in Fig. 5.2 (B) has been utilized and the results have been shown for x = 5 mole% and 25 mole% compositions at 60 and 90 ˚C respectively in Fig. 5.3 (a) & (b). A perfect overlapping of the fitted data with the original impedance plots proves the validity of the circuit in Fig. 5.2 (b).

Series (b) Complex impedance plots for all the compositions of series (b) at various temperatures are shown in Fig. 5.4. As can be noted, the general feature of these Nyquist plots is that one may observe that a small semicircular arc occurs in the high frequency region followed by another, comparatively larger one in the low frequency region.

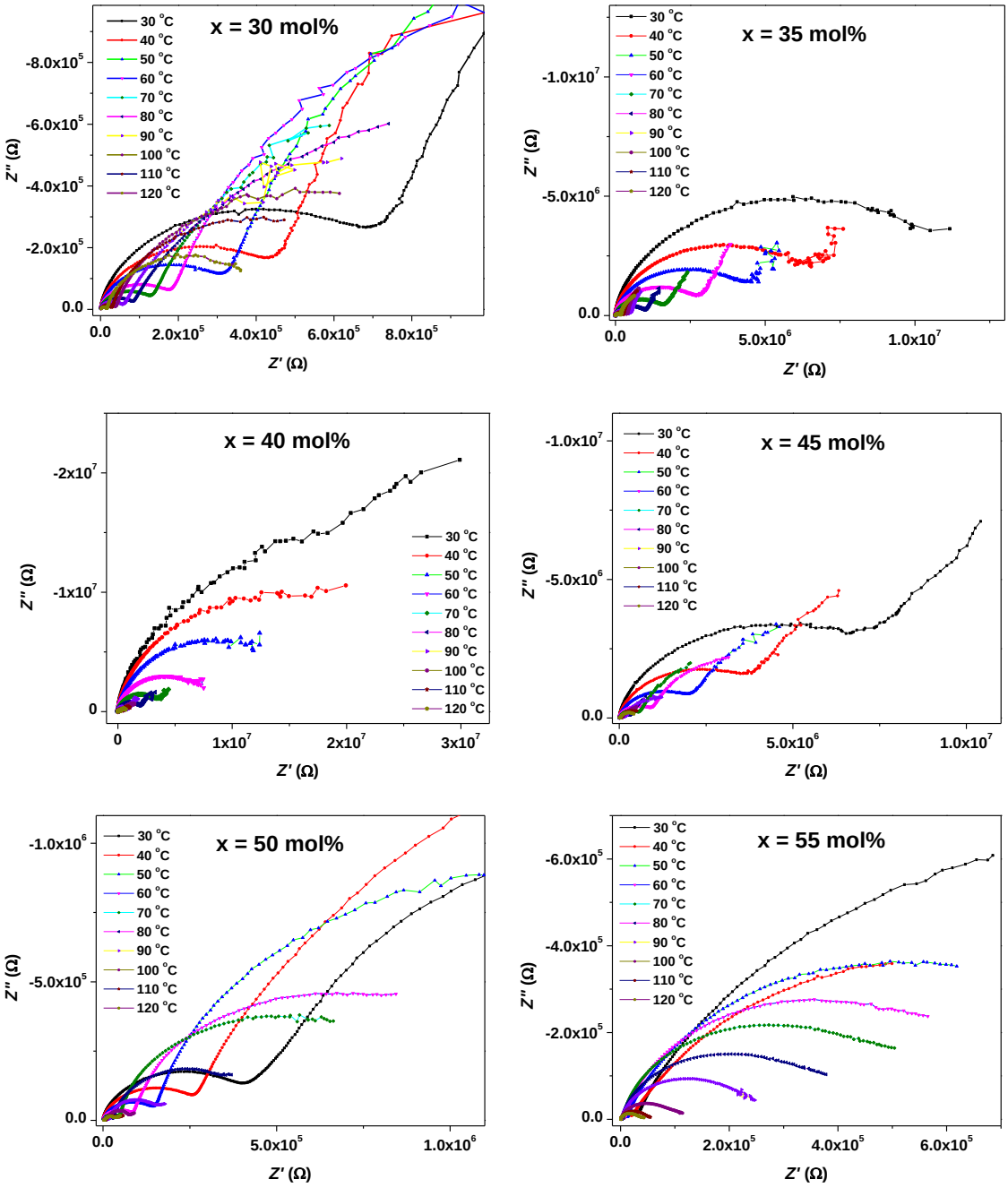

Fig. 5.4. Complex impedance (Nyquist) plots for all compositions of series (b) at various temperatures

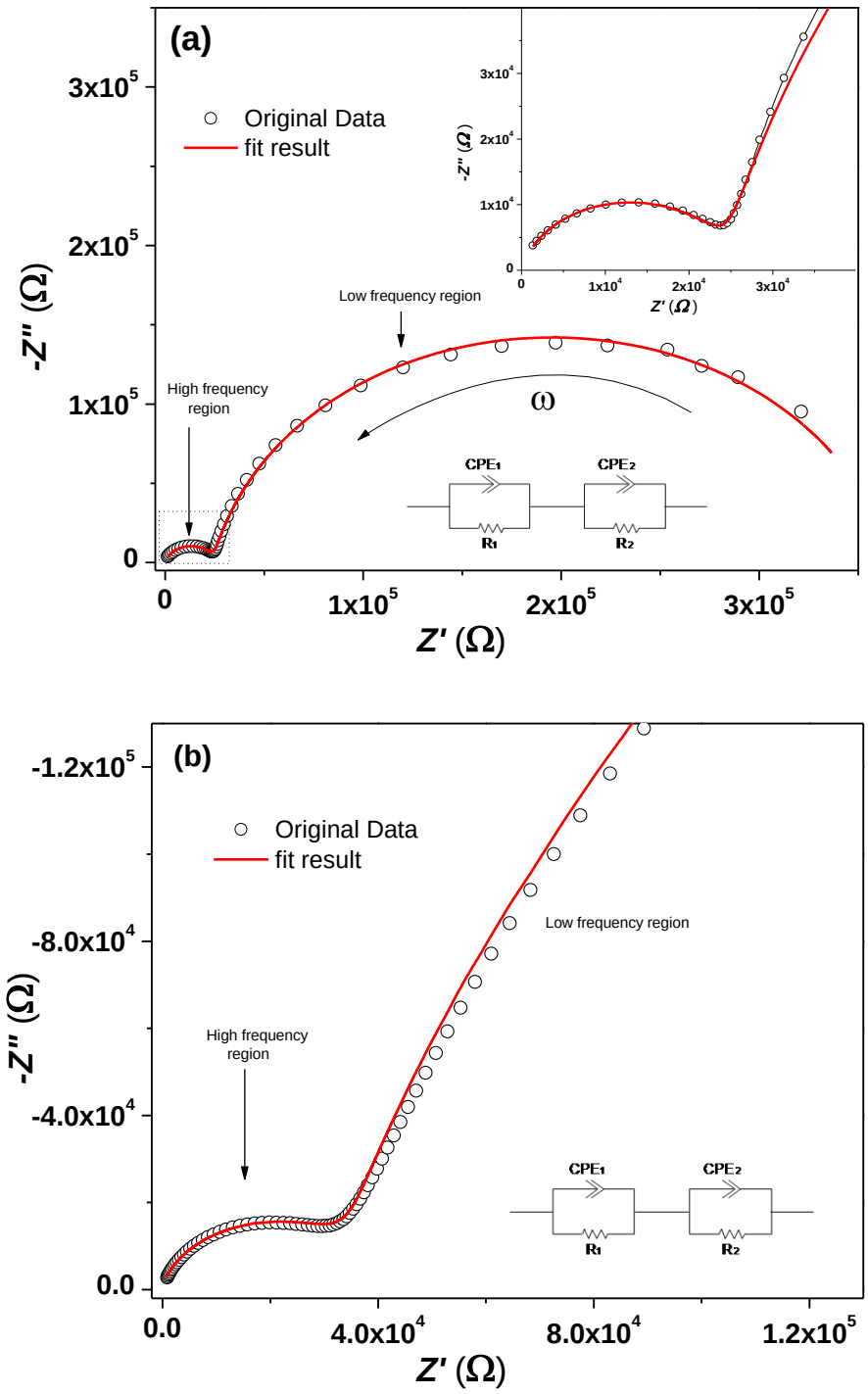

Fig. 5.5. Equivalent circuit fitting of impedance plots using equivalent Circuit of Fig. 5.2 (b) (a) *y* = 45 mole% (100 ˚C) and (b) *y* = 55 mole% (30 ˚C) (*Inset: the high frequency portion in enlarged condition*)

The second semicircular arc/spur which is observed in lower frequency region is a result of polarization of mobile ions at the electrode–electrolyte interface.

As can be observed from the Fig. 5.4 with increasing temperature the impedance plots shrink and tend to shift towards origin, indicating a reduction in overall impedance values with increasing temperature. Similar effect is observed for other compositions at all temperatures.

Fig. 5.5 shows the fitted impedance plot for the same impedance plot of Fig. 5.4 using the second equivalent circuit of Fig. 5.2 (b) containing a Constant Phase Element (CPE) instead of a pure Capacitor in parallel combination with a resistor [32].

Series (c): For glass series (c), the amount of V_2O_5 is being varied (reduced) against a constant ratio of PbI_2:Ag_2O.

Fig. 5.6 shows the complex impedance plots for all compositions of series (c) at different temperatures from 30˚C to 100˚C in steps of 5˚C. It is observed that this system also shows, a semicircular arc in high frequency region and polarization effects in lower frequency regime. With increasing temperature, it is observed that centers of the semicircular arcs in higher frequency region shift towards the origin suggesting a systematic decrease in their bulk resistance due to increase in mobility of Ag^+ ions or an increase in their concentration or a combined effect of the two.

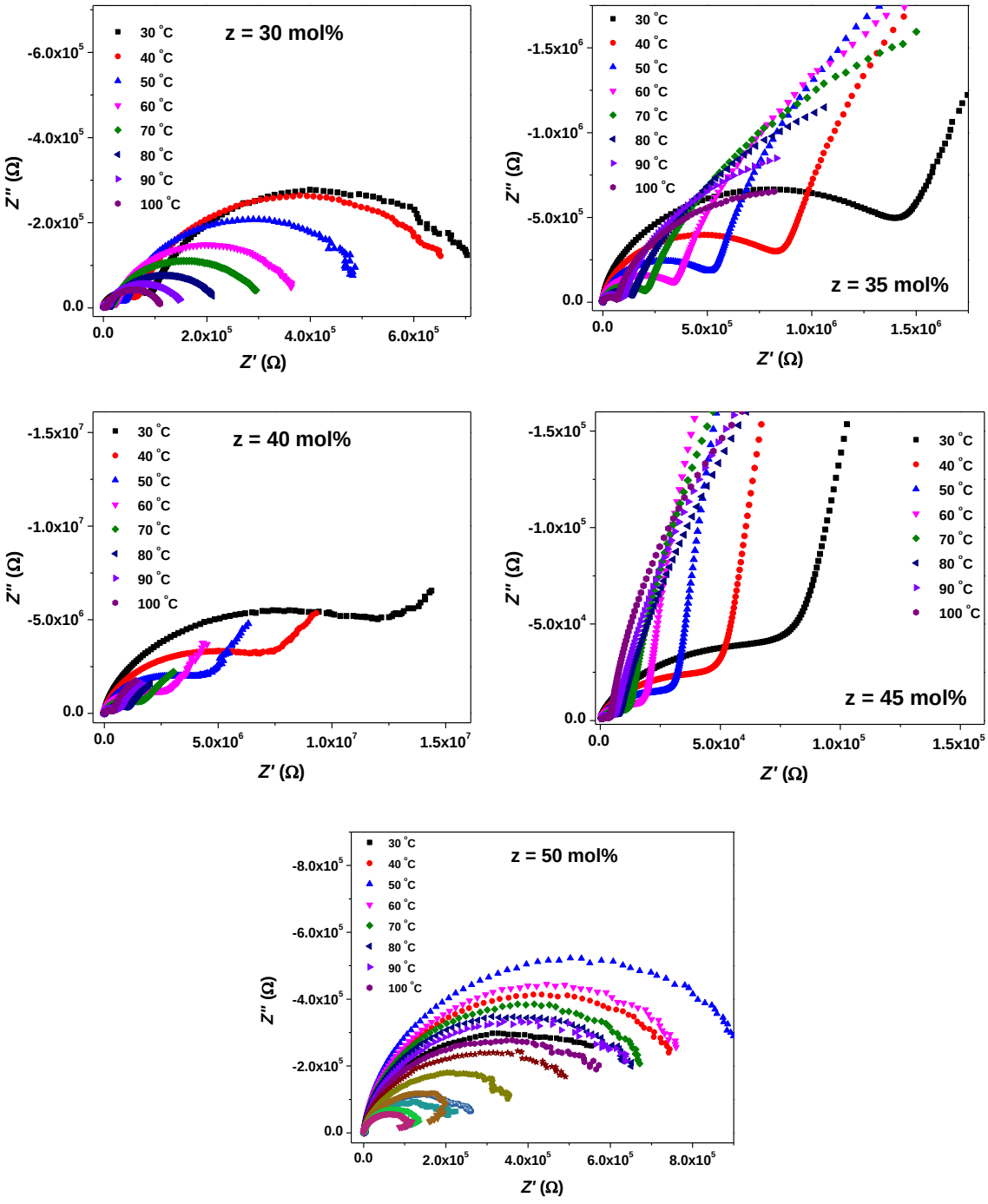

Fig. 5.6. Complex impedance (Nyquist) plots for all compositions of series (c) at various temperatures.

The impedance plots are also fitted using the equivalent circuit given in Fig. 5.2 (b), which contains a series combination of two paralleled lumped Resistance & CPE elements. Fig. 5.7 shows the fitted impedance plots for z = 30, 35 and 50

mole% compositions at 30 ˚C, 55 ˚C and 35 ˚C respectively. Both the curves exhibit a good fitting of the data.

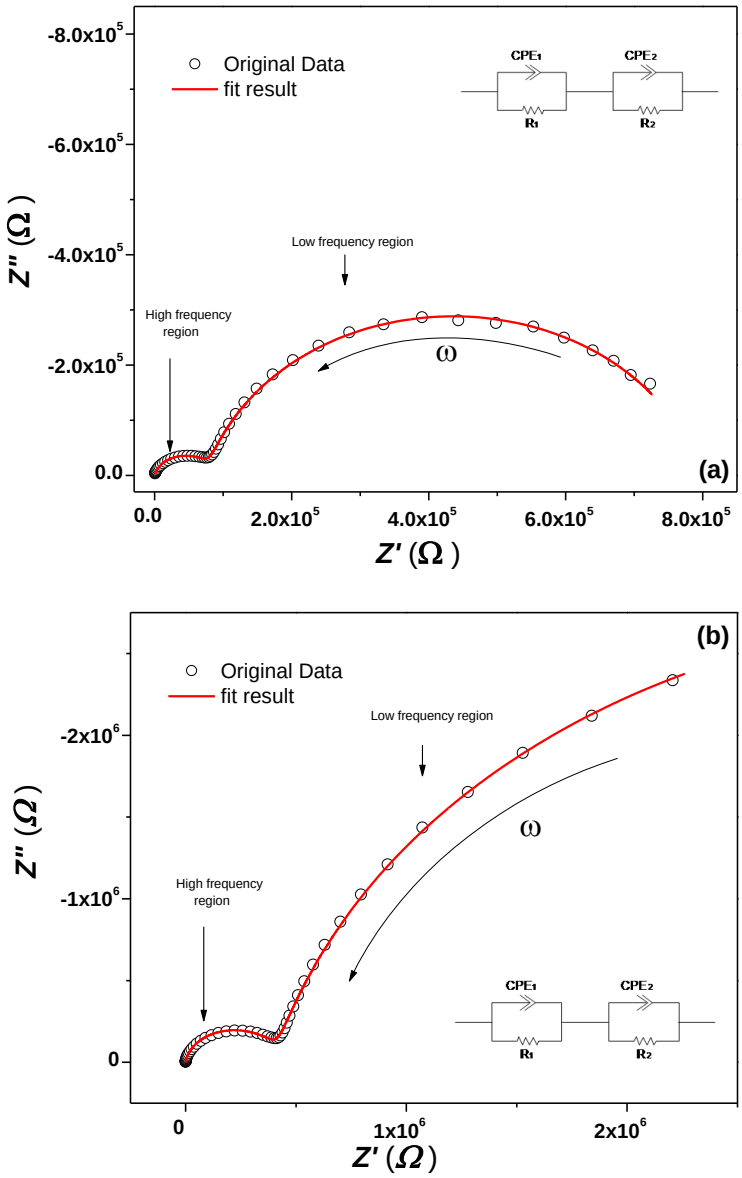

Fig. 5.7. Equivalent circuit fitting of impedance plots using equivalent Circuit of Fig. 5.2 (b) for (a) z = 30 mole% (35 ˚C) & (b) z =35 mole% (55 ˚C)
(*Inset: the high frequency portion in enlarged condition*)

5.3 DC Conductivity

DC conductivity or the bulk conductivity of the specimens was calculated from their known geometrical dimensions and their bulk resistance determined from

their respective complex impedance plots at various temperatures using the following equation.

$$\sigma_{DC} = \frac{1}{R_b} \cdot \frac{t}{a} \qquad \ldots\ldots\ldots (5.2)$$

where, σ_{DC} = DC conductivity or bulk conductivity, R_b = resistance (bulk resistance of the sample, obtained from the complex impedance plot) t = thickness of the specimen and a = cross sectional area of the specimen.

The conductivity of the samples was measured at different temperatures to know its temperature dependence and is shown as a plot of $\log\sigma_{DC} \rightarrow 1000/T$ in Fig. 5.9. It is observed that with increasing temperature, conductivity of all samples enhances. These temperature dependent conductivity plots follow Arrhenius type of equation given below,

$$\sigma_{DC} = \sigma_o \, exp\,(-E_\sigma / kT) \qquad \ldots\ldots\ldots (5.3)$$

where, σ_o = conductivity pre-exponential factor, E_σ = conductivity activation energy, k = Boltzmann's constant = 1.38×10^{-23} J/mole-K and T = absolute temperature in Kelvin scale.

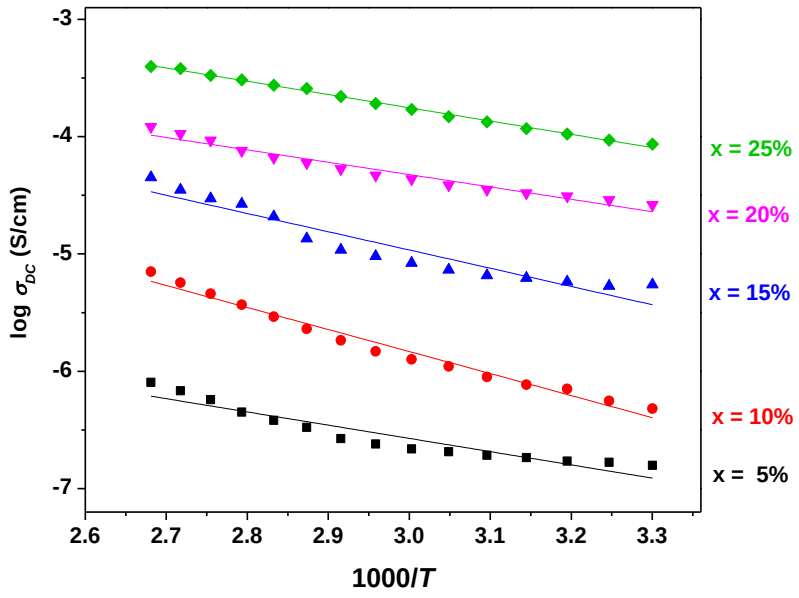

Fig. 5.8. Arrhenius temperature dependent σ_{DC} plots for all compositions of glass series (a) (*Solid lines are the best fits to the Arrhenius equation*)

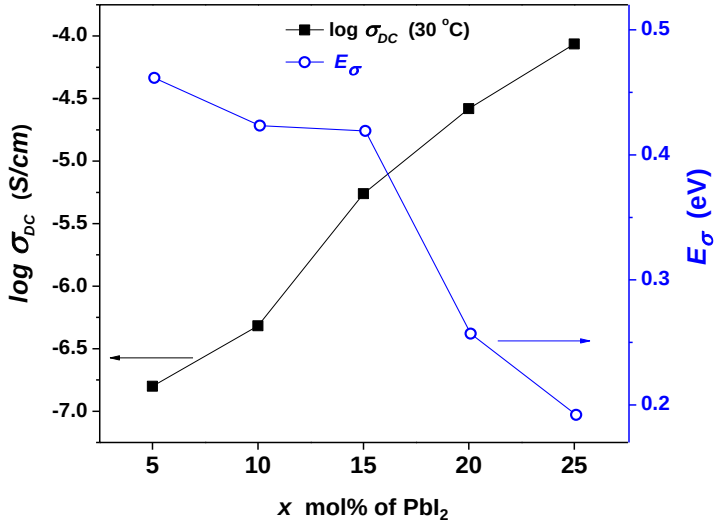

Fig. 5.9. Variation of E_σ, and logσ_{DC} (30 ˚C) with increasing PbI_2 content. (*solid line is just a guide for eyes*)

DC conductivity plots shown in Fig. 5.8 were fitted using the Arrhenius equation to calculate the activation energy E_σ required for migration of ions in the glassy matrix. The variation of conductivity activation energy, E_σ and σ_{DC} (at 30 ˚C) versus PbI_2 concentration are shown in Fig. 5.9.

It is observed that, σ_{DC} increases with PbI_2 concentration consistently and attains maximum value of ~10^{-4} S/cm for 25 mole% PbI_2 concentration. While the activation energy, E_σ, values decrease with lead iodide concentration.

With the addition of PbI_2 in the host glass Ag_2O-V_2O_5-B_2O_3, an exchange reaction between Ag_2O and PbI_2 takes place, in accordance with the HSAB principle, in the glass forming melt and as a result of that two AgI molecules are formed in the host glass network. Formation of AgI in a host glass network results into a highly conducting α-AgI phase at about 147 ˚C. The α phase of AgI contains a body centered cubic (*b.c.c.*) structure and iodide ions lie at the corner and body center positions and two Ag^+ ions are statistically distributed over 42 sites among I^- anions with tetrahedral and trigonal co-ordination. It simply means that the two Ag^+

ions in the unit cell of α–AgI have total 42 equivalent sites to occupy, because they have enough available energy at ambient temperatures which helps them to hop from one site to the next. Maier *et al.* [33] have shown that mobile Ag^{+} ions prefer mixed oxide–iodide coordination, which requires lower activation energy by considering pathway model [34].

Now, according to equation, $\sigma = ne\mu$, conductivity is a function of number of charge carrier concentration, n, and mobility of these charge carriers μ. Hence an increase in mobile ion concentration should lead to increase in conductivity with increasing PbI_2 concentration.

The behavior of lead oxide is unique in oxide glasses. Ganguli *et al.* [35] have reported that it plays a dual role of either a glass network former or as a glass network modifier. In some concentration regions, it enters into the glass network as a glass network former. In other concentration regions it stays as Pb^{+2}, leaving the oxygen ion of PbO and breaks the oxygen bridges when it is acting as a glass modifier. The composition dependent role of lead is dependent on the availability of oxygen coordination that it may get from the host. The conversion reaction is given as follows,

$$2PbO \rightarrow Pb^{+2} + [PbO_{4/2}]^{-2} \qquad \ldots\ldots\ldots (5.4)$$

Now, $[PbO_{4/2}]^{-2}$ unit prefers pyramidal structure with its lone pair of electrons projecting away from the plane of four oxygens. This lone pair of electrons impedes the motion of mobile cations leading to rather low ionic conductivity in spite of the open network structures.

Here, in the first glass series after exchange reaction between Ag_2O and PbI_2, there is sufficient amount of modifier (Ag_2O) is left for in the glass network to

create voids and spaces for transport of Ag cations. The formed PbO may function as glass modifier or network former depending upon the conditions of availability of NBOs and double bonded oxygens for PbO to function as a network former. In this system, the continued increase of conductivity ascribes that thus formed PbO might be behaving as glass modifier.

In the present case, molar volume is found to increase with increasing PbI_2 content, which indicates of gradual expansion of the available free volume. In addition to this, Wicks *et al.* [36], with help of Reverse Monte Carlo models based on neutron and x-ray diffraction, had proposed that the formation of AgI expands the glass network and Swenson *et al.* [37] showed the network expansion and conductivity enhancement in a number of metal halide doped glasses by using EXAFS studies. Damrawi *et al.* [38] found that creation of open volume or expansion of the glass network supports the mobility in fast ion conducting glasses.

The cause of reduction in activation energy may be understood on the basis of the Anderson-Stuart (A-S) model of ion conduction in glasses. According to the Anderson-Stuart model of ion conduction, the total activation energy E_σ, required for a successful hop of an ion may be considered to be a sum of two fractions:

$$\boldsymbol{E_\sigma = E_b + E_s} \qquad \ldots\ldots\ldots (5.5)$$

Here, $\boldsymbol{E_b}$ is the binding energy which is the mean energy that a cation needs to leave its site the other one is $\boldsymbol{E_s}$,the elastic strain energy: it is the mean kinetic energy that a cation needs to open a 'doorway' in the structure of the glass to pass through, which involves the energy to overcome the electrostatic forces between Ag^+ ions and the neighboring oxygen and iodide ions. As discussed, PbO is acting as a glass modifier, which in turn produces a large number of NBOs by breaking the bonds in the glass network. Elliott [39] has pointed out that an increase in modifier

content is likely to reduce the binding energy,whereas the elastic strain energy, E_s, does not get much affected by the changing glass composition. Hence a net reduction in E_b should be occurring due to modified glass network by Ag_2O and PbO, and hence a fall in E_b reflects in total activation energy E_σ with increasing PbI_2 content.

Reduction in impedance of of glass system is supported by the decoupling index values also. In an ionically conducting glass system, decoupling index R_τ is a measure of how strongly the mobile ions are decoupled from the glass matrix [40] and it quantifies, how, as a function of temperature, the electrical relaxation process becomes decoupled from the viscous motion of the glass matrix. In ionically conducting glasses, ion transport is decoupled from the structural dynamics and may be determined using following equation [40].

$$\log R_\tau = 14.3 + \log \sigma_{DC} \qquad \ldots\ldots\ldots (5.6)$$

where, The conductivity σ_{DC}, is at glass transition temperature The calculated values of R_τ and σ_{DC} values at 30˚C for different compositions are shown in Fig. 5.10.

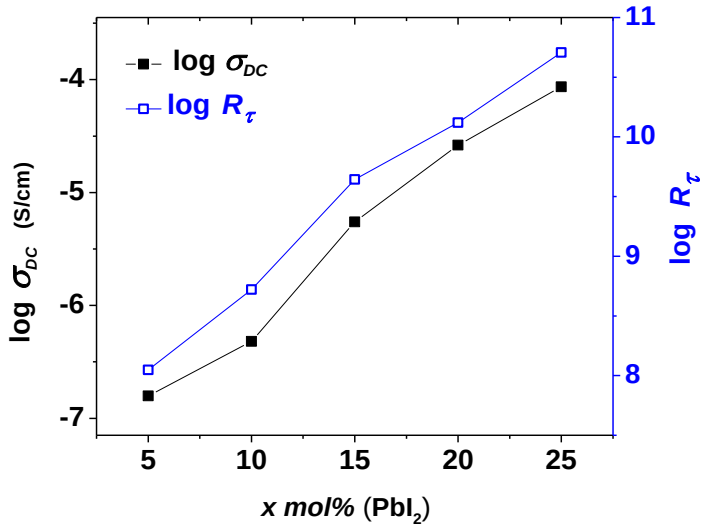

Fig. 5.10. Variation of σ_{DC} (30 ˚C) and R_τ with composition for glass series (a) x PbI_2 - (100-x) [Ag_2O - 2(0.7V_2O_5 – 0.3B_2O_3)]

One may note from the figure that with increasing PbI_2 content, R_τ values steadily increase with PbI_2 content. This rise in decoupling index suggests that the viscosity of the glass structure network must be reducing which favors the migration of Ag^+ ions. Hence, because of the rise in decoupling index with PbI2, the motion of Ag+ ions is becoming easier, because they get more and more decoupled or free from the glass matrix for transport. Kawamura *et al.* [41] in AgI-Ag_2MoO_4 glass system and Bhattacharya *et.al* [42] in the AgI–Ag_2O–V_2O_5 glasses, in their studies, confirmed the dependence of conductivity on decoupling index.

Series (b): In the glass series (b): $y(PbI_2{:}2Ag_2O)$-$(100\text{-}y)[0.7V_2O_5$ - $0.3B_2O_3]$; the iodide salt PbI_2 and the modifier oxide Ag_2O are taken in a ratio of 1:2 is in host glass network $0.7V_2O_5$ - $0.3B_2O_3$. Fig. 5.11 shows the temperature dependence of conductivity for all its compositions at different temperatures as plot of $\log\sigma_{DC} \rightarrow 1000/T$.

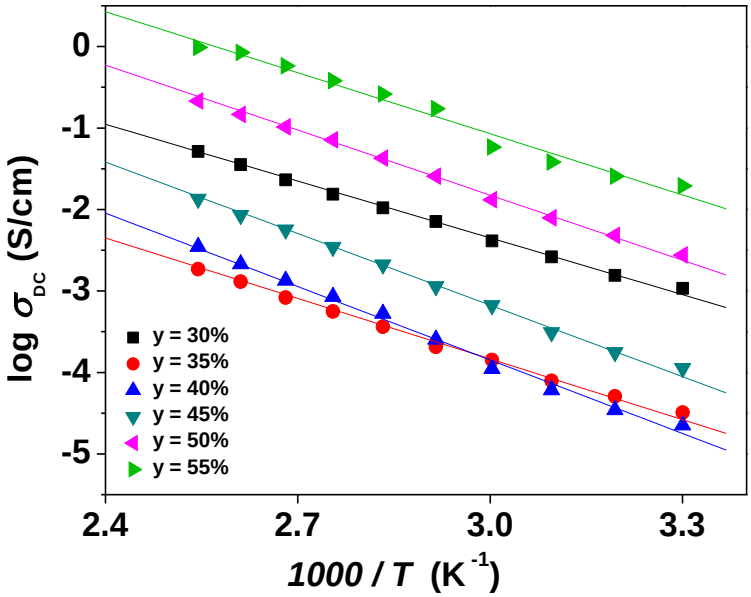

Fig. 5.11. Arrhenius temperature dependent σ_{DC} for all compositions of glass series (b)
(*Solid lines are the best fits to the Arrhenius equation*)

The σ_{DC} plots suggest that conductivity of these glass samples is also thermally activated and rises with increasing temperature. The logσ_{DC} plots are fitted to the Arrhenius equation and the conductivity activation energy, E_σ is obtained. The E_σ and σ_{DC} (at 30 ˚C) values as a function of composition are depicted in Fig. 5.12.

The σ_{DC} isotherm clearly exhibits apparently two distinguishable regions with a minimum at 40 mol%. It is observed that with increasing PbI_2:$2Ag_2O$ content, conductivity decreases initially and attains a minimum for the modifier to glass former ratio M/F = 0.67 (M = PbI_2+Ag_2O, F = V_2O_5+B_2O_3; all values in mole%). After this, as the M/F ratio further increases, conductivity starts increasing and reaches to maximum conductivity (~10^{-2} S/cm) for y = 55 mole% composition. Such variation in σ_{DC} as a function of composition is observable at all temperatures (*not shown here*). The conductivity activation energy values exhibit an exactly opposite trend. E_σ increases initially upto 40 mole% PbI_2:$2Ag_2O$ concentration and is 0.59 eV for y = 40 mole%. Beyond 40 mole%, E_σ decreases gradually and attains a value of 0.49 eV.

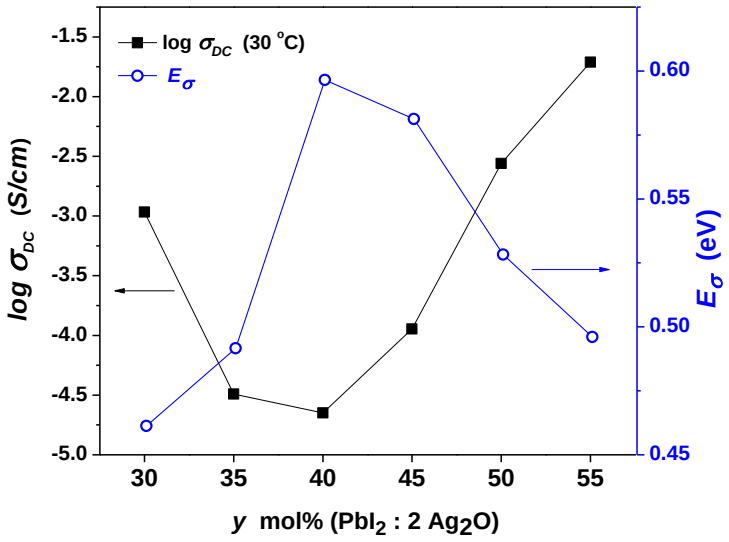

Fig. 5.12. Variation of activation energy and conductivity with (PbI_2:$2Ag_2O$) content at 30 ˚C (*solid line is just a guide for eyes*).

The compositional dependence of conductivity and activation energy for the second glass series (b) may be understood on the basis of A-S model by considering the influence of PbO and other factors on Ag^{+} ion conduction mechanism.

Initially PbO works as a glass former as a $[PbO_{4/2}]^{-2}$ unit due to the availability of large number of NBOs in the host network. The lone pair of electrons projecting away from the plane of four oxygens in $[PbO_{4/2}]^{-2}$ is responsible for impeding the motion of cation through the network.

The lack of availability of sufficient numbers of NBOs due to continuous increase of the *M*/*F* ratio, the Pb^{+2} ions now do not get sufficient NBOs or double bonded oxygens in their vicinity of the glass network and behave as glass modifier at the interstitial sites. At such positions Pb felicitates the motion of cations and ionic conductivity is observed to increase.

It is observed that R_τ values seem to be in consonance with conductivity with the variation of composition (*M*/*F* ratio), i.e. a decrease in R_τ is reflected in the corresponding decrease in σ_{DC} values. The minimum in R_τ and σ_{DC} values coincide at y = 40 mole%.

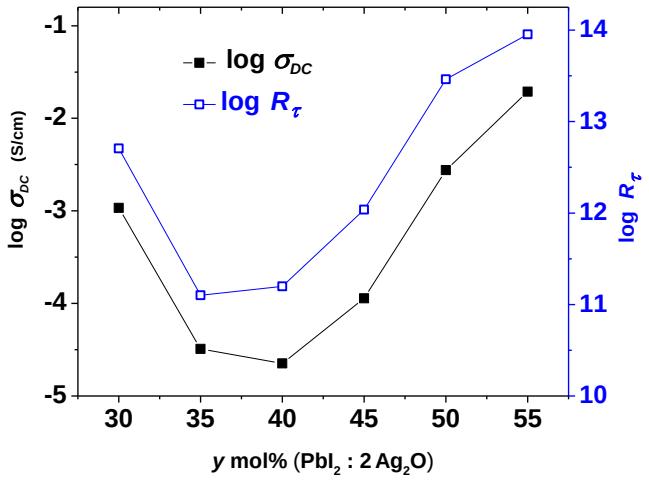

Fig. 5.13. Variation of σ_{DC} (30 °C) and R_τ with composition for glass series (b).

Series (c): In present glass series: z (PbI_2:Ag_2O)-(90-z)V_2O_5-10B_2O_3, the ratio of PbI_2 to Ag_2O has been kept 1 and in addition to that, one of the glass formers, B_2O_3 was fixed at 10 mole% and the other glass former V_2O_5 is varied. PbI_2 has the tendency to completely exchange coordinate with Ag_2O in PbI_2-Ag_2O/$AgPO_3$ glass systems reported by Malugani *et al.* [43] and Sanson *et al.* [44]. In the present system, only a small amount of PbO is left as the glass modifying component.

Temperature dependence of σ_{DC} for all compositions of glass series (c) is presented in Fig. 5.14. It is observed that with increasing temperature, σ_{DC} for all compositions is thermally activated and is also explained according to the Arrhenius equation. Activation energy values alongwith room temperature conductivity are shown in Fig. 5.15 as a function of z mole% of PbI_2:Ag_2O.

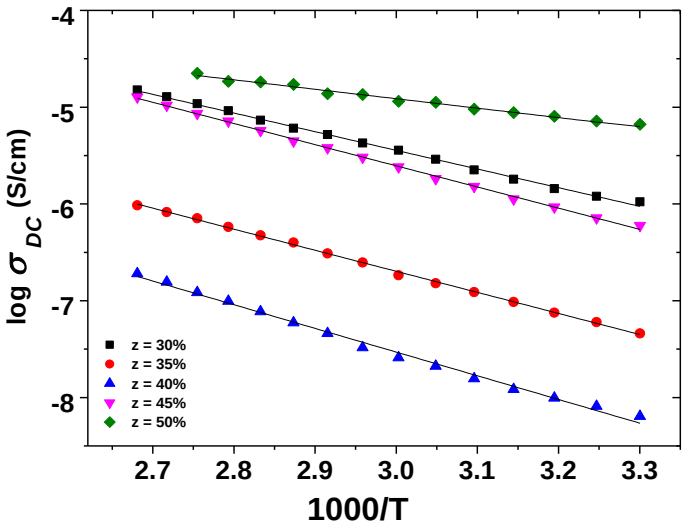

Fig. 5.14. Arrhenius plots of DC conductivity for different compositions of (PbI_2:Ag_2O).
(*Solid lines are the best fits to the Arrhenius equation*)

It is observed that conductivity initially decreases upto M/F = 0.67 ratio and thereafter it starts increasing. On the other hand, activation energy increases with M/F ratio and attains the highest value at M/F = 0.67.The nature of compositional dependence of conductivity and activation energy is similar to that of second glass

series. In this glass system too, PbO works as a glass former for initial compositions when *M*/*F* ratio is smaller than 0.67 as discussed earlier and its role gradually changes from glass network former to glass network modifier beyond this value.

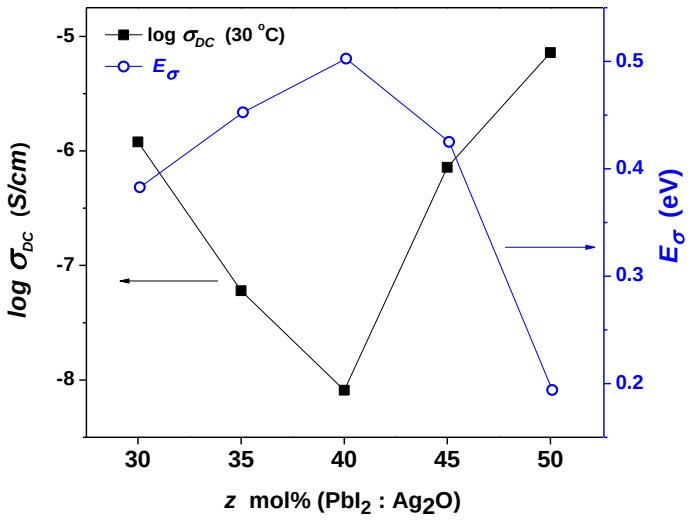

Fig. 5.15. Variation of E_σ, and σ_{DC} (30 °C) with (PbI_2:Ag_2O) content.
(*Solid line is just a guide for eyes*)

When the variation of σDC is correlated with R_τ, it is observed that variation in σ_{DC} with increasing PbI_2:Ag_2O content is in agreement with R_τ. Fig. 5.16 shows R_τ and σ_{DC} as a function of *z* mol% (PbI_2:Ag_2O).

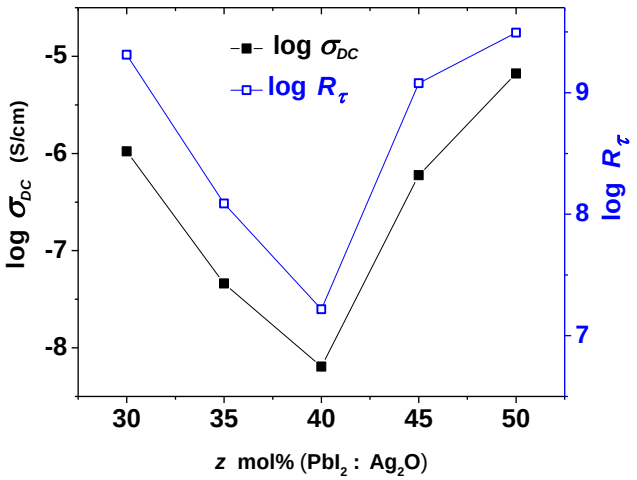

Fig. 5.16. Variation of σ_{DC} (30 °C) and R_τ with composition for glass series (c).

The decoupling index, R_τ (T_g), initially decreases with the increase of modifier content (PbI_2 +Ag_2O) and shows a minimum at z = 40 mole% (M/F = 0.67) an enhancement in σDC is observed beyond this limit. It means that the role of PbO is as a former at lower concentrations and thereafter it gradually changes to the role of glass modifier.. Similar is the variation of conductivity with PbI_2:Ag_2O content. The decrease in of R_τ (T_g) suggests that Ag^+ ions are coupled more with the glass network, hence a consequent decrease in conductivity also is expected. The coupling of Ag^+ increases with further increase of M/F ratio consequently and the conductivity shows increasing trend. However, overall conductivity of glass samples of series (c) is lower than that of the two glass series (a) and series (b).

In the earlier two glass series, after exchange reaction, some amount of Ag_2O is always left to function as a glass modifier along with PbO and is able to create more NBOs in the host glass network. But, in the present and last glass system, wherein the ratio of PbI_2 to Ag_2O has been fixed at 1:1, no excess Ag_2O is available after exchange reaction [45] in all glass samples. PbO, thus formed, plays partly the role of the glass network former and partly as modifier depending upon the amount of M/F ratio. The molar volume also decreases continuously with the increase of M/F ratio (given in Table 5.1) and the values of the decoupling index are lower than those in the first two glass series.(Table 5.1). Hence, lower value of conductivity is expected.

A summary of compositional dependence of conductivity, activation energy and decoupling index for all compositions of all three glass series is presented in Table 5.1.

Table 5.1: Compositional dependence of conductivity, activation energy and decoupling index for all compositions of all glass series

	Glass composition								σ_{DC} (30 °C)	E_σ	$logR_\tau$
	x	PbI_2	Ag_2O	V_2O_5	B_2O_3	$M = PbI_2+Ag_2O$	$F = V_2O_5+B_2O_3$	M/F			
	mole%	mole%	mole%	mole%	mole%	mole%	mole%		S/cm	eV	
	5	5	31.67	44.33	19	36.67	63.33	0.58	1.58×10^{-7}	0.46	8.05
	10	10	30	42	18	40	60	0.67	4.81×10^{-7}	0.42	8.72
Series (a)	15	15	28.33	39.67	17	43.33	56.67	0.76	5.49×10^{-6}	0.42	9.64
	20	20	26.67	37.33	16	46.67	53.33	0.88	2.63×10^{-5}	0.26	10.12
	25	25	25	35	15	50	50	1.00	8.65×10^{-5}	0.19	10.71
	30	10	20	49	21	30	70	0.43	1.08×10^{-3}	0.45	12.71
	35	11.67	23.33	45.5	19.5	35	65	0.54	9.07×10^{-5}	0.47	11.10
Series (b)	40	13.33	26.67	42	18	40	60	0.67	5.24×10^{-5}	0.60	11.20
	45	15	30	38.5	16.5	45	55	0.82	2.62×10^{-4}	0.56	12.04
	50	16.67	33.33	35	15	50	50	1.00	3.23×10^{-3}	0.50	13.46
	55	18.33	36.67	31.5	13.5	55	45	1.22	1.94×10^{-2}	0.49	13.95
	30	15	15	60	10	30	70	0.43	1.41×10^{-6}	0.38	9.31
	35	17.5	17.5	55	10	35	65	0.54	4.70×10^{-8}	0.43	8.09
Series (c)	40	20	20	50	10	40	60	0.67	1.04×10^{-8}	0.49	7.22
	45	22.5	22.5	45	10	45	55	0.82	5.57×10^{-7}	0.43	9.08
	50	25	25	40	10	50	50	1.00	6.66×10^{-6}	0.19	9.49

5.4 AC conductivity

Analysis of Impedance data of ionically conducting glasses adds a new dimension towards understanding of the ion transport phenomena occurring at different length and time scales. The frequency dependence of conductivity at different temperatures for all compositions of glass series (a) in which concentration of PbI_2 is varied with respect to the host silver-vanadoborate glass is presented in Fig. 5.17.

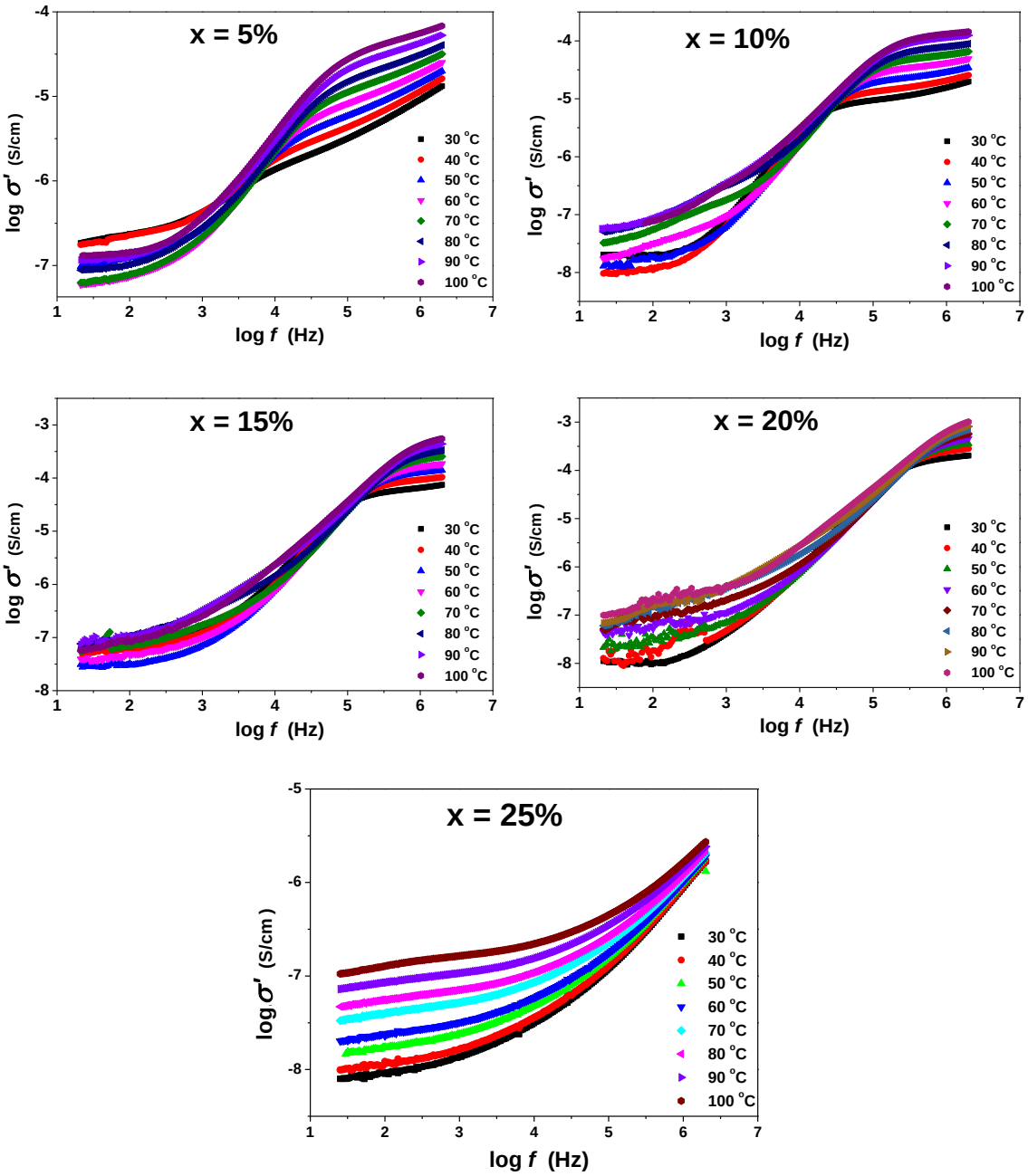

Fig. 5.17. Frequency dependent conductivity at different temperatures for *x* = (a) 5 mol%, (b) 10 mol%, (c) 15 mol%, (d) 20 mol% and (e) 25 mol% compositions of glass series (a).

In glasses, AC conductivity spectra exhibit a frequency independent conductivity plateau at lower frequencies followed by dispersion (increase of conductivity with increasing frequency) at higher frequencies. In the present case, it may be noted that the AC conductivity spectra for x = 5, 10, 15 and 20 mole% PbI_2 containing glass compositions possess two distinct regimes: (**1**) in low frequency

side below 10 kHz with a plateau like shape and (**2**) in higher frequency side (above ~ 10 kHz) with a plateau like region followed by high frequency dispersion.

It may be noted that for 15 and 20 mole% of PbI_2, a plateau is visible in high frequency side and dispersion region is not observable in the measured frequency range. With increasing temperature, the plateau region is visible and seems to be shifting towards high frequency side. At lower frequencies ($f \leq 10$ kHz), the time intervals available to mobile cations at these frequencies are so large that they are able to make successful translational hops to nearby sites and this usually results into polarization at the electrode-electrolyte interface [46, 47]. For x = 25 mole% PbI_2 composition, polarization behavior at low frequency is not observed and only a plateau region followed by the high frequency dispersion is observed.

These frequency dependent conductivity spectra follow the Jonscher's universal power law [48],

$$\sigma'(\omega) = \sigma_{DC} + A\omega^n \qquad \ldots\ldots\ldots (5.7)$$

where, σ_o is the bulk conductivity, A is an arbitrary constant, ω is the radial frequency $\omega = 2\pi f$ and n is a constant called frequency exponent with its value lying generally between 0 and 1 [49]. Since the calculated values of exponent n lie in the range 0.4-0.8, the correlation motion is sub-diffusive and indicates a preference on the part of ions that has hopped away to return to where it started. The AC conductivity spectra were fitted according to the Jonscher universal power law equation. Fig. 5.18 depicts the obtained frequency exponent values with changing temperature for all glass compositions. It is observed that the n is nearly temperature independent for all except x = 5 mole% PbI_2 doped composition.

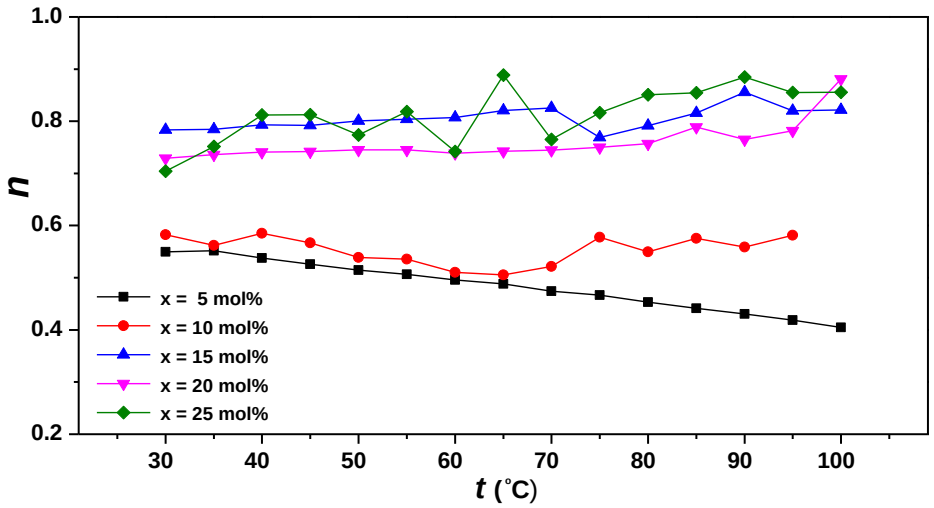

Fig. 5.18. Frequency exponent *n* as a function of temperature for all compositions of glass series (a).

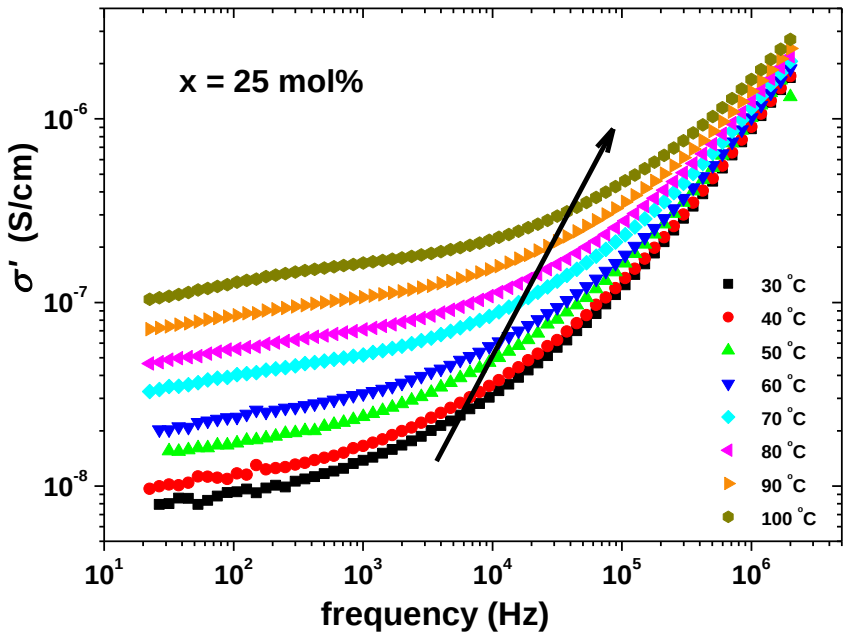

Fig. 5.19. Position of hopping frequency, ω_p, (*shown by arrow*) shifting towards higher frequency side with increasing temperature.

Hopping Frequency

A close inspection of the AC conductivity spectra in Fig. 5.18 reveals that the onset frequency (of dispersion) is shifting towards higher frequency side with increasing temperature. This particular frequency is termed as hopping frequency of

mobile cations and is denoted by ω_p. It is the frequency at which relaxation effects begin to dominate and conductivity makes a transition from frequency independent (low frequency plateau) to frequency dependent (dispersive) behavior. Shifting of hopping frequency with increasing temperature has been marked by an arrow for x = 25 mole% PbI_2 containing glass composition as shown in Fig. 5.19.

Almond and West [50-53] have developed a special formalism based on Jonscher's Universal Power law to estimate the hopping frequency of ions as well as carrier concentration from AC conductivity spectra. In Almond-West formalism, the universal power law is represented in the following form [54],

$$\sigma'(\omega) \propto \omega\left[\left(\frac{\omega}{\omega_o}\right)^{a} + \left(\frac{\omega}{\omega_o}\right)^{b-1}\right] \qquad \ldots\ldots\ldots (5.8)$$

where, ω_o is the characteristics frequency. Now, assuming a single proportionality constant K and taking the characteristics frequency as hopping frequency, and taking a = -1 and $b = n$, following expression for AC conductivity occurs [51],

$$\sigma'(\omega) = K\omega\left[\left(\frac{\omega}{\omega_p}\right)^{-1} + \left(\frac{\omega}{\omega_p}\right)^{n-1}\right] \qquad \ldots\ldots\ldots (5.9)$$

$$\sigma'(\omega) = K\omega_p + K\omega_p^{1-n}\omega^{n} \qquad \ldots\ldots\ldots (5.10)$$

where, K is a constant.

Comparing equation 5.10 and equation of Jonscher's Power Law (equation 5.7), one gets,

$$\sigma_{DC} = K\omega_p \qquad \ldots\ldots\ldots (5.11)$$

& $$A = K\omega_p^{1-n} \qquad \ldots\ldots\ldots (5.12)$$

And, comparing equations 5.11 and 5.12,

$$\sigma_{DC} = A\omega_p^n \quad or \quad A = \frac{\sigma_{DC}}{\omega_p^n} \qquad \ldots\ldots\ldots (5.13)$$

Substituting equation 5.13 in equation 5. 7,

$$\sigma' = \sigma_{DC}\left[1+\left(\frac{\omega}{\omega_p}\right)^n\right] \qquad \ldots\ldots\ldots (5.14)$$

Now, when the frequency of the hopping becomes equal to hopping frequency of the ions, i.e. when $\omega = \omega_p$ in equation 5.14, one gets,

$$\sigma' = 2\sigma_{DC} \qquad \ldots\ldots\ldots (5.15)$$

Thus, hopping frequency should be taken as the particular frequency at which AC conductivity becomes twice of DC conductivity. Substituting equation 5.15 in Jonscher's universal power law (equation 5. 7), the expression for hopping frequency ω_p occurs

$$\omega_p = \left(\frac{\sigma_{DC}}{A}\right)^{\frac{1}{n}} \qquad \ldots\ldots\ldots (5.16)$$

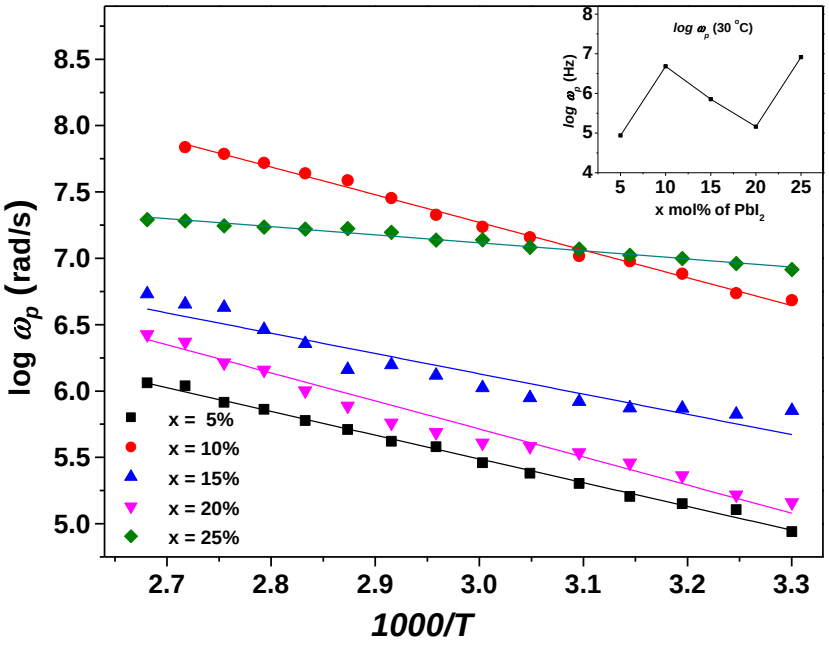

Fig. 5.20 $log\omega_p \rightarrow 1000/T$ plots for hopping frequency
(*Solid lines are the best fits to the Arrhenius law*)

The hopping frequency values at different temperatures are plotted with 1000/T and shown in Fig. 5.20for all compositions of glass series (a Hopping process of ions is thermally activated as is evident from the Fig. 5.20. It means that the rate of attempt to hop from one site to the next available site increases with increasing temperature. In the inset in Fig. 5.20, the compositional dependence of hopping frequency depicted and its is observed to be almost independent of PbI_2 in the host glass system and does not seem to be in consonance with compositional variation of bulk conductivity. Table 5.2 shows of the values of activation energies for conduction as well as hopping of ions and their hopping frequency at 30˚C.

Table 5.2: Conductivity activation energy, E_σ and hopping frequency activation energy, E_ω, and room temperature hopping frequency, ω_p , as a function of x mole% of PbI_2 for glass series (a).

x mole% of PbI_2	E_σ (eV)	E_ω (eV)	ω_p (30 ˚C) (Hz)
5	0.46	0.36	8.72×10^4
10	0.42	0.41	4.83×10^6
15	0.42	0.30	7.12×10^5
20	0.26	0.42	1.45×10^5
25	0.19	0.12	8.22×10^6

It may be noted from Table 5.2 that activation energies for hopping of ions are lower than that for conduction processes except for 20 mole% of PbI_2, which suggests that the ions that are participating in the conduction process have to face different potential barriers due to the localized electrons of the amorphous matrix in the conduction process.

The observed frequency dependence of conductivity in the present glass systems can be understood on the basis of jump relaxation model [55, 56]. According to this model, at lower frequencies (f < 1k Hz-10k Hz), a mobile ion can make successful hops to its neighboring vacant site due to long time periods

available at these frequencies. And such successive jumps result in a long range translational motion of ions contributing to DC conductivity and as a result the low frequency plateau occurs. Once an ion has completed its "initial hop" from initial site to the neighboring site, two competing relaxation processes may be visualized at higher frequencies: first, the ion may hop back to its initial position (correlated forward–backward hopping) and second, the surrounding ion cloud (neighborhood) will relax with respect to its new position thereby shifting its cage potential. At higher frequencies, the probability for the ion to go back again to its initial site increases due to the short time intervals. This increased probability of correlated forward–backward hopping at higher frequencies along with relaxation of the cage potential leads to the observed high frequency conductivity dispersion in AC conductivity spectra.

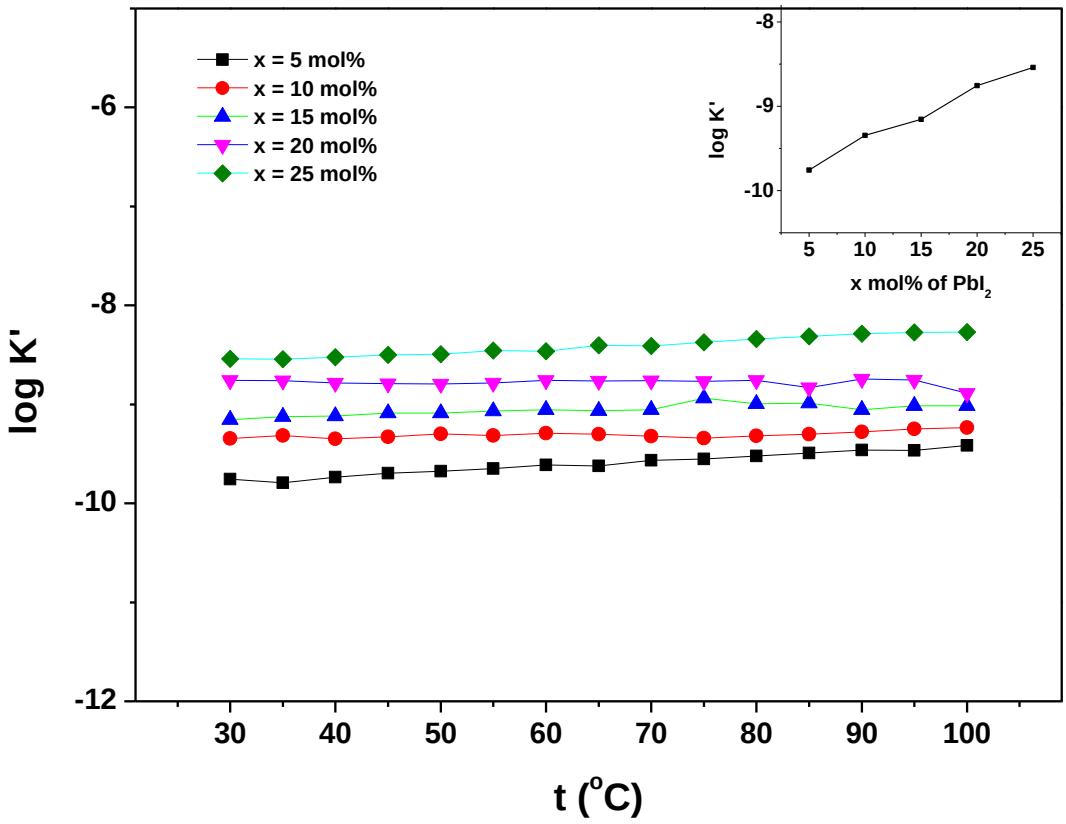

Fig. 5.21. log$K' \rightarrow t$ plots for the mobile ion concentration factor for glass series (a)
(***Solid lines are the guides for eyes*****)**

The mobile ion concentration factor *K'* may be calculated using the following relation [57],

$$K' = \frac{\sigma_{DC} T}{\omega_p} \qquad \ldots\ldots\ldots (5.17)$$

Fig. 5.21 shows the variation of mobile ion concentration factor as a function of temperature in glass series (a). it is observed that log*K'* remains almost invariant with changing temperature. It implies charge carrier concentration factor varies almost linearly with increasing PbI_2 content at 30 ˚C as shown in the inset of Fig. 5.21.

Now, in order to identify the effect of variation of composition and /or influence of temperature on ion conduction mechanism, scaling analysis is helpful. Different scaling laws had been applied to scale the AC conductivity spectra of a large number of ion conducting glass systems by various workers [58-61].

The first ever scaling of σ' spectra was attempted by Summerfield [62] in semiconductors and this approach has been widely utilized by Roling *et al.* [63] and its modified version by others [64] for scaling different relaxation spectra of ionically conducting glass systems. In its simplest form, the Summerfield scaling is given as,

$$\frac{\sigma'}{\sigma_o} = F\left(\frac{f}{\sigma_o T} \cdot x\right) \qquad \ldots\ldots\ldots (5.18)$$

where, f = frequency, σ_o = conductivity at given temperature, T = absolute temperature, x = concentration factor.

Now, as stated earlier, the cross-over frequency or hopping frequency is given as: $\sigma'(\omega_p) = 2\,\sigma_{DC}$

And it has been already found that ω_p is thermally activated with the same energy as $\sigma_{DC}T$. Moreover,

$$\sigma_{DC} = N_v \cdot q \cdot \mu_{DC} \qquad \ldots\ldots\ldots (5.19)$$

where, N_v = number density of mobile charges, q = electronic charge of the mobile cation and μ_{DC} = mobility of charge carriers.

For simplicity, it may be assumed that charge carrier concentration remains constant with temperature, the scaling law may be written as [65]

$$\frac{\sigma'}{\sigma_o} = F\left(\frac{f}{\sigma_{DC}T}\right) \qquad \ldots\ldots\ldots (5.20)$$

In this equation, the ion dynamics is described by the universal function ***F*** that is independent of both temperature and composition. Main advantage of this scaling law is that it utilizes the directly available quantities as scaling parameters. Fig. 5.22 shows the scaled spectra for AC conductivity spectra for all compositions of series (a). It is observed that AC conductivity spectra for different temperatures merge near perfectly onto a single master curve which indicates the existence of a time temperature superposition (TTS) and a temperature independent relaxation mechanism. Such scaling has been named canonical scaling by Sidebottom [66] where shape of the AC conductivity spectra is preserved with changing temperature and ion concentration remains invariant. According to Dyre *et al.* [67], TTS is observed in single ion conducting glasses and crystals with structural disorder. It means that disorder is intimately linked to presence of TTS [68-70] because the disorder of the glass matrix leads to a broad distribution of ion site energies and barrier heights and thus to a broad distribution of jump rates [71, 72] and the Coulombic interactions cause a significant spread in the potential energies of the ions.

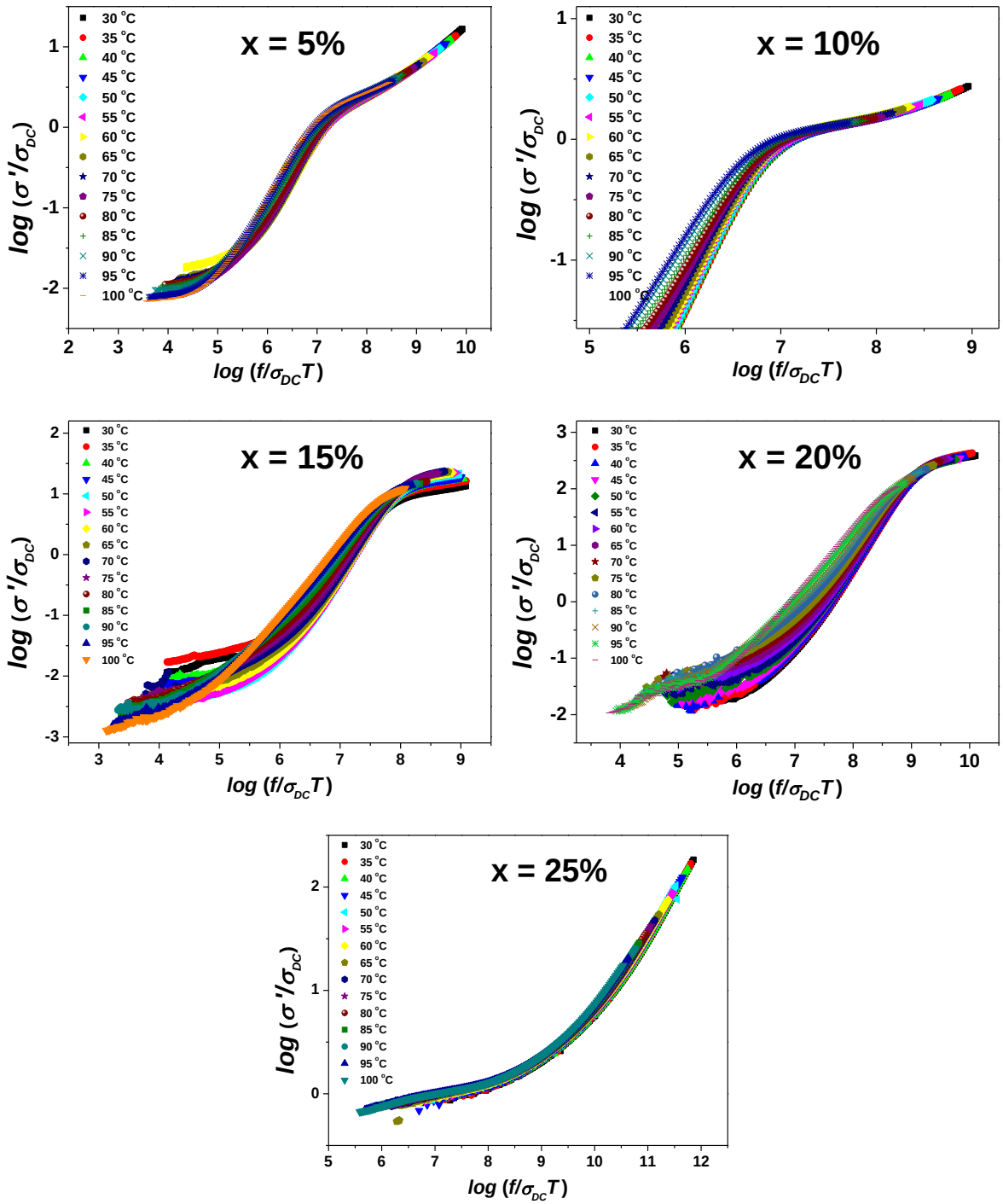

Fig. 5.22 Scaling of σ' spectra as a function of temperature for all compositions of glass series (a).

Scaling of σ' spectra as a function of PbI_2 concentration is presented in Fig. 5.23 in order to see the effect of change of mobile Ag^+ ion concentration as well as variation of the glass structure. It is observed that the σ' spectra for different compositions do not superpose on a single curve.

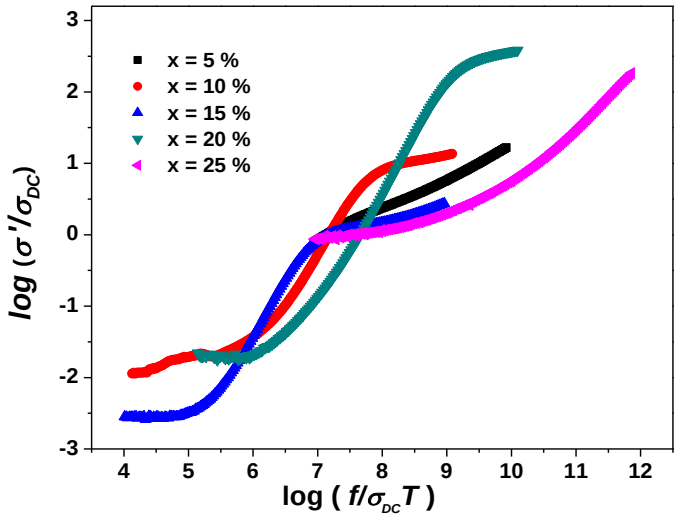

Fig. 5.23. Conductivity scaling spectrum for different compositions at 30 ˚C as a function of composition for glass series (a)

It should be noted that mobile ion concentration *K'* is increasing with PbI_2. It has been reported by Roling [73], that variation in ion concentration affects the ion relaxation process significantly and hence violation of scaling as a function of composition is generally observed in glasses with significant variation of mobile ion concentration with changing glass composition. This indicates that Ag^+ ion conduction mechanism might not be uniform over the studied compositional range.

Series (b): The AC conductivity spectra for all compositions of series (b), where the ratio of PbI_2 to Ag_2O has been kept 1:2, are presented in Fig. 5.24 at different temperatures.

It is observed that for *y* = 35, 40 and 45 mole% compositions, at low temperatures (below 50 ˚C) only a low frequency plateau followed by high frequency is observed. And at higher temperatures it exhibits polarization effects. Kuwata *et al.* [74], Karan *et al.* [75] and others [76-79] also reported similar behavior in different Li^+ and Ag^+ superionic conducting glass systems. However, for *y* = 30, 50 and 55 mole% compositions, the low frequency dispersion due to polarization effects is present right from room temperature. The plateau region shifts

towards higher frequencies with increasing temperature. All AC conductivity spectra were found to obey Jonscher universal power (equation 5. 7).

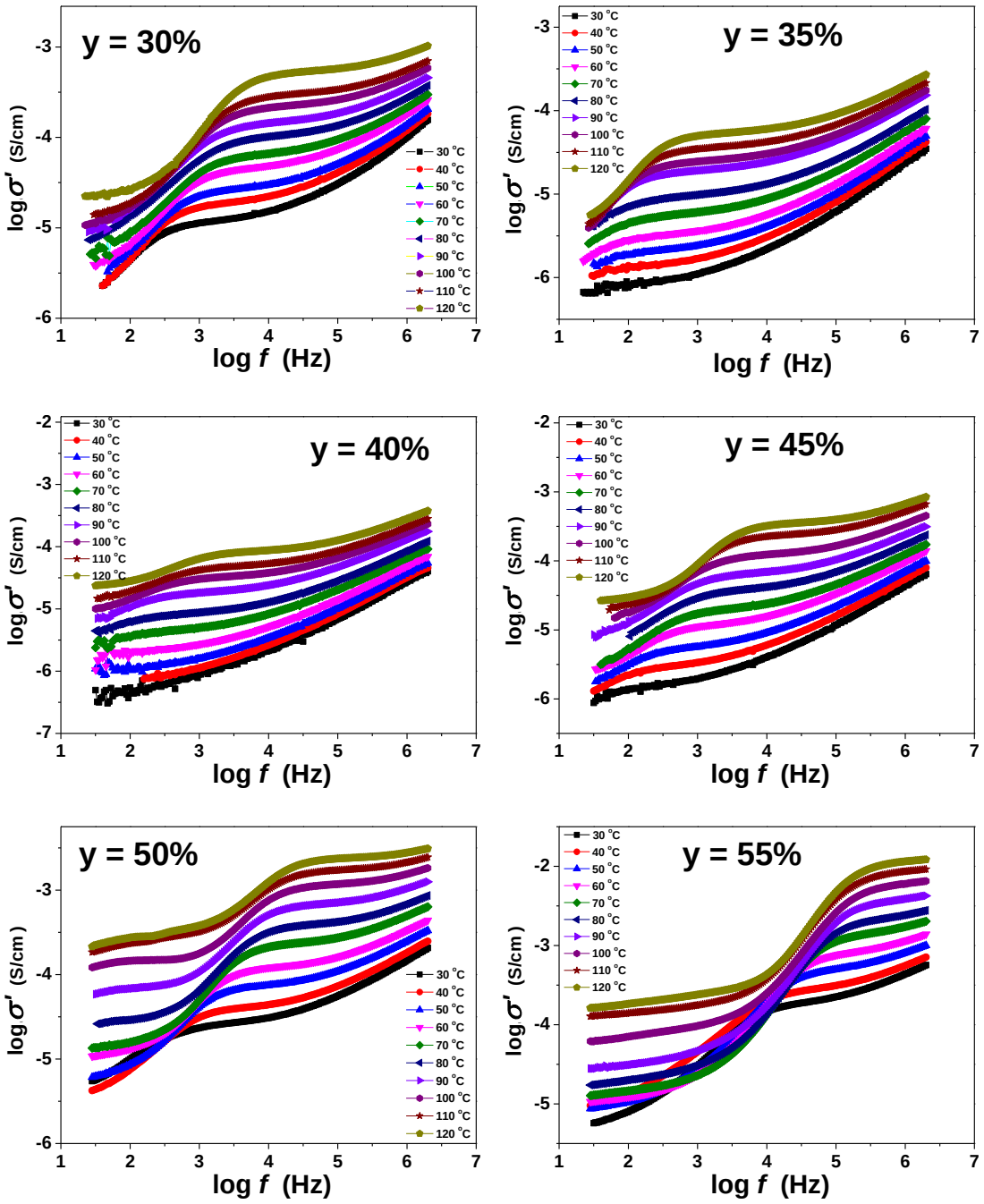

Fig. 5.24. Frequency dependent conductivity at different temperatures for *y* = (a) 30 mol%, (b) 35 mol%, (c) 40 mol%, (d) 45 mol%, (e) 50 mol% and (f) 55 mol% compositions

The frequency exponent, *n*, is calculated, which is in the range of 0.5 to 0.9, is independent of temperature as well as composition. For composition, *y* = 55 mole%, *n* shows a weak temperature dependence, increasing steadily from 0.56 at 30 ˚C to 0.79 at 120 ˚C.

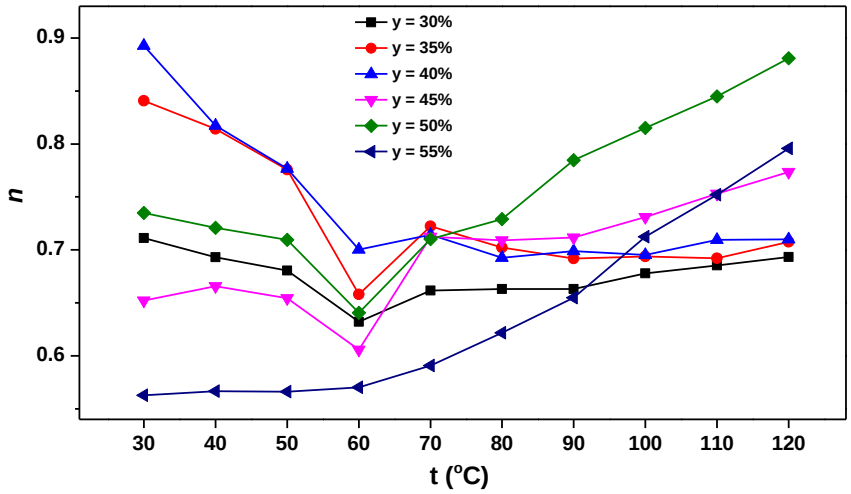

Fig. 5.25. Frequency exponent *n* as a function of temperature for all compositions of series (b).
(*Note: Solid line is just a guide for eyes*)

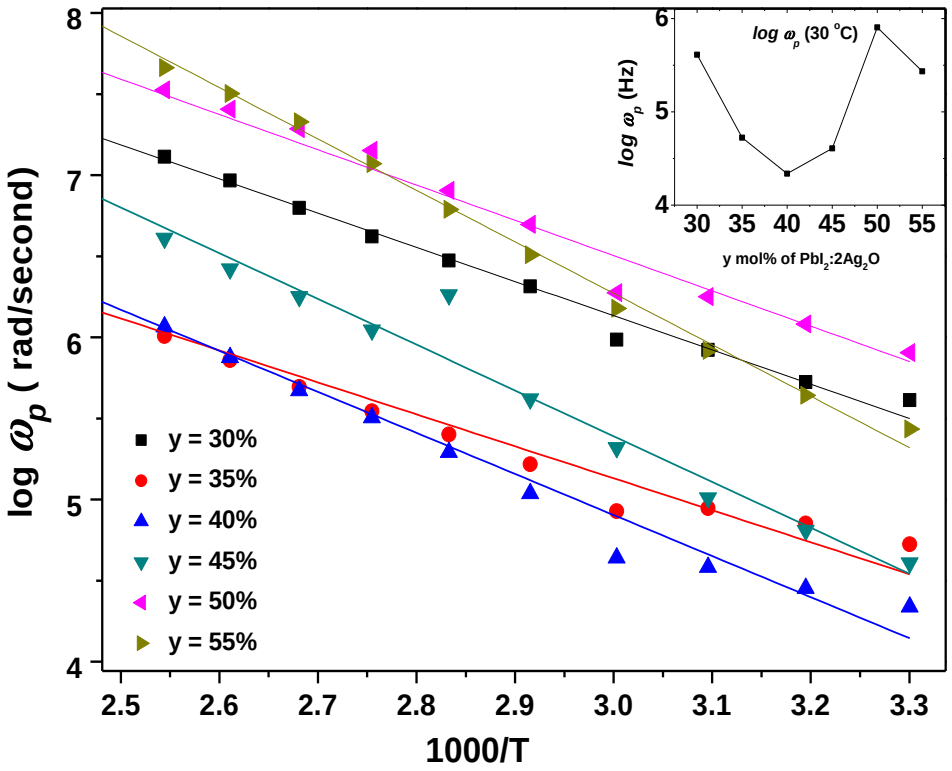

Fig. 5.26. logω_p → 1000/T plots for hopping frequency. *Inset*: logω_p at 30 ˚C for all compositions.
(*Solid lines are the best fits to the Arrhenius equation*)

The linear variation of logω_p with1000/T for different compositions is shown Fig. 5.26. which confirms the thermally activated nature of hopping frequency in the present system. The the variation of logω_p as a function of different amount of (PbI_2:$2Ag_2O$) is shown in the inset of Fig. 5.26. It is observed that with changing composition, ω_p decreases initially upto 40 mole% and after that it increases. Such variation at y =40 mole% is observed in DC conductivity as well.

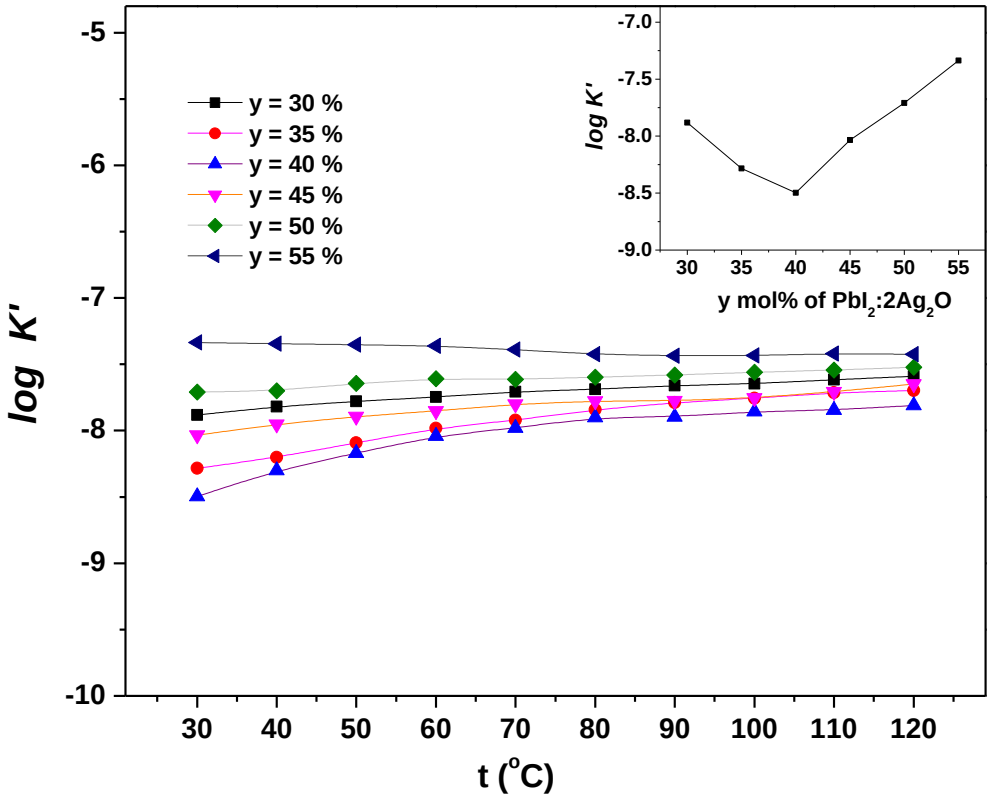

Fig. 5.27. log$K' \rightarrow t$ plots for the mobile ion concentration factor for glass series (b)
(*Solid lines are the guides for eyes*)

The carrier concentration factor K' as a function of temperature for all glass compositions of series (b) is plotted in Fig. 5.27. It is observed that logK' remains almost invariant with changing temperature, whereas, it shows a minimum K' for y = 40 mole% PbI_2:$2Ag_2O$ concentration.. Thus, such a variation in conductivity is

observed near y = 40 mole% and increases beyond y = 45 mole% PbI_2:2Ag_2O concentration.

Scaling of AC conductivity spectra is carried out using the scaling law mentioned in equation 5.20 and is presented in Fig. 5.28 & 5.29 as a function of composition and temperature respectively.

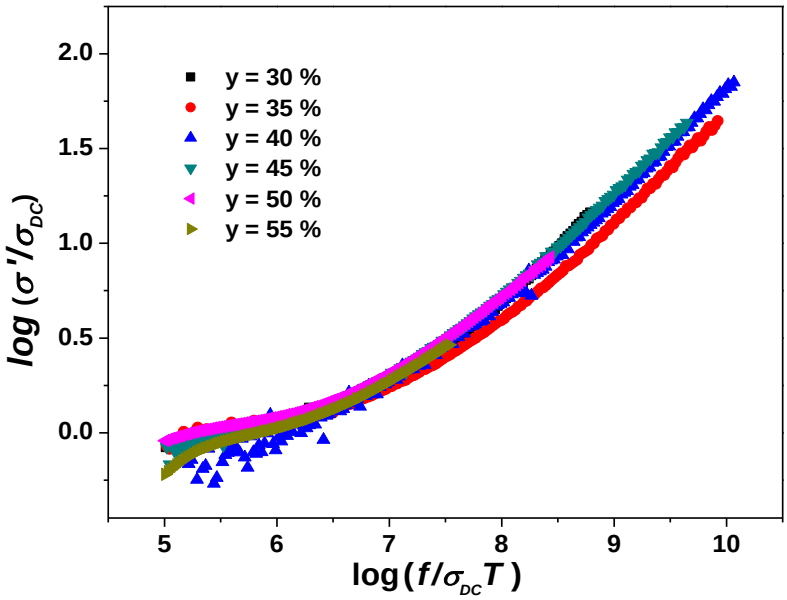

Fig. 5.28. Conductivity scaling spectrum for different compositions at 30 ˚C as a function of composition for series (b)

In a composition dependent scaling given in Fig. 5.28, it is observed that σ' spectra merge near perfectly onto a single master curve In addition to this, scaling as a function of temperature is also observed for all compositions of the glass series (b). The polarization effects at electrode-electrolyte interface, observed at low frequency region are not merging after scaling. Thus, the scaling of σ' spectra as a function of temperature as well as composition suggests that ion conduction mechanism in the present glass series is independent of variations of temperature as well as glass composition.

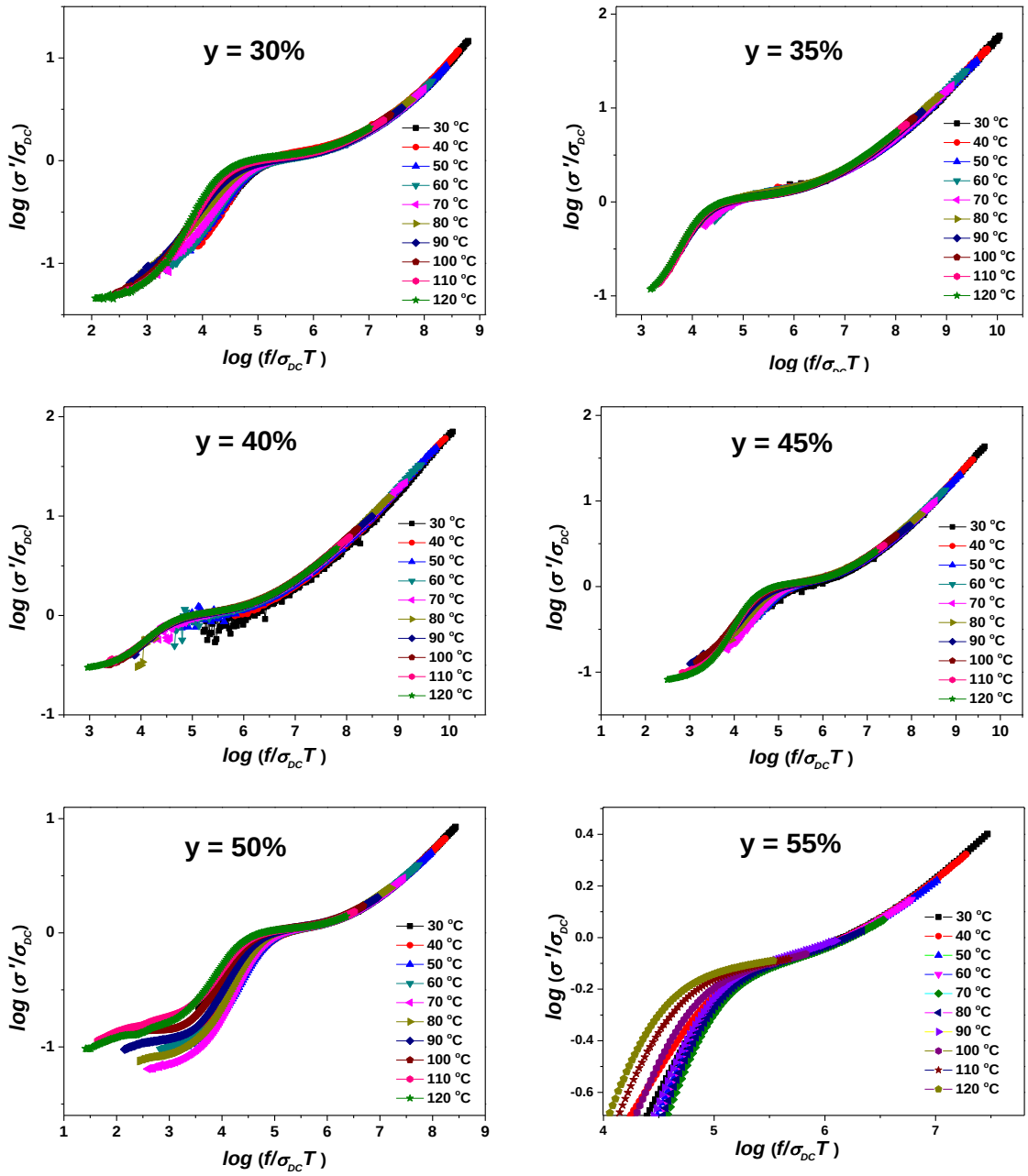

Fig. 5.29. Scaling of *σ'* spectra as a function of temperature for all compositions of glass series (b).

Series (c): In glass series $z(PbI_2{:}Ag_2O)$-$(90\text{-}z)V_2O_5$-$10B_2O_3$, where one of the glass formers, B_2O_3 is fixed at 10 mole% while other glass former V_2O_5 is varied. AC conductivity spectra for all glass compositions at different temperatures are shown in Fig. 5.30.

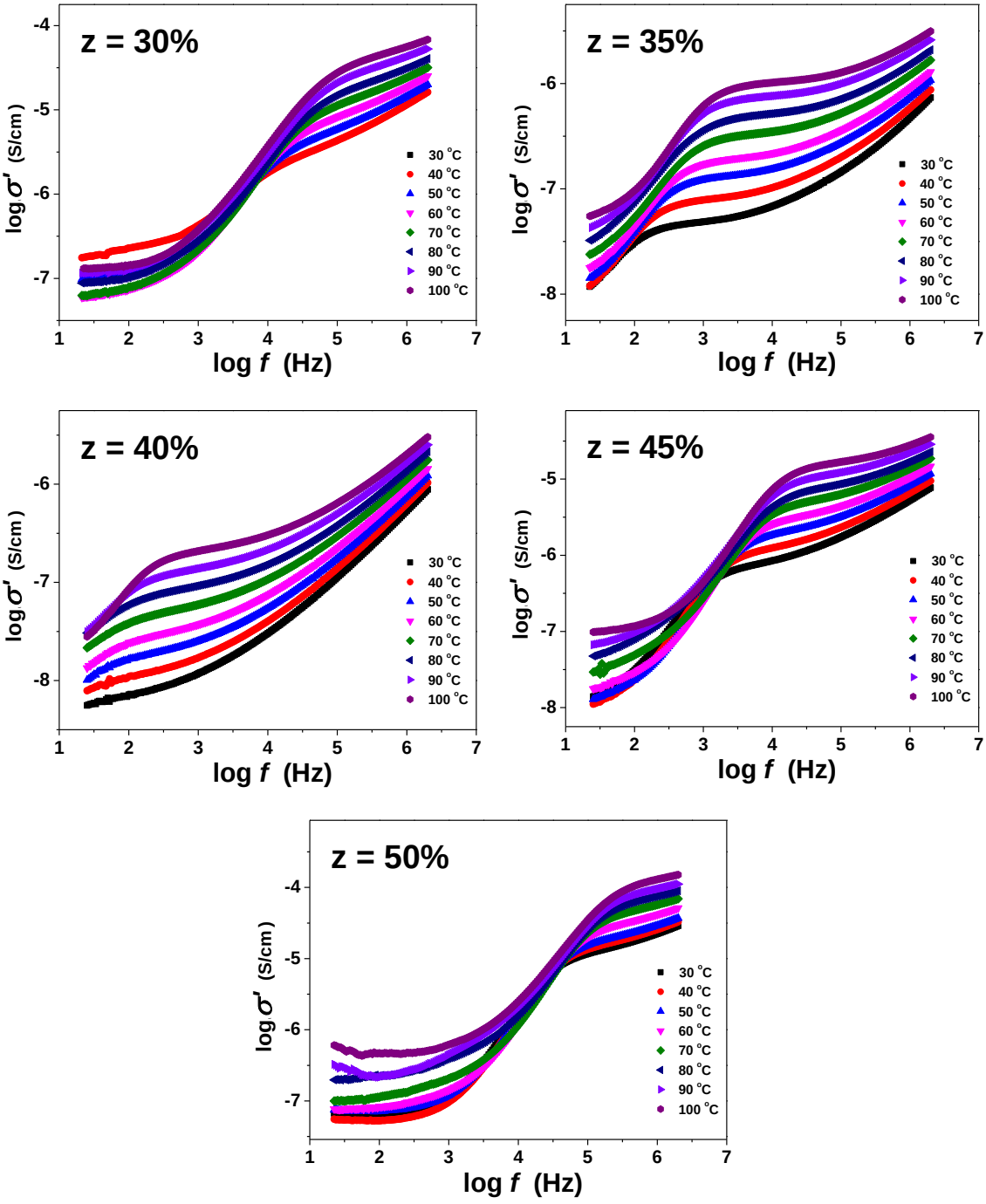

Fig. 5.30. Frequency dependent conductivity at different temperatures for *z* = (a) 30 mol%, (b) 35 mol%, (c) 40 mol%, (d) 45 mol% and (e) 50 mol% compositions

One may note two dispersive regimes; one in low frequency side and other in high frequency region are present. The observed frequency dispersion in low frequency side is attributed to electrode polarization effects which mask the ionic

conduction of the bulk. The plateau region in high frequency side is thermally activated. Moreover, the hopping frequency, ω_p shifts consistently towards higher frequency side with increasing temperature. The observed frequency dispersion spectra are fitted to the Jonscher's universal power law and the hopping frequency ω_p and the frequency exponent n are plotted in Fig. 5.31 and 5.32 respectively.

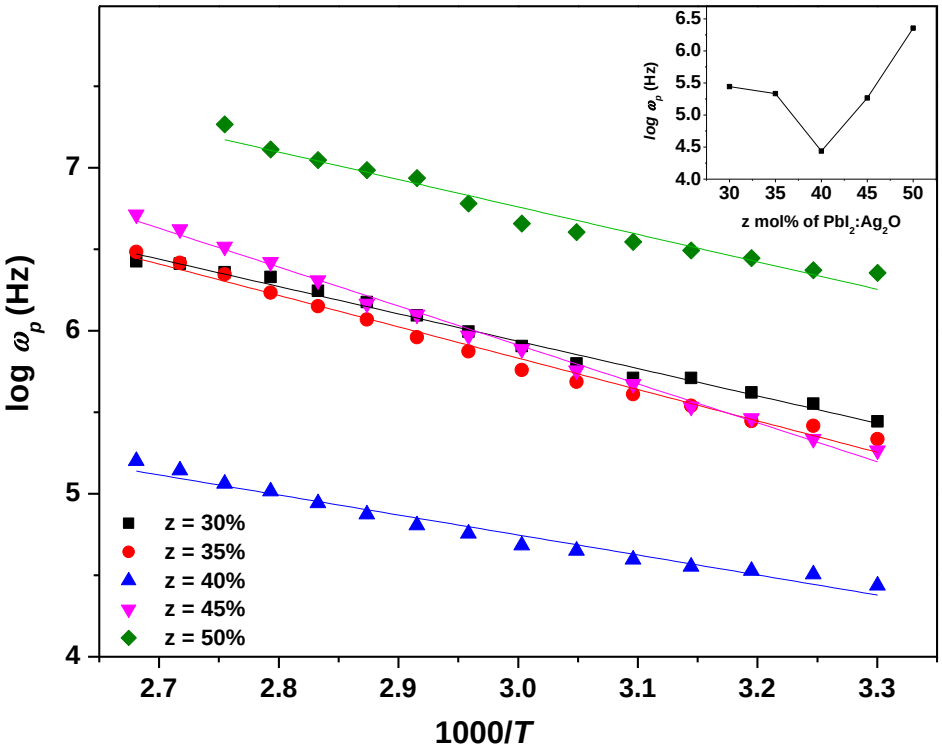

Fig. 5.31. logω_p → 1000/T plots for hopping frequency. *Inset*: logω_p at 30 ˚C for all compositions. (*Continuous lines are the best fits to the Arrhenius equation* 5.15)

The hopping frequency when plotted with 1/T (Fig. 5.31) showed the linear behavior following the Arrhenius behavior [81] and inset of the figure shows variation of hopping frequency with composition. The hopping frequency is observed to decrease till M/F ratio = 0.67 and starts increasing thereafter only PbO is available in the network. As discussed earlier, PbO plays a role of glass former initially upto z = 40 mole% and forms $[PbO_4]^{-2}$ which impedes the motion of Ag^+ ions and hence the conductivity and ωp exhibit a decreasing behavior. Beyond this,

available PbO acts as glass modifier and supports the transport of Ag+ ions in the glass matrix.

The frequency exponent *n* does not exhibit any systematic dependence on composition, whereas, it is noticeable that it decreases weakly with increasing temperature for all glass compositions except *z* = 35 mole% glass composition. For *z* = 35 mole% composition a shallow minimum around 60˚C is observable. Presence of such a minimum was first reported by Jain *et al.* [82] and later followed by other workers [76, 83] in different ion conducting glass systems. As discussed by Elliott *et al.* [84] and Rao *et al.* [83], presence of such a minimum in the temperature dependent frequency exponent *n* can be understood using the Diffusion Controlled Relaxation model [81, 85].

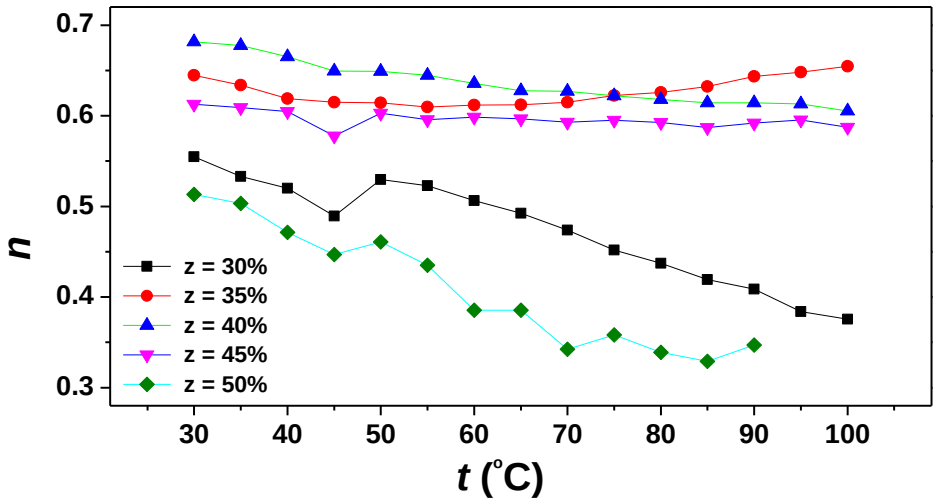

Fig. 5.32. Frequency exponent *n* as a function of temperature for all compositions of glass series (c). (*Continuous lines are just a guide for eyes*)

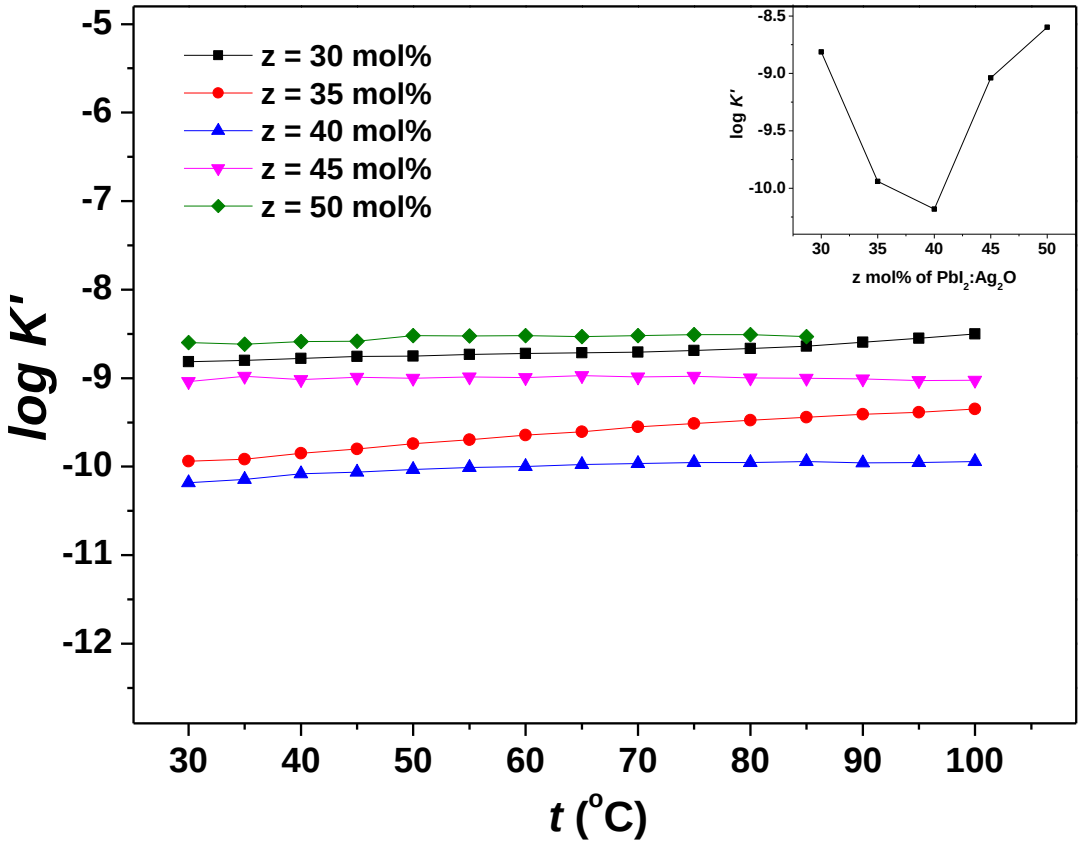

Fig. 5.33. log$K' \rightarrow t$ plots for the mobile ion concentration factor for glass series (c) Inset: log K' as a function of composition at room temperature (*Solid lines are guides for eyes*)

The variation of mobile ion concentration factor *K'* for this glass series is depicted in Fig. 5.33. And it is observed that no change in mobile ion concentration with temperature, whereas, the variation of ion concentration factor *K'* is in good agreement with the observed variation of conductivity as well as hopping frequency with PbI_2:Ag_2O.

Scaling of AC conductivity spectra of the present glass system is carried out using scaling procedure adopted in previous glass systems and is presented in Fig. 5.34 and Fig. 5.35 as a function of temperature and composition respectively.

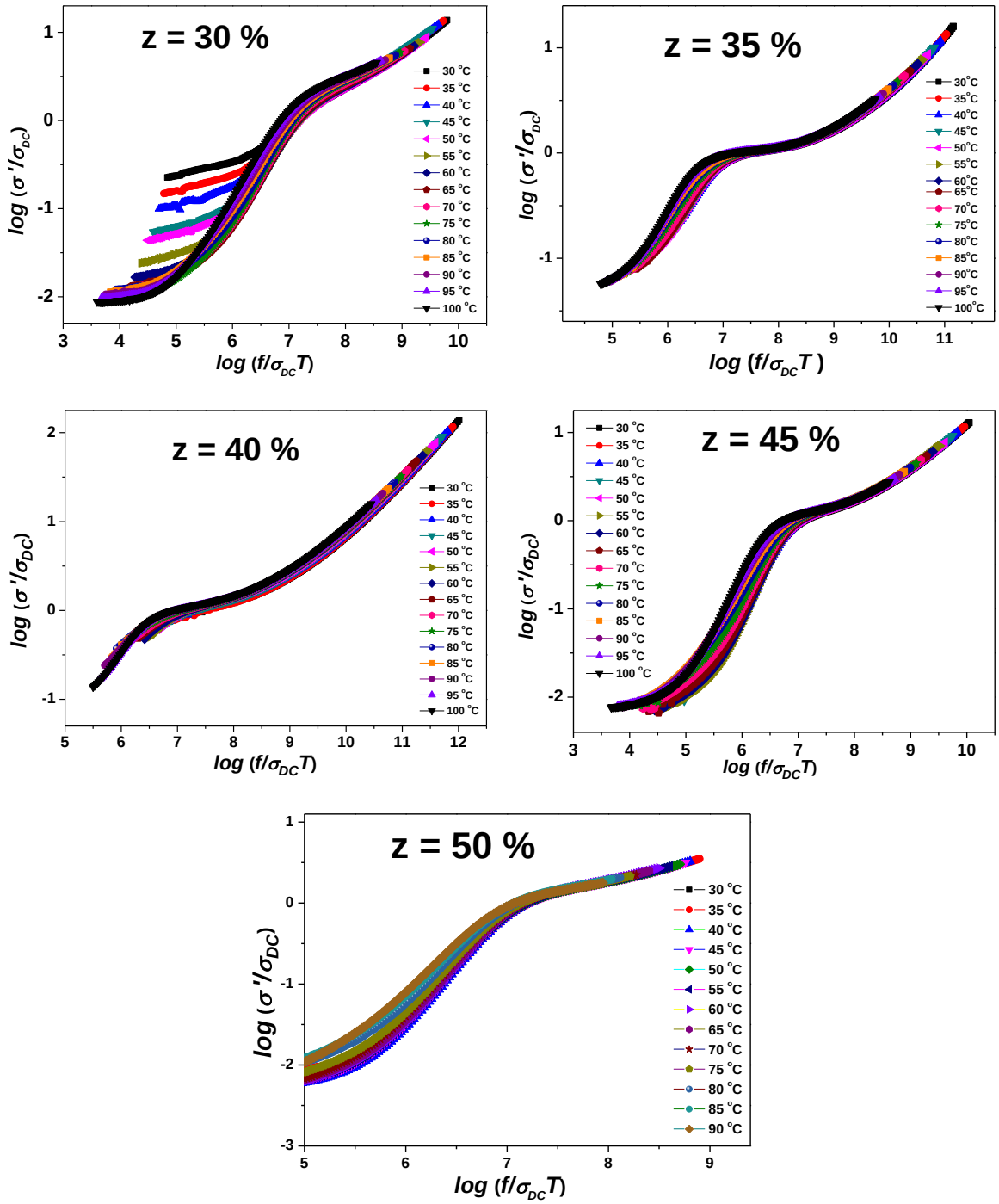

Fig. 5.34. Scaling of *σ'* spectra as a function of temperature for all compositions of glass series (c).

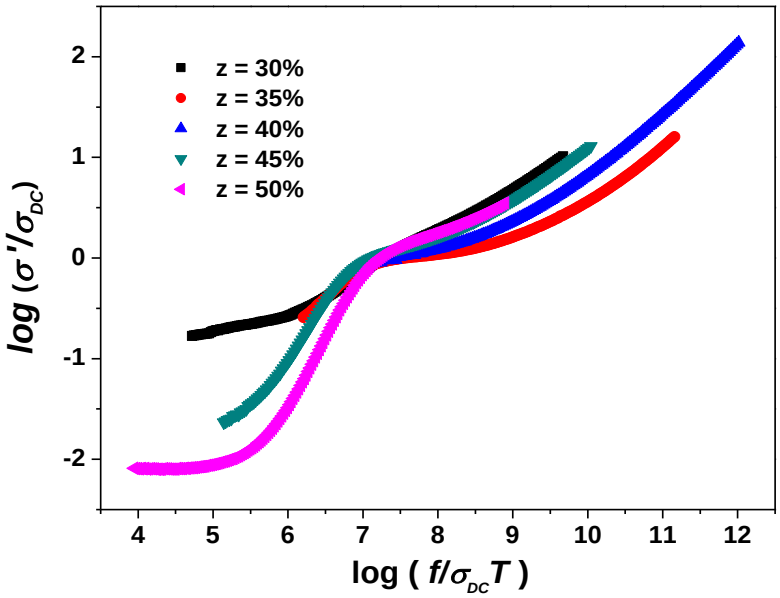

Fig. 5.35. Conductivity scaling spectrum for different compositions at 30 ˚C as a function of composition for series (b)

It is observed that the AC conductivity spectra merge onto a single master curve for all glass compositions for different temperatures. This concludes the invariance of ion dynamics remains at different temperatures for all glass samples. At low frequency, deviation of scaling in conductivity is observed and is ascribed due to the polarization effects reported In Ag^{+} ion conducting lead-bismuthate and tellurite glasses, Ghosh *et al.* [86, 87] have also reported the non superposition of conductivity spectra with composition, while conductivity mechanism follows the time-temperature scaling behavior.

Thus, it may be deduced that, motion of Ag^{+} ions in the present glass systems is hopping in nature and their hopping rate is thermally activated. Time Temperature Superposition is observed for all glass samples suggesting that ion relaxation process is only thermally activated for all glass samples suggesting that the relaxation process is independent of temperature but is dependent on composition. .

5.5 Frequency Dependent Dielectric Permittivity Analysis

Dielectric formalism of impedance spectroscopy has been traditionally applied to investigate dipolar relaxation in liquids and solids where reorientation of permanent dipoles gives rise to characteristic frequency-dependent features of dielectric permittivity [88]. Hence, studying the dielectric properties of an electrically conducting material may seem deceptive, however that *in ion conducting materials, polarization is inseparable from the eventual conduction process* [89]. *Because, the mobile ion, which creates polarization by reorienting locally, is the same ion that later separates from its immediate neighborhood to produce conduction at lower frequencies. Therefore, in ion conducting materials, polarization and conduction are integrated into a single & continuous process.* And hence it is reasonable to consider that dielectric analysis may add complimentary knowledge towards understanding of the ion transport process in ion conducting materials. Details on dielectric formalism are given in section 2.3.3 in chapter 2. The complex dielectric function ε^* is related to complex impedance and complex conductivity functions and is given as [90],

$$\varepsilon^*(\omega) = \frac{1}{i\omega C_o}\cdot\frac{1}{Z^*} = \frac{\sigma^*(\omega)}{i\omega\varepsilon_o} = \varepsilon'(\omega) - i\,\varepsilon''(\omega) \qquad \ldots\ldots\ldots (5.21)$$

where, ε_o is the permittivity of free space, ω is radial frequency, $C_o = \varepsilon_o (a/t)$ and a & t are cross sectional area and thickness of the sample specimen respectively. The Complex dielectric function ε^* is separated into its real and imaginary parts as follows,

$$\varepsilon' = \frac{-1}{\omega C_o}\left(\frac{Z''}{Z'^2 + Z''^2}\right) \qquad \& \qquad \ldots\ldots\ldots (5.22)$$

$$\varepsilon'' = \frac{1}{\omega C_o}\left(\frac{Z'}{Z'^2 + Z''^2}\right) \qquad \ldots\ldots\ldots (5.23)$$

The real part ε' is considered to be the dielectric constant and ε'' is considered to be the dielectric loss that occurs due to conduction process. For an ideal Debye type system, $\varepsilon'(\omega)$ spectra exhibit a step-like change from low to high frequency with two plateau regions in lower and higher frequency regions designated as ε_s and ε_∞ respectively, where, ε_∞ is the high frequency permittivity value determined from the $\varepsilon'(\omega)$ plots at sufficiently high frequencies and ε_s is static dielectric constant, or static permittivity [91]. The difference $\Delta\varepsilon = \varepsilon_s - \varepsilon_\infty$ (the change in the dielectric permittivity) represents dielectric relaxation strength and it is a cumulative result of various relaxation processes [92]. Sidebottom [93] suggested that the hop of an ion between equivalent anionic sites is analogous to the rotation of a permanent dipole and can be approximated to the Debye model of dipolar relaxation. And the permittivity change, $\Delta\varepsilon$, can be given as [94],

$$\Delta\varepsilon = \frac{\gamma N (qd)^2}{3\varepsilon_o kT} \qquad \ldots\ldots\ldots\ldots (5.24)$$

where, N = total mobile-ion concentration, γ = fraction of N ions that are mobile, q = the charge of the mobile ions, d is the distance traversed in a single hop, a resultant of the product *'qd'* is the effective dipole of a hopping ion, k = Boltzmann's constant and T is absolute temperature.

The imaginary part, ε'' corresponds to dielectric loss, that, is a manifestation of motion of mobile ions when an electrical field is applied across the material specimen. Due to their large inertia, the mobile ions are unable to follow to the quick reversal of the applied electric field. And it causes a delayed response to the applied electric field, which results into a loss peak in the high frequency side.

Fig. 5.36 depicts the frequency dependent ε' spectra at different temperatures for all glass compositions of glass series (a).

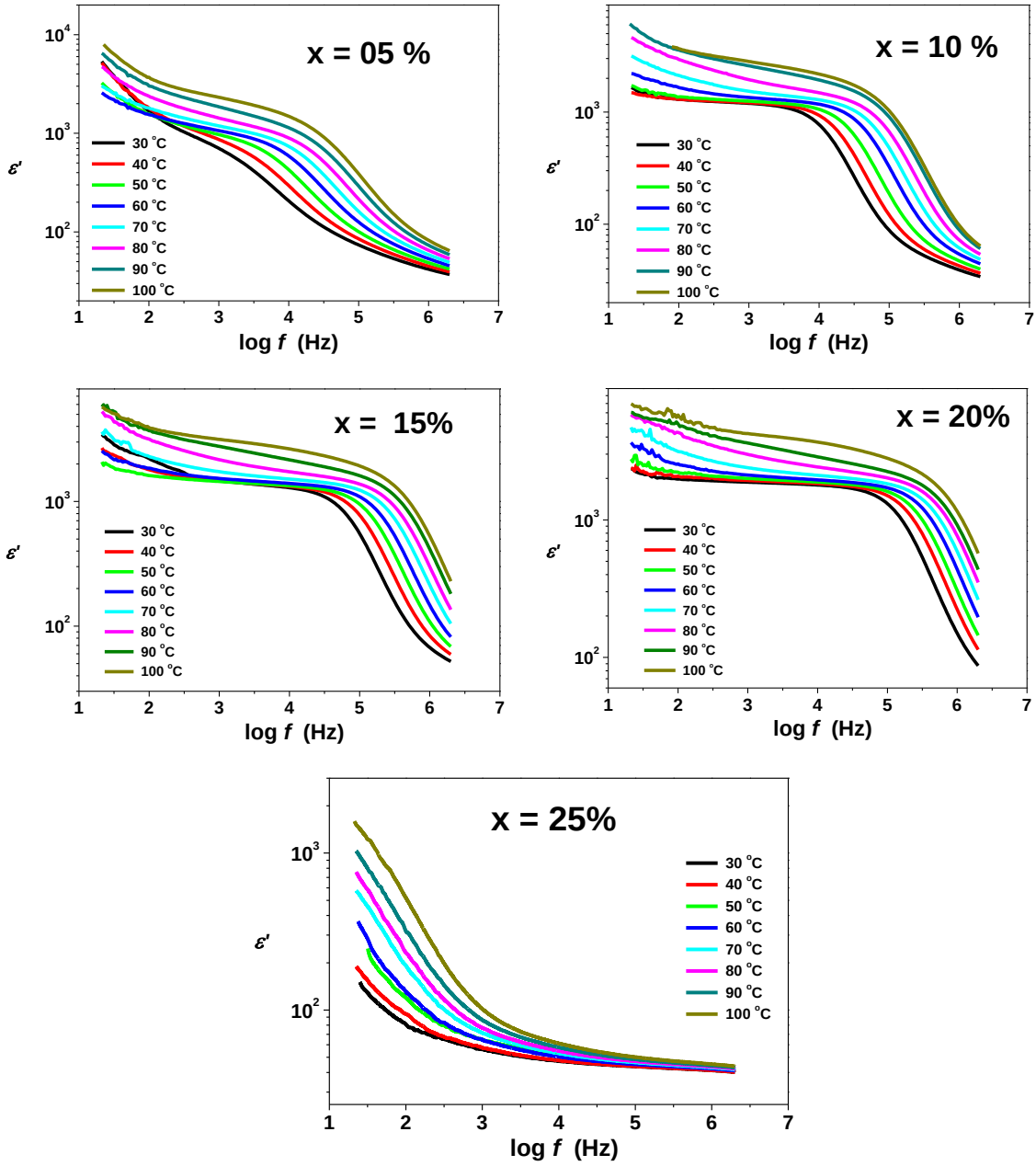

Fig. 5.36. ε' spectra for all compositions of glass series (a) at different temperatures.

It is observed that the resultant ε' spectra have three distinct regions, namely low frequency plateau (ε_s), mid frequency dispersion and finally high frequency saturation plateau (ε_∞). For x = 5 and 10 mole% compositions, all three regions are present, whereas for x = 15 and 20 mole% compositions, the high frequency

saturation plateau is not observable. And for x = 25 mole% composition, the low frequency plateau (ε_s) seems to have merged with that due to the polarization effects and hence it is not distinguishable. The rapid rise in the dielectric constant ε' at lower frequencies (below 50 Hz -1kHz) is due to the electrode polarization effects which is caused by blocking of mobile cations at the interface between glass sample and the electrodes, where metallic electrodes do not permit transfer of the mobile ions into the external circuit [89]. As a consequence of this, mobile Ag^+ ions get piled up near the electrodes and a large bulk polarization of the specimen occurs.

At higher frequencies, periodic reversal of the applied electric field is so rapid that no excess ionic jumps in the field direction occur, and polarization due to pile up of mobile cations at high energy barrier sites disappears and the observed value of ε' saturates at ε_∞. Above results are in conformity with observations made by earlier workers in various ion conducting glass systems [95-99]. Similar features of dielectric dispersion are exhibited by all glass compositions. To quantify the magnitude of polarization, dielectric relaxation strength, $\Delta\varepsilon$ (= ε_s - ε_∞) was calculated. Fig. 5.37 and 5.38 depict the $\Delta\varepsilon$ values as a function of temperature and composition respectively.

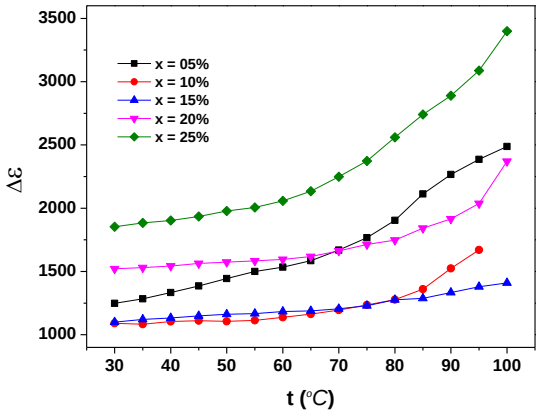

Fig. 5.37. $\Delta\varepsilon$ as a function of temperature for all compositions of glass series (a).

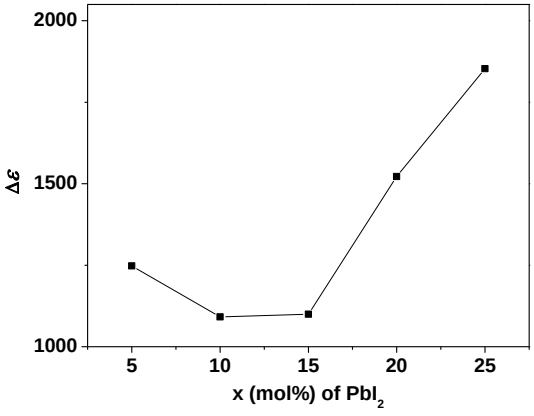

Fig. 5.38. $\Delta\varepsilon$ as a function of x mole% of PbI_2 At 30 °C.

From Fig. 5.37, it is observed that the dielectric relaxation strength $\Delta\varepsilon$ is thermally activated and increases gradually with temperature. According to equation 5.24, $\Delta\varepsilon$ is a result of microscopic phenomena and it is affected by variations in mobile ion concentration, *N*, as well as the hoping distance, *d*.

Further, in order to examine the universality of the relaxation process, scaling analysis of the ε' spectra has been utilized [100, 101]. The scaling approach undertaken for scaling the AC conductivity spectra can be simply modified to include the hopping length, which is an ultimate quantity concerning the nature of the hopping process of ions, however is not measurable directly or indirectly. Sidebottom [102] proposed the following scaling law to scale the frequency dependent dielectric permittivity spectra:

$$\frac{\sigma'}{\sigma_{DC}} = F\left(\frac{f\varepsilon_o\Delta\varepsilon}{\sigma_{DC}}\right) \qquad \ldots\ldots\ldots (5.25)$$

And the scaling constant for frequency axis is given as,

$$f_o = \frac{\sigma_{DC}}{\varepsilon_o\Delta\varepsilon} \qquad \ldots\ldots\ldots (5.26)$$

where, $\Delta\varepsilon = \varepsilon_s - \varepsilon_\infty$. This form of f_o (scaling frequency) is consistent with the Barton-Nakajima-Namikawa relation [103-105] as well as theoretical work by Dyre [106]. The dielectric relaxation strength $\Delta\varepsilon$, on the basis of analogy of ionic relaxation to the rotation of a dipole of dipole moment $p=qd$, the dielectric relaxation strength $\Delta\varepsilon$ may be expressed using equation (5.24) as follows

$$\Delta\varepsilon = \frac{\gamma N(qd)^2}{3\varepsilon_o kT}$$

And if this analogy is valid, this choice for f_o (the scaling frequency) should account for changes in the hopping distance and it tends to the expression of a direct proportionality between f_o and hopping rate. It was demonstrated that this choice for

f_o could scale σ' spectra for Na_2O-GeO_2 glass system at different concentrations [102] and later in F^- ion conducting polycrystalline $PbSnF_4$ by Ahmad *et al.*[101].

Now, in order to scale the ε' spectra, the high frequency dielectric constant ε'_∞ (saturation value of ε' at higher frequency saturation) should be removed, as it is a consequence of faster polarization mechanisms and not of ionic motion. The ε' spectra should be scaled by $\Delta\varepsilon$ and the magnitude of permittivity change due to ionic relaxation. Thus, permittivity can be scaled as [89]

$$\frac{\varepsilon' - \varepsilon_\infty}{\Delta\varepsilon} = F_2\left(\frac{f}{f_o}\right) \qquad \ldots\ldots\ldots (5.27)$$

where,
$$f_o = \frac{\sigma_{DC}}{\varepsilon_\infty \Delta\varepsilon} \qquad \ldots\ldots\ldots (5.28)$$

The scaling law given in equation 5.27 has been applied to scale the ε' spectra and the scaled permittivity spectra are depicted for the present glass series (a) in Fig. 5.39.

It is observed here that the dielectric spectra merge near perfectly onto a single master curve for all glass compositions at different temperatures, except a at lower frequencies. The polarization effects at sample-electrode interface at lower frequencies does not merge at any temperatures. Such a deviation at lower frequencies is also observed in scaled AC conductivity spectra as well [107]. Scaling as a function of composition at any particular temperature is not observed. This means that the dielectric relaxation in different glass compositions might be occurring at different time scales. In other words, even though the characteristic frequency scale governing the transport processes might be thermally activated, the characteristic spectral features of the relaxation remain in the same proportion, *i.e.*

the ion dynamics mechanism does not get altered in the studied frequency range and temperature window.

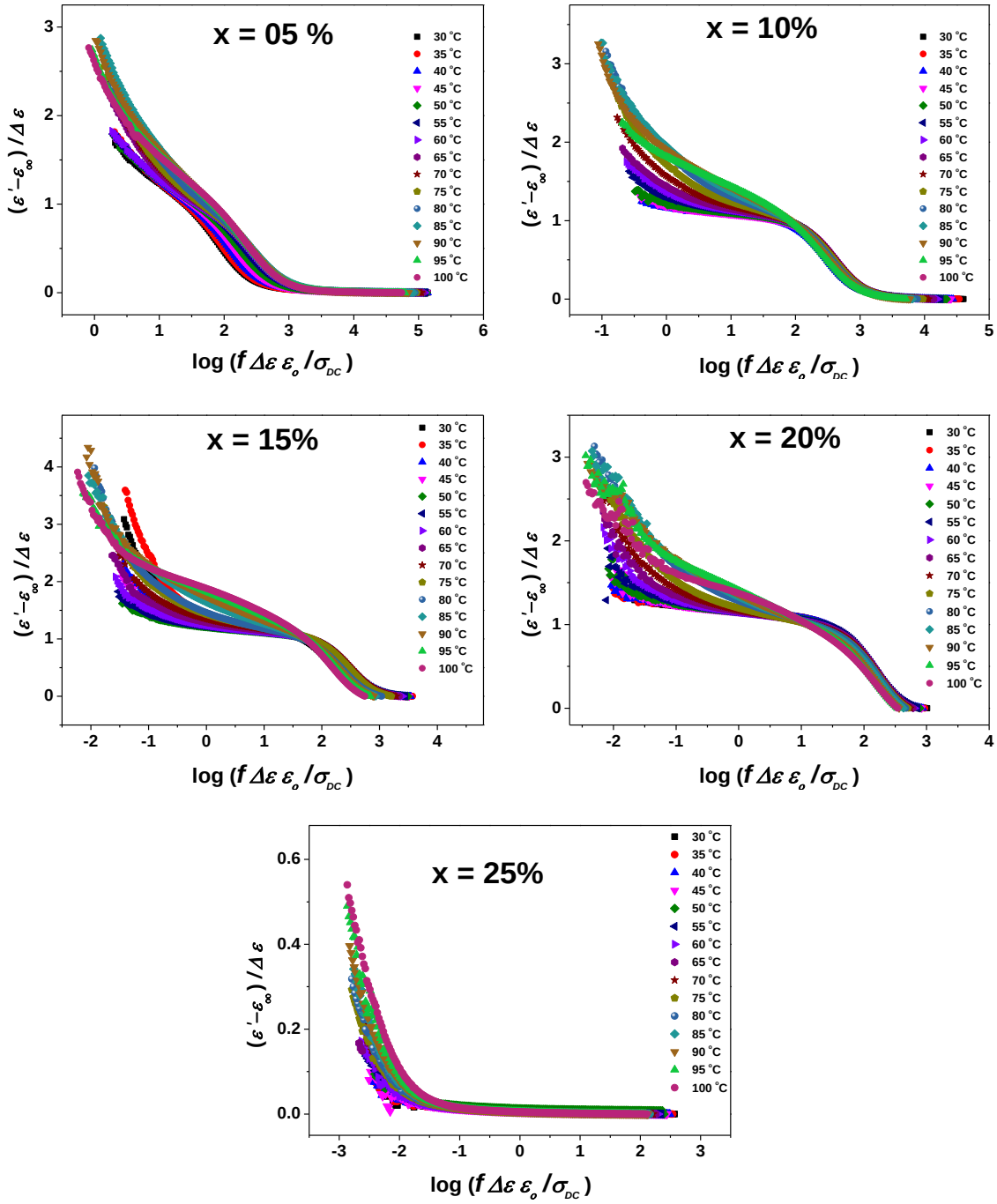

Fig. 5.39. Scaling of ε' spectra as a function of temperature for all compositions of glass series (a).

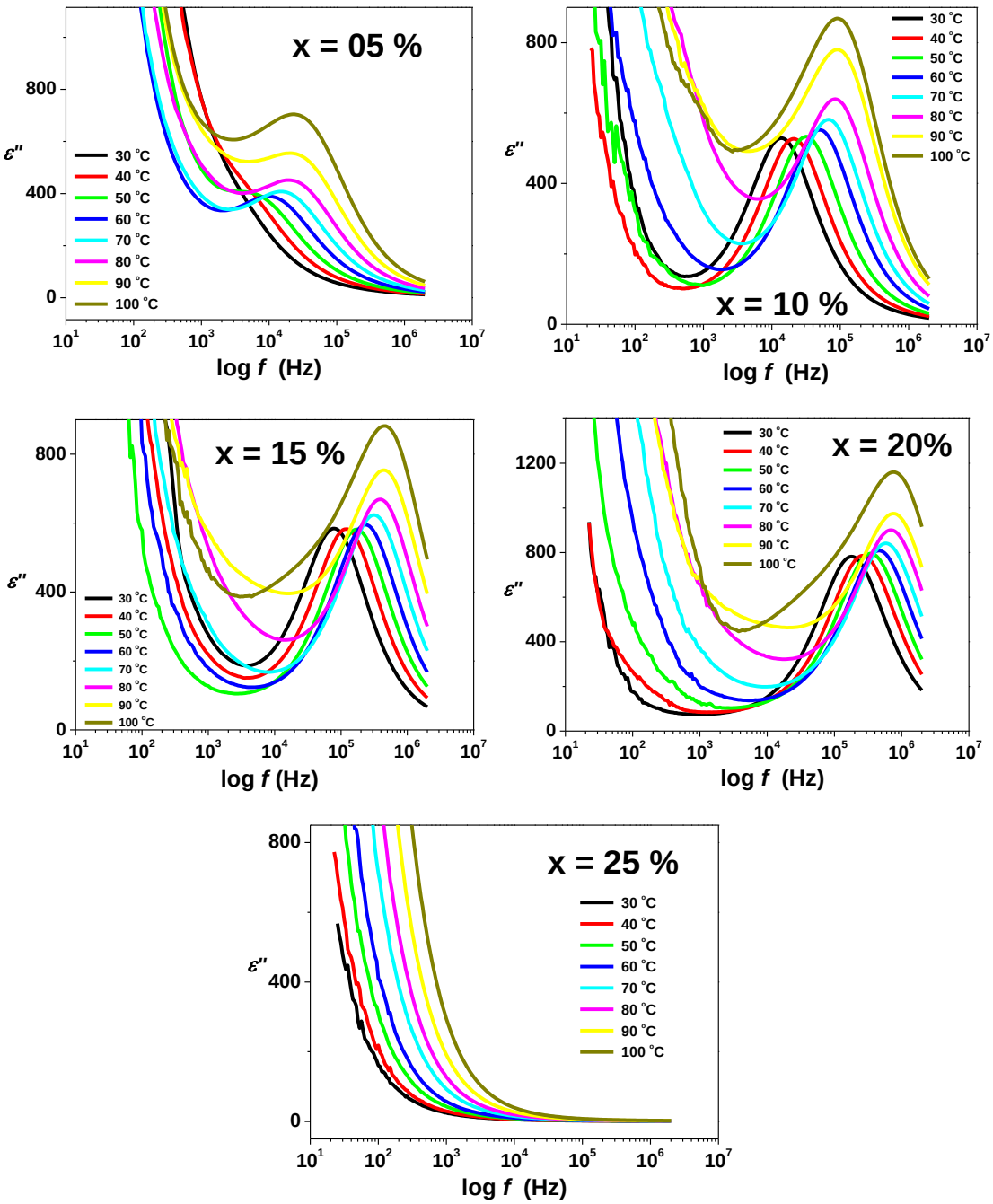

Fig. 5.40. Dielectric loss *ε″*, spectra for all compositions of glass series (a) at different temperatures.

In order to evaluate the effect of PbI_2 dopant salt concentration on the dielectric loss spectra ε'' for all compositions of glass series (a) at different temperatures are shown in Fig. 5.40. It is clear that all ε'' spectra exhibit a well developed dielectric loss peak for x = 5 to 20 mole% PbI_2 between mid frequency to high frequency side. The observed dielectric loss peak can be attributed to

combination of dipole relaxation loss and conduction losses that occur due to migration of Ag^+ ions in the glass matrix. Both these losses are collectively termed as migration losses. Conduction losses increase with the rise in temperature. It has been mentioned that conductivity is thermally activated and increases with increasing temperature.

This implies that with increasing temperature, the losses associated with conduction also increase. For x = 25 mole% no loss peak is observed in the studied range of frequency.

Series (b): The Dielectric permittivity spectra for glass series (b) are presented in Fig. 5.41 for all of its compositions. It is observed that similar to glass series (a), the $\varepsilon'(\omega)$ spectra exhibit a step-like change from low to high frequency with a saturation plateau at higher frequency.

It is interesting to note here that with increasing y mole%, the onset frequency of dielectric dispersion initially reduces from y = 30 mole% compositions to 40 mole%, and after that it starts shifting towards higher frequency side; this effect is more pronounced at higher temperatures.

Table 5.3: Onset Frequency of ε' dispersion at 100 ˚C as a function of composition

Sample	Onset Frequency of ε' dispersion
y mole% of PbI_2:2Ag_2O	(Hz)
30	768
35	131
40	109
45	757
50	5087
55	62475

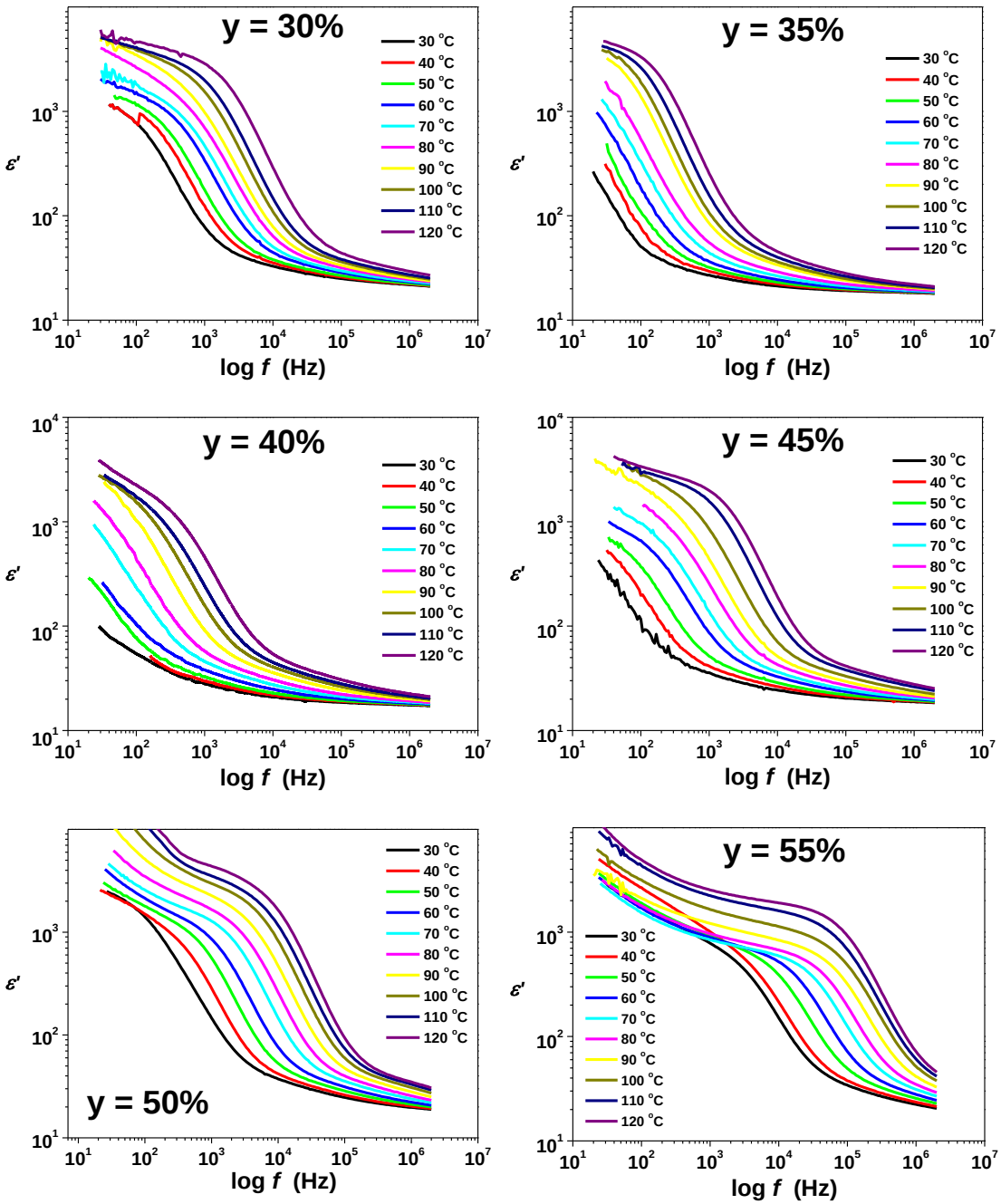

Fig. 5.41. ε' spectra at different temperatures for all compositions of glass series (b).

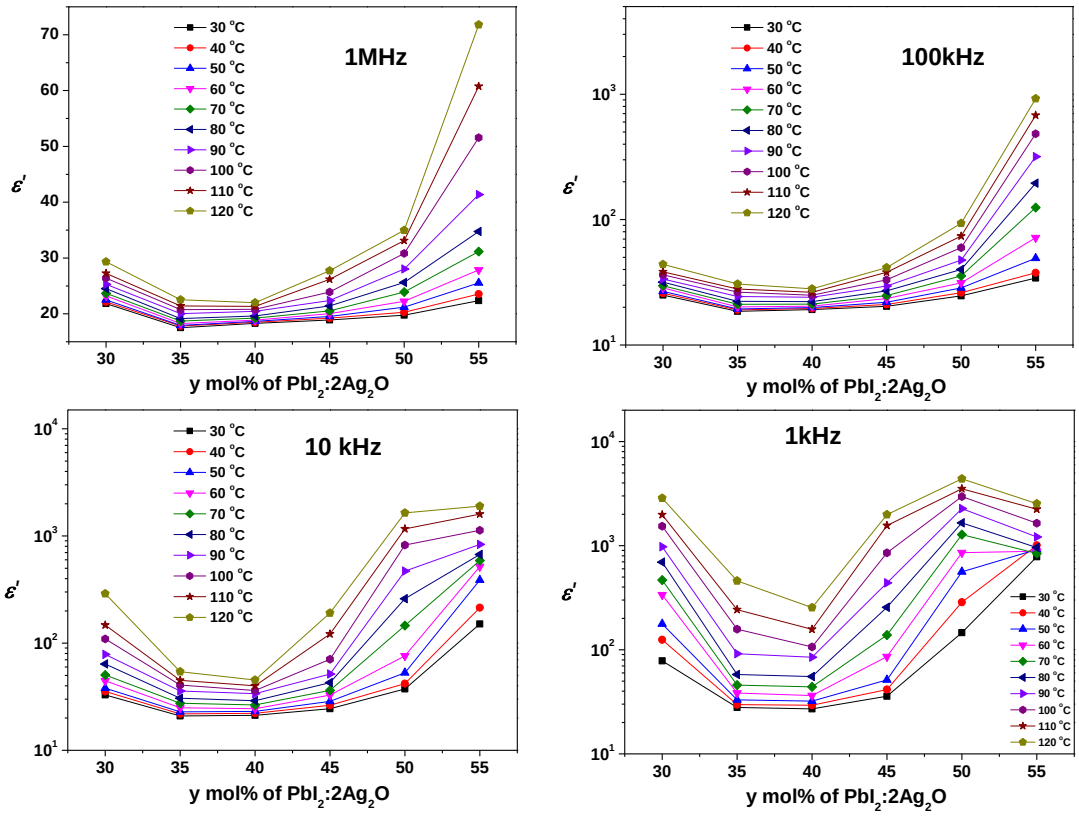

Fig. 5.42. ε' as a function of glass composition at fixed frequencies at different temperatures.

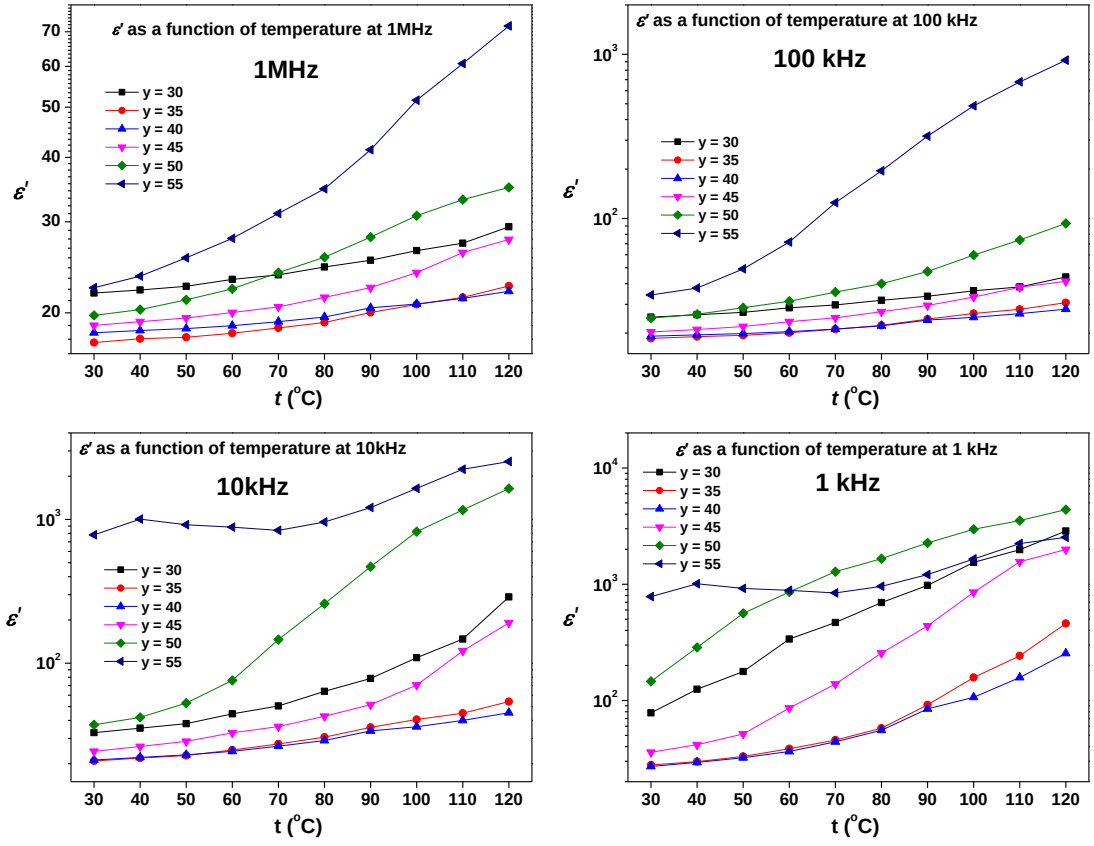

Fig. 5.43. ε' as a function temperature for various glass compositions at some fixed frequencies.

Table 5.3 shows onset frequency of dispersion for different compositions at 100 ˚C and the effect of change in glass composition on the onset frequency of dispersion is easily noticeable. The minimum onset frequency occurs at 109 Hz for y = 40 mole% whereas it rises up to nearly 62 kHz for y = 55 mole% composition. Alongwith that Fig. 5.42 shows ε' isotherms at different frequencies as a function of composition. It is remarkable here that this behavior is similar to as observed for isotherms of DC conductivity, σ_{DC} as well as hopping frequency, ω_p; in both cases the minimum occurs nearly at y = 40 mole% PbI_2:$2Ag_2O$ containing glass sample. As we know that hopping frequency ω_p (in AC conductivity spectra) marks the transition of ion conduction process from long range to short range order, (*-or-* in other words, from frequency independent to frequency dependent behavior) and any influence on hopping frequency are a collective response of variations in mobile ion concentration, hopping distance and conductivity.

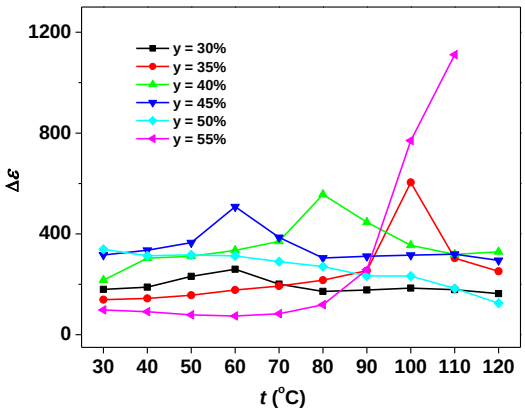

Fig. 5.44. Δε as a function of temperature for all compositions of glass series (b).

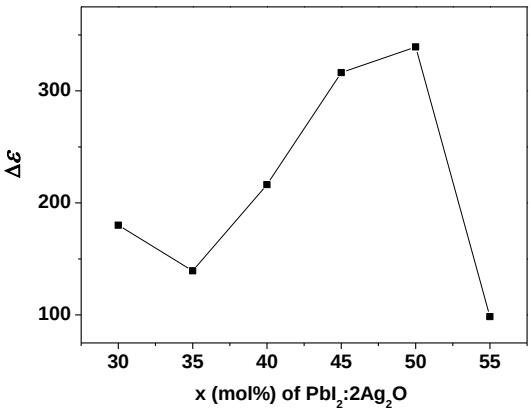

Fig. 5.45. Δε as a function of *x* mole% of PbI_2:$2Ag_2O$ At 30 ˚C.

The dielectric strength, $\Delta\varepsilon$ values as a function of temperature for all compositions of glass series (b) are depicted in Fig. 5.44. It is noteworthy here that $\Delta\varepsilon$ values are almost independent of temperature except for y = 55 mole% PbI_2:$2Ag_2O$ containing composition, which is constant till 70 ˚C and then after it

steeply increases. In addition to this, $\Delta\varepsilon$ does not exhibit any specific compositional dependence as can be observed from Fig. 5.45. Nevertheless, $\Delta\varepsilon$ values are lower due to higher ionic conductivity of the present glass system.

The ε' spectra were scaled and the results are depicted in Fig. 5.46. A near perfect scaling with a little deviation at lower frequency side is observed to materialize, which suggests that the overall dielectric relaxation process is independent of temperature for all glass compositions in the studied temperature range. And the microscopic nature of ionic relaxation remains invariant under the influence of temperature. Occurrence of scaling suggests suitability of the chosen scaling frequency, $f_o = \sigma_{DC} / \varepsilon_o \Delta\varepsilon$, which is in confirmation with the Barton–Nakjima–Namikawa relation [108] for dielectric relaxation.

$$\sigma_{DC} = P\omega_o \varepsilon_o \Delta\varepsilon \qquad \ldots\ldots\ldots (5.29)$$

where, P is a constant of order one and ω_o is the relaxation frequency. From equation 5.29, it is apparent that the dielectric relaxation strength, $\Delta\varepsilon$ is directly dependent on the hopping frequency. Dygas [109] has suggested that when P≈1, in the glasses, the onset frequency and the relaxation frequency are approximately equal. Thus it may be said that, this might be the reason why such a strong correlation between onset frequency and hopping frequency are observed for the present glass series (b).

Fig. 5.46 depicts the scaled ε' spectra for all glass samples using equation 5.27 for scaling. It is observed that all ε' spectra at different temperatures merge perfectly onto a single master curve near perfectly. The deviation is observed only at lower frequencies due to polarization effects. The near perfect scaling in the high frequency region suggests that though the characteristic frequency scale governing

the transport processes is thermally activated, the characteristic spectral features of ion relaxation process or the ion dynamics mechanism does not get altered in the studied frequency range and temperature window.

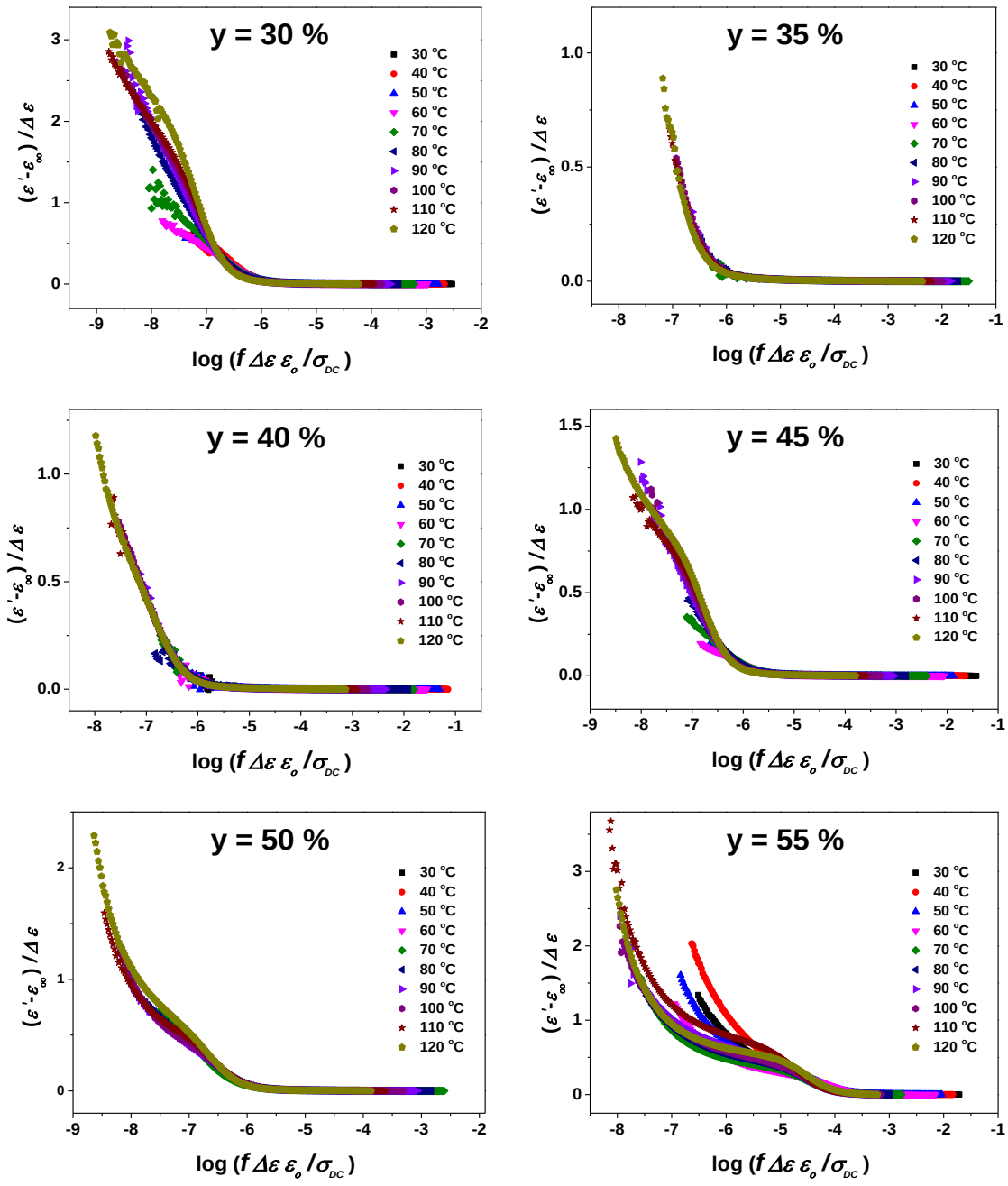

Fig. 5.46. Scaling of ε' spectra as a function of temperature for all compositions of glass series (b).

The dielectric loss spectra at different temperatures for the glass series (b) are presented in Fig. 5.47. Composition y = 30 mole% shows the presence of a

dielectric loss peak in the mid frequency region, with the loss peak frequency shifting towards higher frequency side with temperature.

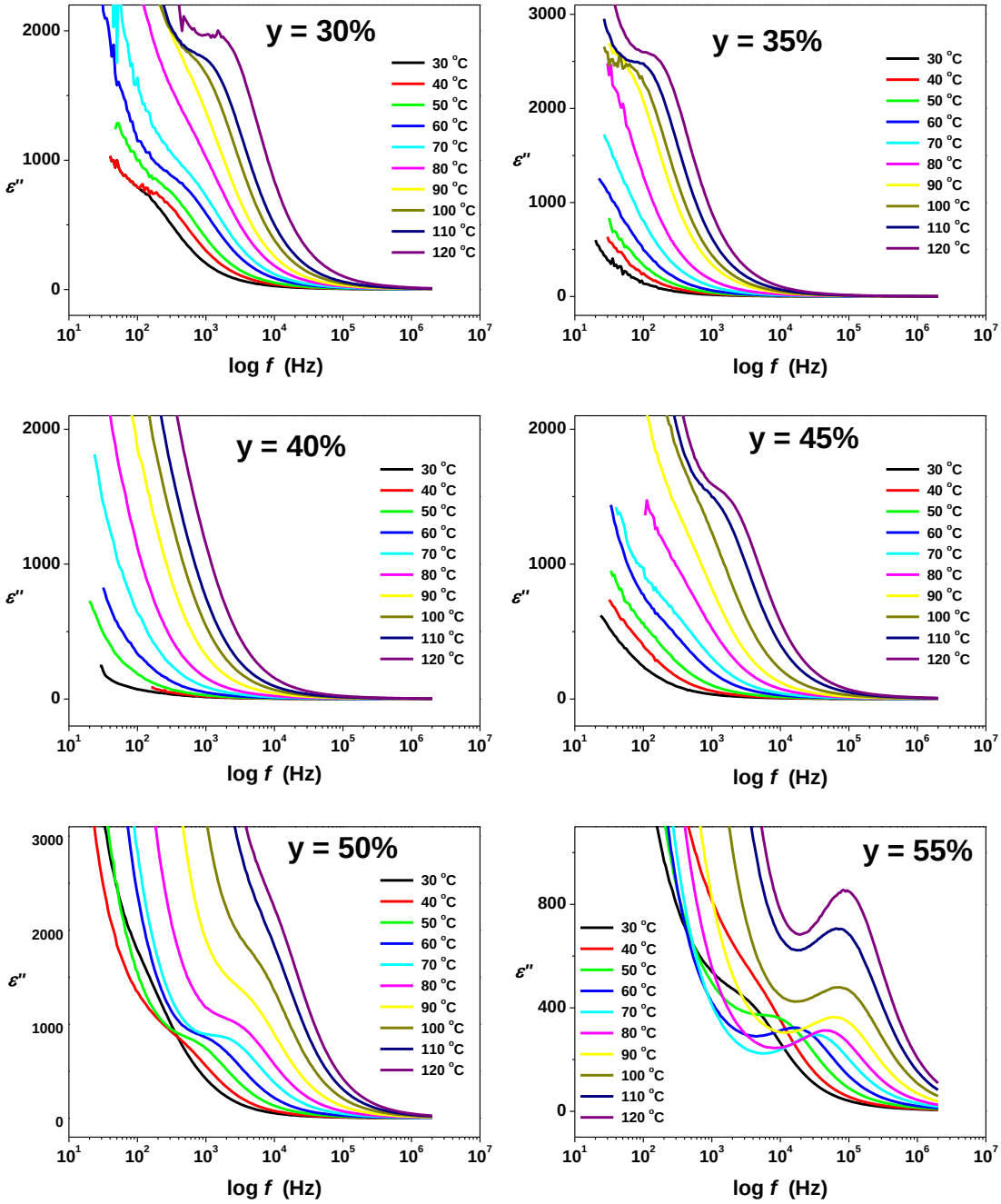

Fig. 5.47. *ε″* spectra for all compositions of glass series (b) at different temperatures.

For y = 35 mole% composition, small dielectric loss peak appears at 90˚C onwards. For y = 40 mole% composition, no dielectric peaks are observable at any temperatures which is the lowest conducting composition in the present glass series.

The relaxation peak appears at 100˚C for y = 35 mole% only, whereas for *y* = 50 & 55 mole% compositions, the relaxation peak appears right from 40˚C and peak frequency shifts towards higher frequency side. Hariharan *et al.* [110] and Chowdari *et al.* [111, 112], too, reported similar features for different Ag^+ ion conducting glass systems.

Series (c): In glass series (c), the glass former V_2O_5 is being varied and the dielectric spectra are presented in Fig. 5.47. It is observed that for all glass samples a plateau like region in high frequency regime is observed which undergoes a mid frequency dispersion and then saturates at low frequency side in a plateau like shape. The low frequency plateau gets merged with the polarization effects and it is difficult to extract the value of ε_s graphically. All spectra show the shifting of dispersion towards higher frequency side with the increase in temperature. Such behavior is observed for all other compositions. For *z* = 40 mole%, the low frequency plateau is completely absent, however a well defined high frequency saturation plateau is readily observed. It is interesting to see that the onset frequency of ε' dispersion initially decreases with increasing PbI_2:Ag_2O content and attains a minimum at *z* = 40 mole% PbI_2:Ag_2O content and then after shifts towards higher frequency side.

The dielectric relaxation strength for these glass compositions is also calculated. Fig. 5.48 shows $\Delta\varepsilon$ at different temperatures for all compositions of glass series (c). It is noted here that $\Delta\varepsilon$ changes very slowly between 30 ˚C to 60 ˚C and beyond this, it increases linearly. The sample with *z* = 40 mole% possesses minimum $\Delta\varepsilon$ value, as expected.

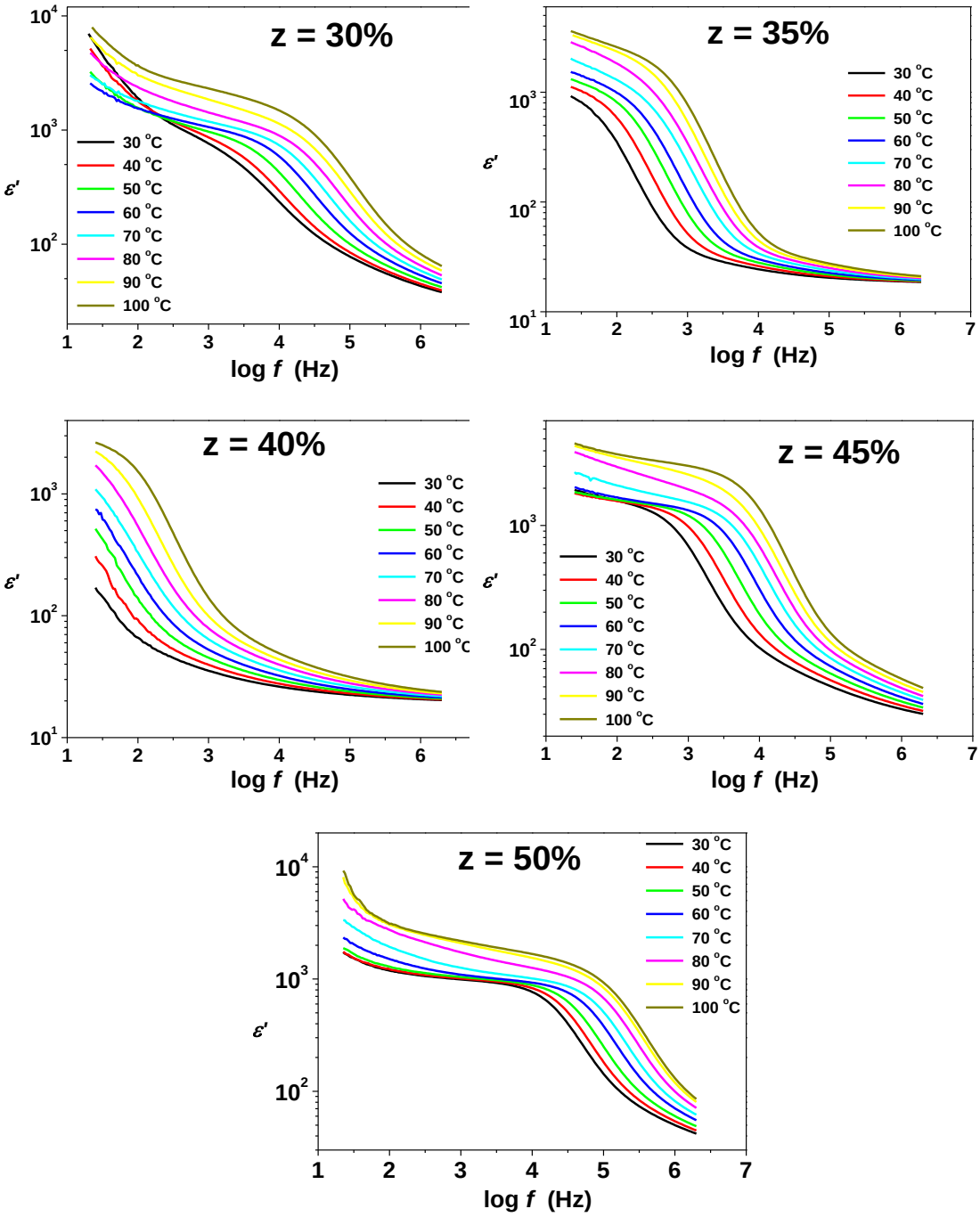

Fig. 5.48. ε' spectra for all compositions of glass series (c) at different temperatures.

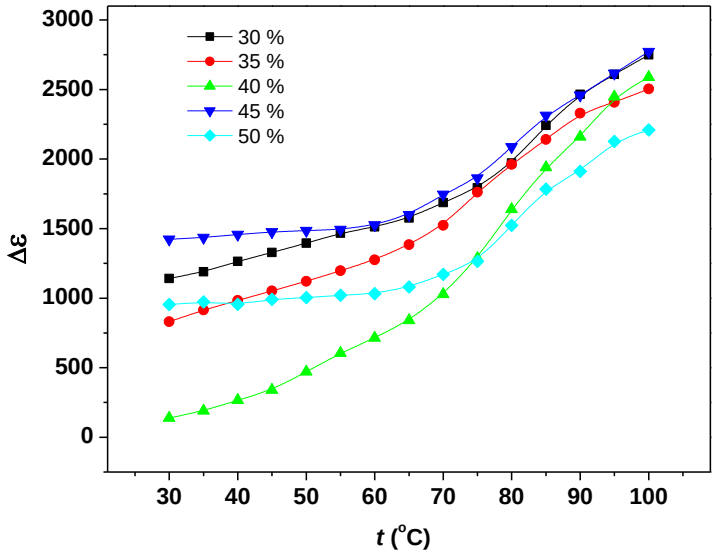

Fig. 5.49. Δε as a function of temperature for all compositions of glass series (c).

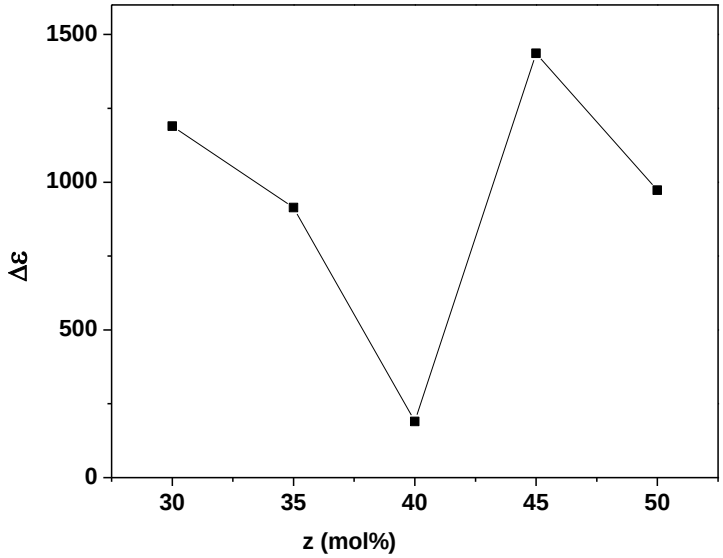

Fig. 5.50. Δε as a function of z mole% of PbI_2:Ag_2O At 30 ˚C.

Scaling of ε' spectra is undertaken and results are depicted in Fig. 5.50. All ε' spectra merge onto a single curve for respective glass compositions. It means, time temperature superposition holds well for these glass compositions, even when the glass former is being varied. Here, the deviation observed at lower frequencies are similar to as observed in other glass systems.

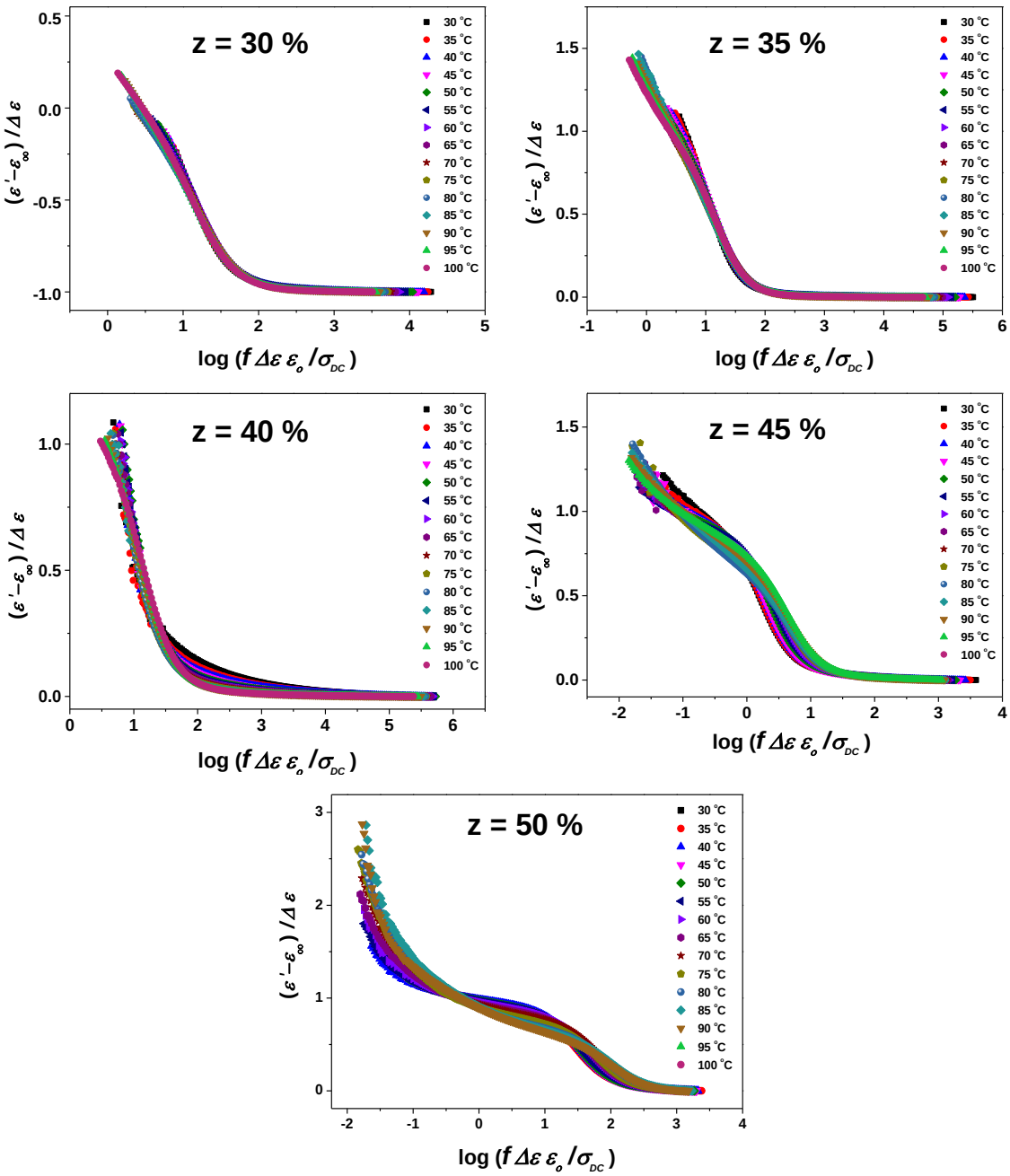

Fig. 5.51. Scaling of ε' spectra as a function of temperature for all compositions of glass series (c).

The dielectric loss spectra for all compositions of the glass series (c) are given in Fig. 5.52 at different temperatures. It is noteworthy here that similar to glass series (b), except for the least conducting composition, z = 40 mole%, for rest of the compositions, a distinguishable loss peak in the mid frequency region is observable. Similar features are observed at different temperatures.

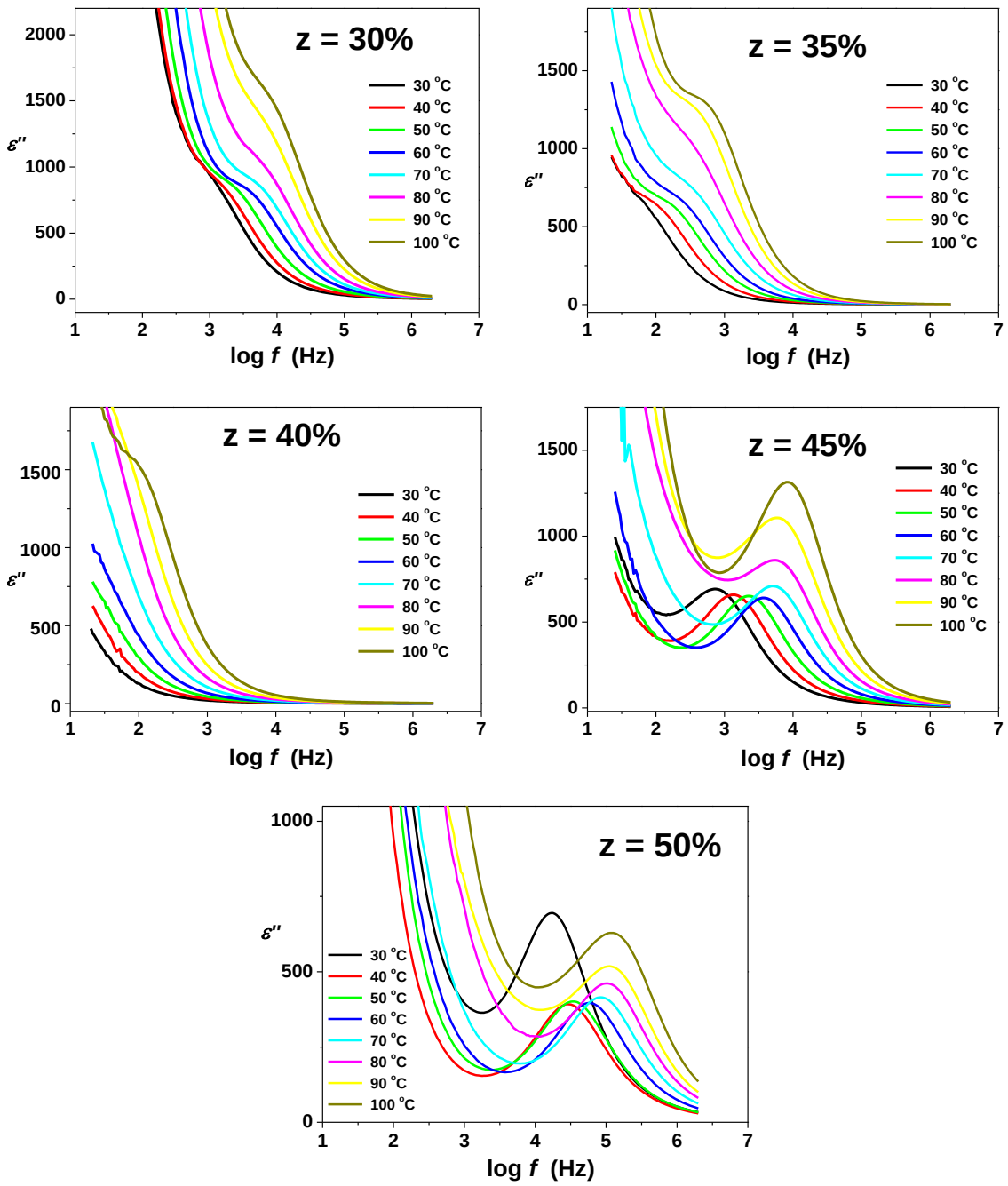

Fig. 5.52. *ε″* spectra for all compositions of glass series (c) at different temperatures.

For z = 30 and 35 mole% PbI_2:Ag_2O compositions, the ε'' loss peaks seem to be merged with low frequency polarization which occurs due to accumulation of mobile Ag^+ ions at electrode-electrolyte interface (generally below 1 kHz). However for other compositions, namely z = 45 and 50 mole%, well formed sharp loss peaks are observable. The frequency of dielectric loss peaks are thermally activated and

shift towards higher frequency side. It Here also, the lowest conducting composition i.e. z = 40 mole% of PbI_2:Ag_2O content, does not exhibit any dielectric loss peak..

5.6 Modulus function analysis

In dielectric analysis, it is generally noticed that at low frequencies, there are unavoidable electrode polarization effects and the dielectric constant is rather high. This often yields a large experimental error during the separation of dc conductivity from the total conductivity; and separation of true relaxation behavior from polarization effects becomes quite a challenging task in itself. To overcome these difficulties, a new formalism of relaxation spectroscopy, often called modulus formalism, has been given by Macedo *et al.* [46] and over the years has been applied by others [113-115] effectively to analyze the relaxation spectra. Modulus formalism helps in understanding relaxation process by suppressing these polarization effects. Details on modulus formalism are given in chapter 2 (section 2.3.4); it is defined as the inverse of the complex dielectric function as follows,

$$M^* = \frac{1}{\varepsilon^*} \qquad \ldots\ldots\ldots (5.31)$$

$$M^* = \frac{\varepsilon'}{\varepsilon'^2 + \varepsilon''^2} + i\frac{\varepsilon''}{\varepsilon'^2 + \varepsilon''^2} \qquad \ldots\ldots\ldots (5.31)$$

$$M^* = M' + iM'' \qquad \ldots\ldots\ldots (5.32)$$

M^* can be separated into its real and imaginary parts as follows,

$$M' = \frac{\varepsilon'}{\varepsilon'^2 + \varepsilon''^2} \qquad \ldots\ldots\ldots (5.33)$$

$$M'' = \frac{\varepsilon''}{\varepsilon'^2 + \varepsilon''^2} \qquad \ldots\ldots\ldots (5.34)$$

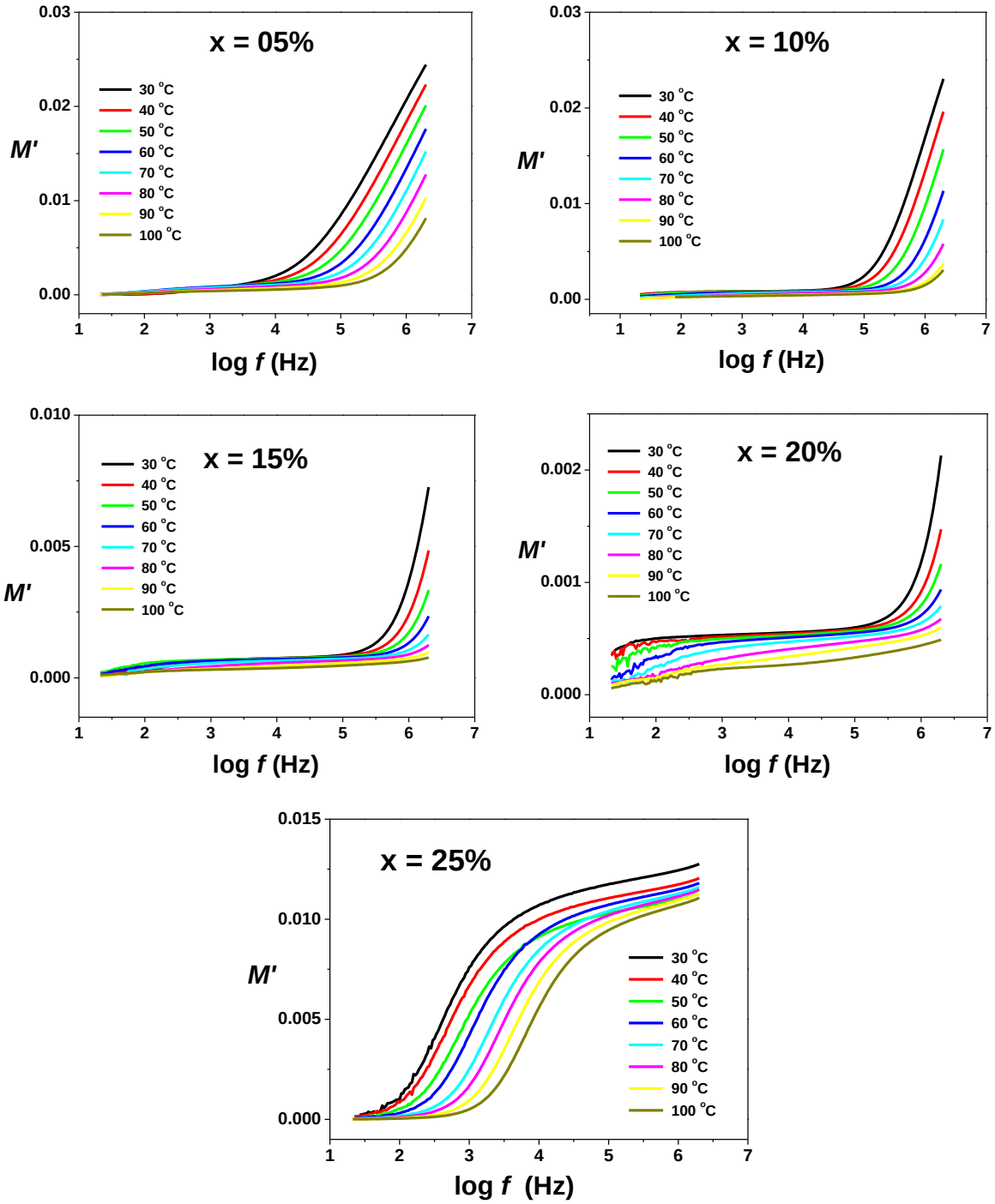

Fig. 5.53. *M'* spectra for all compositions of glass series (a) at different temperatures.

Fig. 5.53 depicts the frequency dependent real part of the modulus, *M'* for all compositions of glass series (a): xPbI$_2$–(100–x)[Ag$_2$O–2(0.7V$_2$O$_5$–0.3B$_2$O$_3$)] at different temperatures when the concentration of dopant salt PbI$_2$ is being changed against the host glass Ag$_2$O-V$_2$O$_5$-B$_2$O$_3$. It is observed that *M'* spectra tend to

saturate to zero at lower frequencies and exhibit dispersion till 2 MHz frequency (upper frequency limit). The high frequency saturation effects are not observed for *x* = 5 to 20 mole% compositions. In addition to this, *M' s*pectra do not exhibit any saturation effects in high frequency regime. The low frequency plateau indicates the suppression of polarization effects [116, 117]. It is noticeable here that the onset frequency of dispersion shifts towards higher frequency side with increasing PbI_2 content till *x* = 20 mole%. This means that with increasing mobile ion concentration, the mobile Ag^+ ions have to spend less and less time at their resting sites. Absence of high frequency saturation in these compositions suggests that it might be occurring outside the upper limit of the measured frequency range. With rise in temperature, the onset frequency of dispersion shifts towards higher frequency side indicating a thermal activation. And similar behavior is observed for all glass compositions. For *x* = 25 mole% composition, both the lower frequency plateau and high frequency saturation effects are observed.

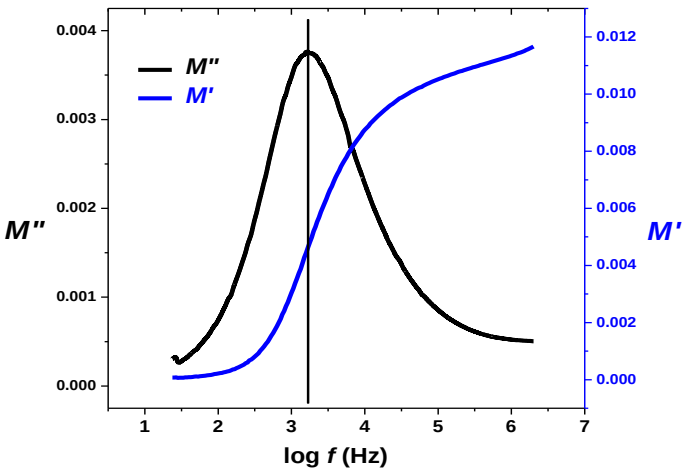

Fig. 5.55. Real and imaginary parts of modulus at 60 ˚C for *x* = 25 mole% PbI_2 glass composition in series (a).

Fig. 5.54 depicts Real and imaginary parts of modulus at 60 ˚C for x = 25 mole% composition. It is observed that M'' spectra exhibit a relaxation peak centered at dispersion region of corresponding M' spectra.

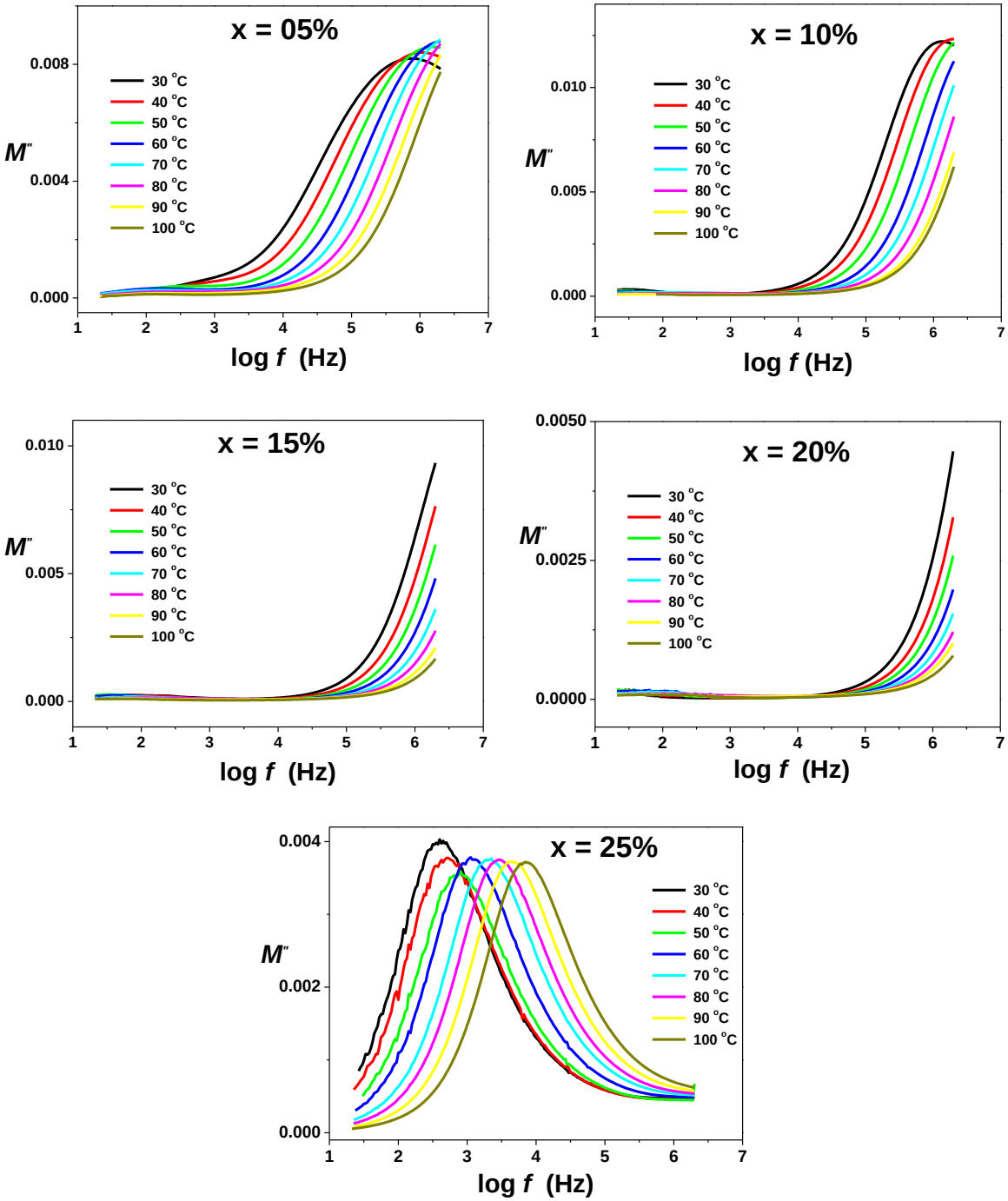

Fig. 5.55. M'' spectra for all compositions of glass series (a) at different temperatures.

The frequency dependent imaginary part of modulus is presented as plot of $M'' \rightarrow \log f$ in Fig. 5.55 for all compositions of glass series (a) at different temperatures. The $M'' \rightarrow \log f$ plot is popularly called modulus spectrum. Unlike M' spectra, the M'' spectra generally exhibit an asymmetric peak.

From Fig. 5.55, it is noted that except for x = 25 mole% PbI_2 composition, other glass compositions exhibit either a partial or no peak. This means that M'' peak for other glass compositions must be occurring outside the measured frequency range and it implies that relaxation of Ag^+ ions might be occurring beyond the measured frequency window of 20 Hz to 2 MHz range on the higher frequency side. In addition to this, the peak shape as well as the peak height is apparently not affected with increasing temperature.

The frequency corresponding to peak value of M'' is called the characteristics relaxation frequency f_{max}. And it is found to shift towards higher frequency side with increasing temperature, implying that relaxation of mobile silver ions is of thermally activated nature. The frequency range below M''_{max} determines the range where charge carriers are mobile over long distances and contribute to DC conductivity, whereas in the higher side of the f_{max} the mobile charge carriers are confined to their potential wells and are able to make hops of short ranges only. The relaxation frequency, f_{max}, is related to the conductivity relaxation time by the following equation, [118, 119],

$$\omega_{max}\tau_\sigma = 1 \qquad \ldots\ldots\ldots (5.35)$$

where, $\omega_{max} = 2\pi f_{max}$.

The reciprocal temperature dependence of the relaxation time, τ_σ , for all the glass compositions is depicted in Fig. 5.56. And it is observed to follow the Arrhenius relation of type given as follows [76],

$$\tau_\sigma = \tau_o \exp(E_\tau / kT) \qquad \ldots\ldots\ldots (5.36)$$

where, τ_σ is the characteristic relaxation time or conductivity relaxation time mentioned in equation 5.35, τ_o is a constant and E_τ is the activation energy for τ_σ.

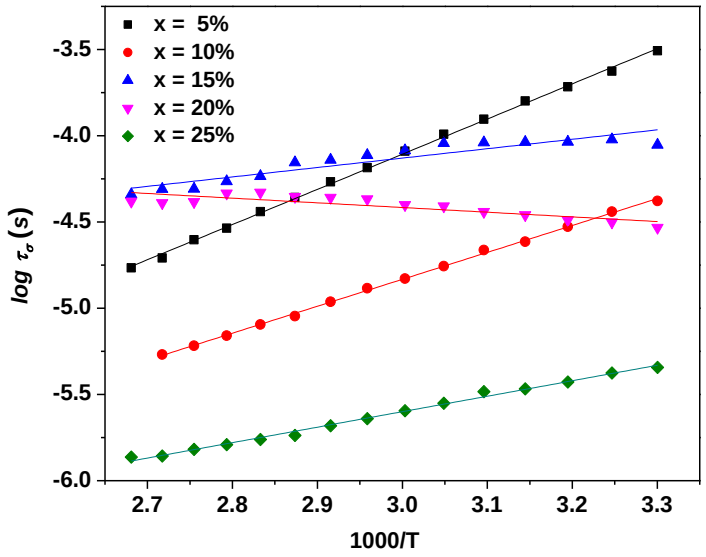

Fig. 5.56. Relaxation time τ_σ for x PbI_2 - (100-x) [Ag_2O - 2($0.7V_2O_5$ – $0.3B_2O_3$)] glass series.

The activation energy E_σ values, obtained from DC conductivity, which is the activation energy for long range charge transport and E_τ values from the relaxation time plots corresponds to short range migration, are given in Table 5.4. And both are found to be nearly same in magnitude.

Table 5.4: E_σ and E_τ as a function of x mole% of PbI_2 content for glass series (a)

x mol% of PbI_2	E_σ (eV)	E_τ (eV)
5	0.46	0.36
10	0.42	0.41
15	0.42	0.42
20	0.26	0.30
25	0.19	0.12

The comparable values of E_σ and E_τ (Table 5.4) suggest that for long range migration of ions and for relaxation process, both mechanisms require similar activation energies [120,121].

The M'' spectra can be best fitted to the stretched exponential *KWW* (Kohlrausch-Williams-Watts) function [122, 123 described by Moynihan *et al.* [124].

$$\phi(t) = \phi_o e^{-\left(\frac{t}{\tau}\right)^{\beta}} \quad \ldots\ldots\ldots (5.37)$$

where, τ is the characteristic relaxation time and β ($0 < \beta < 1$) is a relaxational parameter representative of distribution of relaxation times and ϕ_o is a constant.

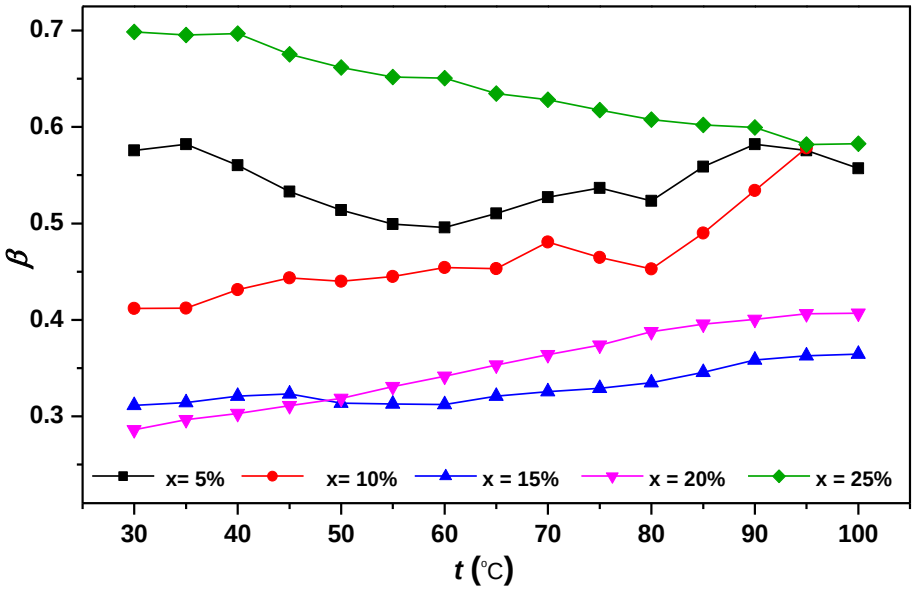

Fig. 5.57. Stretched exponential constant, *β*, as a function of temperature for all glass compositions of glass series (a). (*Solid lines are as a guide for eyes*)

Fig. 5.57 depicts the obtained β values from fitting of M'' spectra to the KWW equation. The β values are found to be in the range of 0.3 to 0.7 at room temperature and are almost independent of temperature, moreover they also do not exhibit any significant dependence on composition which indicates that the ion-ion interactions are independent of composition or charge concentration [121]. In addition to this, the β parameter shows the extent to which the mobile ions, here Ag^+ ions, couple during the conduction process [125]. The concept of the cooperative motions in glass is derived from the universal behavior discussed by Jonscher [126].

As discussed by Elliott [127], it implies that hop of a mobile ion in a glass matrix may not be treated as an isolated event, i.e. when ions hop from one equilibrium site to the next, it causes a time dependent movement of other ions in its vicinity, which leads to additional relaxation of the applied electrical field [128].

Series (b): The *M'* and *M"* spectra for glass series (b), are shown in Fig. 5.58 and 5.59 for all of its glass compositions at different temperatures. The *M'* spectra show a typical behavior having a low frequency tail that slowly converges with increasing frequency to a dispersive behavior in mid frequency region and exhibits a sign of saturation in the high frequency region. It is noticeable that position of onset frequency of dispersion shifts towards higher frequencies with rise in temperature for each glass composition. In addition to that the saturation behavior also reduces with increasing temperature and only a low frequency tail followed by dispersion is observed. This behavior is more pronounced for x = 50 and 55 mole% PbI_2:$2Ag_2O$ containing compositions, which are highly conducting.

Frequency dependent $M'' \rightarrow \log f$ plots at different temperatures for all compositions of glass series (b) is presented in Fig. 5.59. Here, it is noteworthy that all modulus spectra at all temperatures are having a similar shape with a long and flat tail extending from the low-frequency region up to the intermediate frequency region. This type of behavior may be attributed to the large capacitance associated with the electrodes while that part of the peaking curve occurring at higher frequencies may be due to the bulk effect. The non-perturbed shape of the modulus spectra obtained at various temperatures has indicated the temperature independence of the distribution of relaxation times. It is also clear from these modulus spectra that it is possible effectively to suppress the electrode-electrolyte interface effects in

the modulus formalism and the true relaxational behavior appears in form of the relaxation peak.

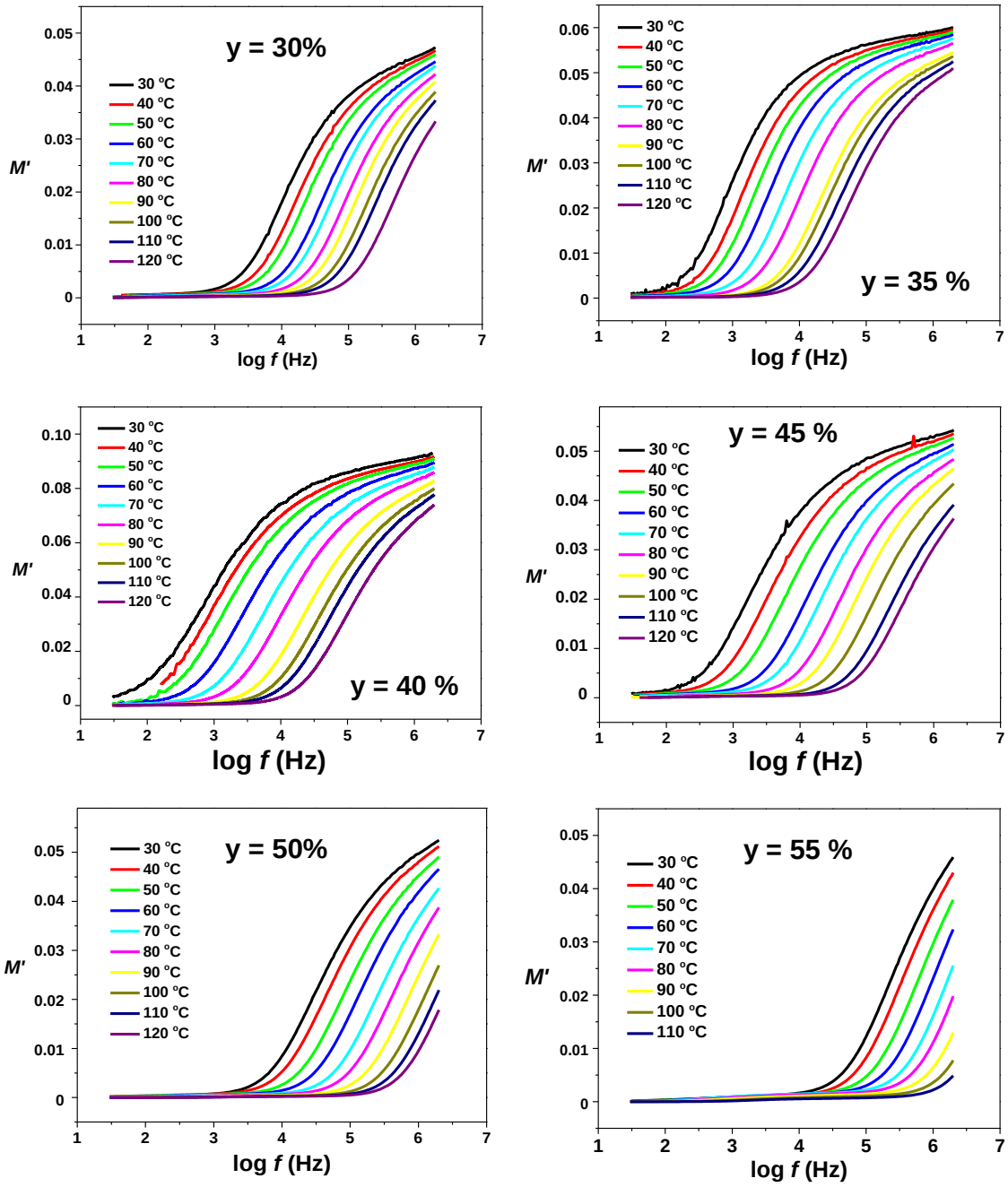

Fig. 5.58. *M'* spectra for all compositions of glass series (b) at different temperatures.

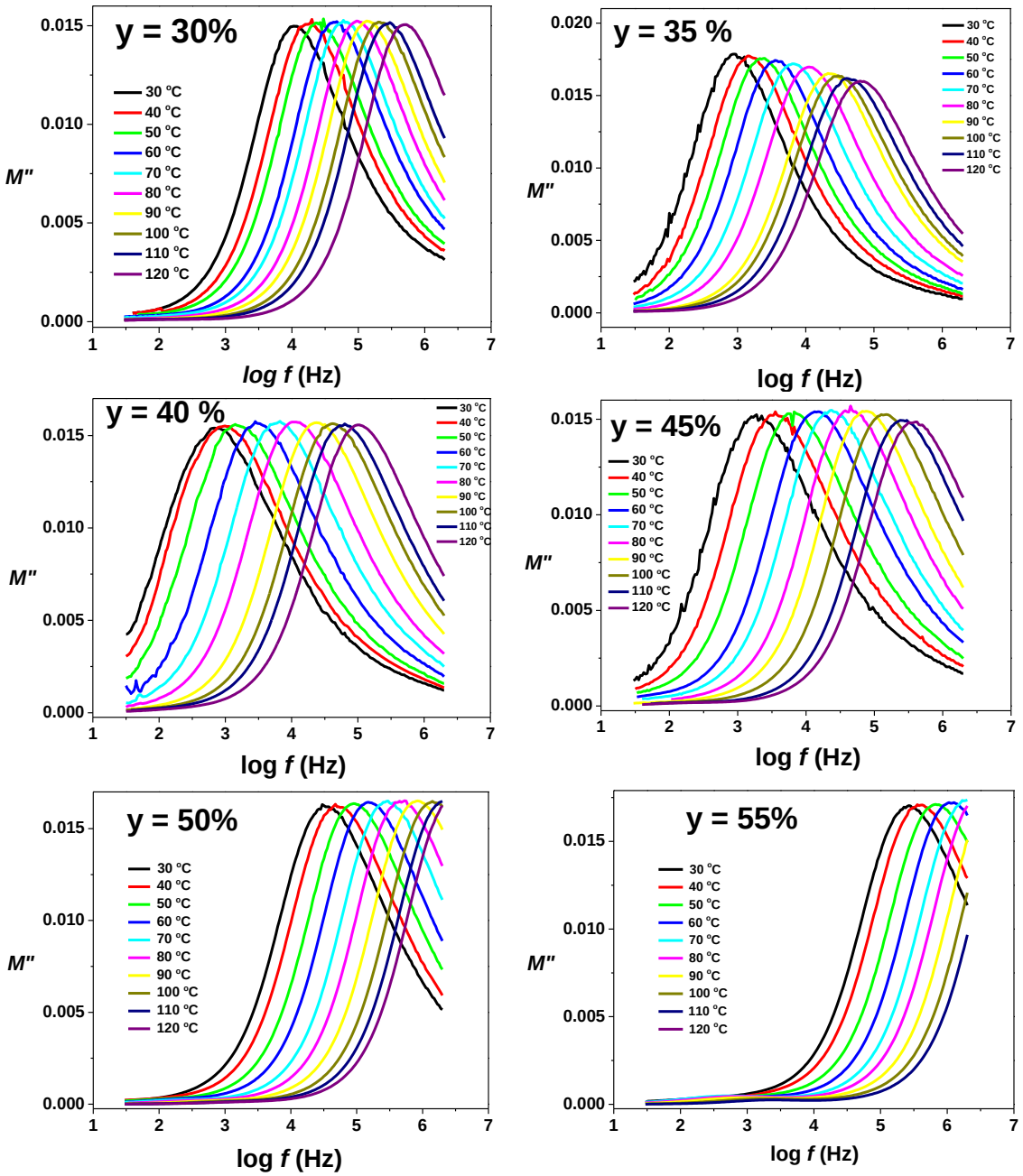

Fig. 5.59. M'' **spectra for all compositions of glass series (b) at different temperatures.**

It is observed that the frequency position f_{max} of the M'' peak shifts systematically towards higher frequency side with increasing temperature, confirming the thermally activated nature of the relaxation process. The f_{max} isotherm at 30˚C is shown in Fig. 5.60 as a function of y mole% of PbI_2:$2Ag_2O$.

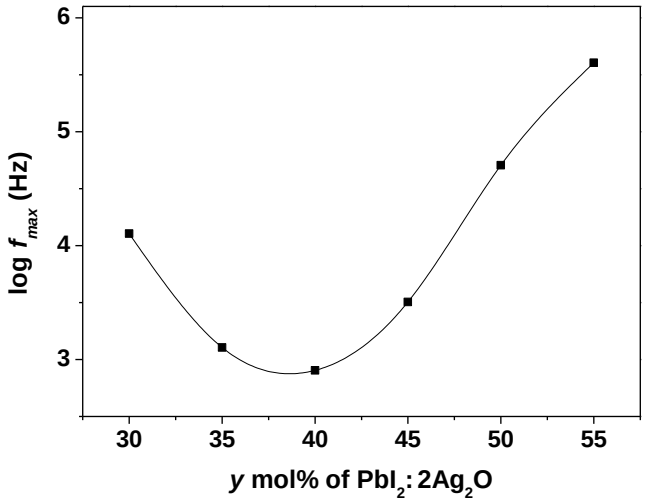

Fig. 5.60 Variation of peak frequency f_{max} (30 ˚C) with increasing y mole% of PbI_2:$2Ag_2O$.

It may be noted that f_{max} tends to show a minimum at 40 mole% PbI_2:$2Ag_2O$; to decoupling index R_τ and DC conductivity σ_{DC} isotherms. This compositional dependence of f_{max} and its correlation with conductivity suggests that the hopping rate of Ag^+ ions initially decreases and it attains a minimum at y = 40 mole% and after this, M''_{max} (f_{max}) starts shifting towards higher frequency side. [129]. When PbO is in glass network former role, Ag^+ ions do not get easily decoupled and as a result, Ag^+ ions have to spend longer times before they could make any successful jumps. And hence the frequency of the relaxation peak reduces. Beyond y = 40 mole%, PbO changes its role from former to network modifier gradually and decoupling of Ag^+ ions from the glass matrix gets stronger and as a result of this, a decrease in the mean relaxation time is expected and a shift inthe f_{max} position towards higher frequency side with increasing PbI_2:$2Ag_2O$ concentration is observed.

The temperature dependence of relaxation time, τ_σ, is depicted as a plot of $\log\tau_\sigma \rightarrow 1000/T$ in Fig. 5.61 for all compositions, and they closely fit to the Arrhenius equation. It is observed that with increasing temperature the τ_σ values are

decreasing. The activation energy for relaxation time obtained from τ_σ plots is presented alongwith conductivity activation energy values for each composition in table 5.16. The activation energies for the conductivity relaxation time and DC conductivity are nearly same indicating that the mobile Ag^+ ions have to overcome the similar potential barriers while relaxing as well as while conducting.

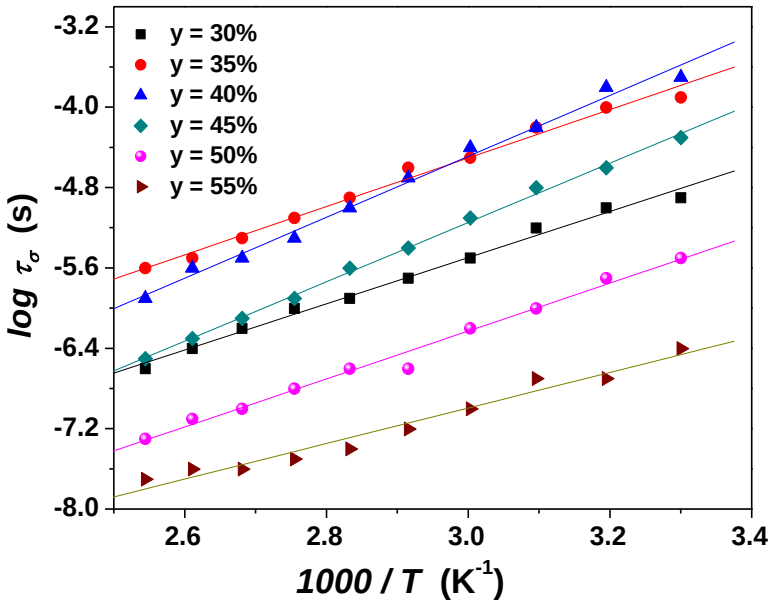

Fig. 5.61. Arrhenius plot of relaxation time for *y* (PbI_2 2:Ag_2O) -(1-y) [0.7V_2O_5 - 0.3B_2O_3] glass series (b).

Table 5.5: E_σ and E_τ as a function of *x* mole% of PbI_2:2Ag_2O content for series (b).

y mol% of PbI_2:2Ag_2O	E_σ (eV)	E_τ (eV)
30	0.45	0.46
35	0.47	0.48
40	0.60	0.60
45	0.56	0.59
50	0.50	0.47
55	0.49	0.35

The stretched exponential constant β is obtained by fitting of M'' spectra to the KWW equation and is depicted in Fig. 5.62. It is observed that β has no uniform trend with increasing temperature and seems to be independent of temperature and

its value lies between 0.4-0.8. These results are quite in conformity with the results for other ion conducting glass systems by Dutta *et al.* [121].

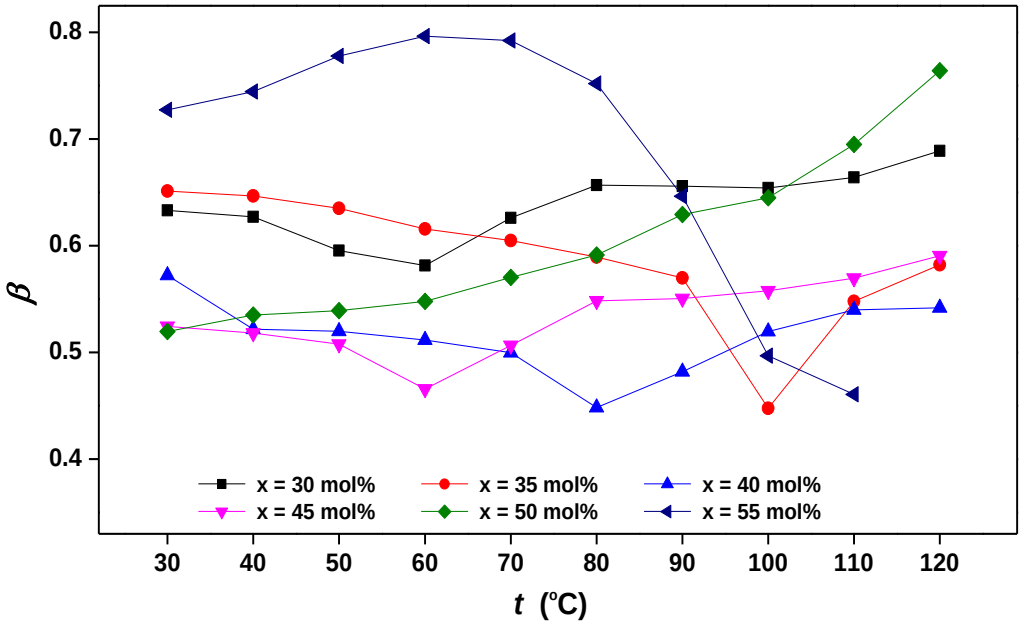

Fig. 5.62. Stretched exponential constant, *β*, as a function of temperature for all glass compositions of glass series (b). (*Solid lines are as a guide for eyes*)

Series (c): In this glass series, the effect of variation of glass former V_2O_5 on ion relaxation process is undertaken. The real and imaginary parts of the complex modulus at different temperatures for all compositions are shown in Fig. 5.63 & 5.64 respectively. It is noted from the Fig. 5.63 that the real modulus *M'* shows a long tail in low frequency side which converts to a dispersive behavior in mid frequency region and tends to saturate at M_∞ at higher frequencies. It is marked that the high frequency saturation is pronounced only for z = 35 and 40 mole% compositions only; i.e. the high frequency saturation effects might be occurring outside the measured frequency range. A close examination of these plots reveals that the dispersion frequencies at different temperatures for different samples initially shift towards low frequency side and the high frequency saturation effect is observed

within the measured frequency range. after z = 40 mole%, a sudden shift of dispersive frequencies towards higher frequency side is the feature of the samples.

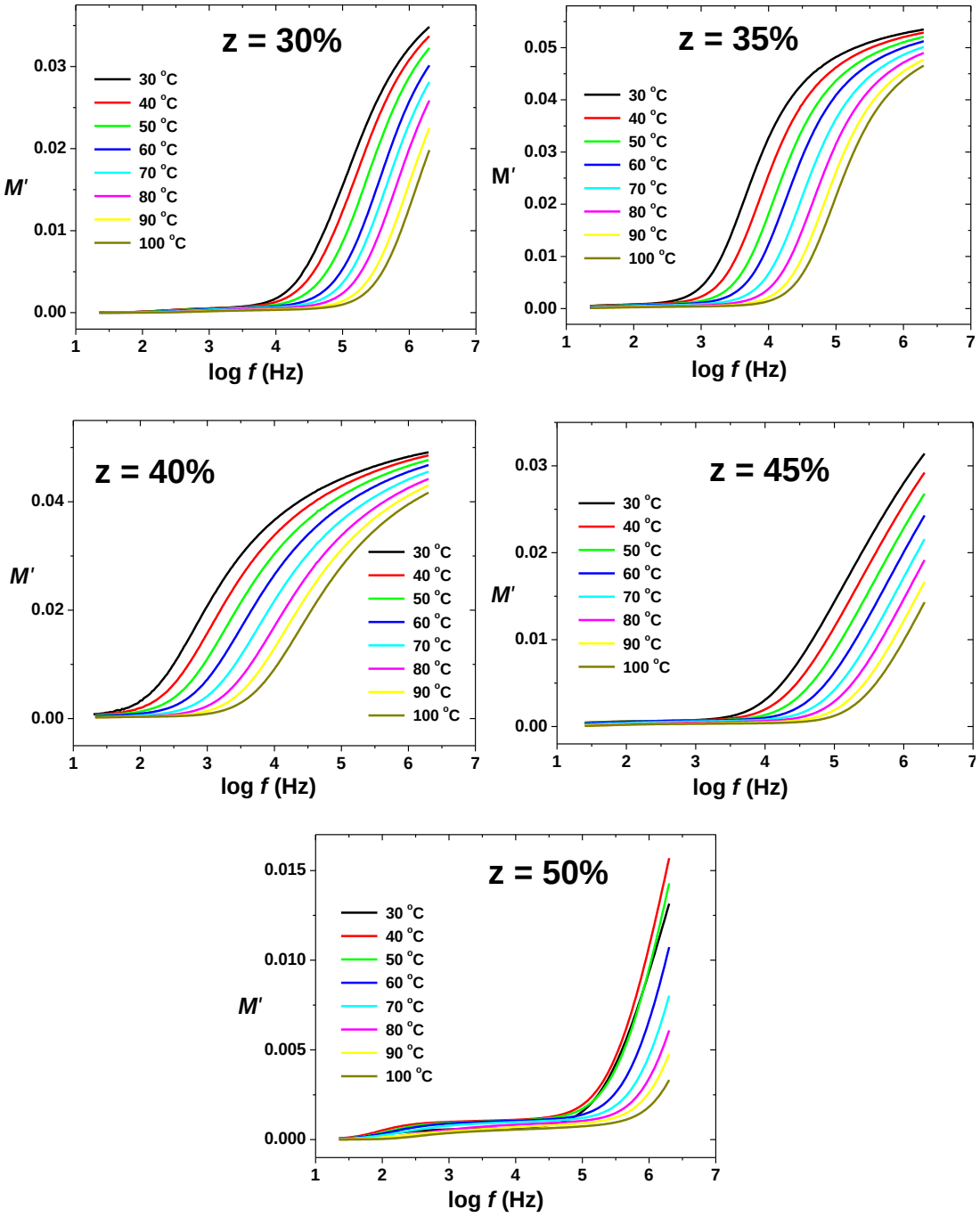

Fig. 5.63. *M′* spectra at different temperatures for all compositions of glass series (c).

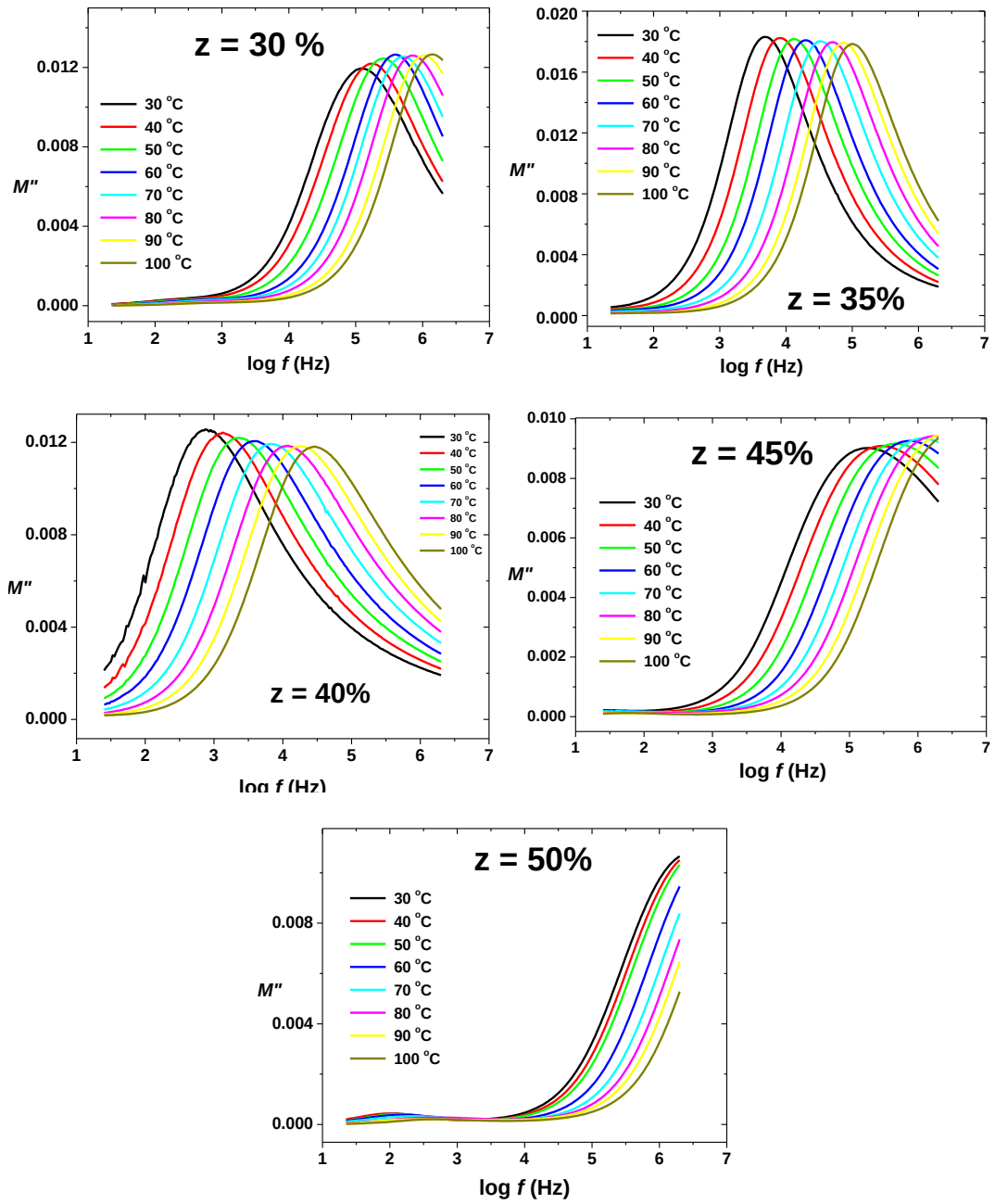

Fig. 5.64. *M''* spectra at different temperatures for all compositions of glass series (c).

The *M''* spectra in Fig. 5.64 show the presence of an asymmetric peak, with a tail towards low frequency side Similar to the M' spectra behavior, the dispersion peaks, in M", too, initially shift towards low frequency side thaen after 40% at different temperatures, the peaks now start shifting towardsa high frequency side and consequently the peaks in z = 50 mole% are not observed and are beyond the measured frequency range. It is also noted that with decreasing V_2O_5 content

(increasing z mole% of PbI_2:Ag_2O) the width of the *M″* spectra first decreases upto 40 mole% and then after starts to increase. However, for each composition, the shape of the *M″* spectra does not change at different temperatures, suggesting that ion dynamics might not be getting affecting by change in temperature.

The f_{max} values at 30 ˚C, as a function of composition are given in Fig. 5.65 and its variation is similar to σ_{DC}. It means that the glass structure changes with z mole% of PbI2:Ag2O in such a way to decrease the conductivity and relaxation frequency upto 40 mole% where PbO acts as a glass former and after that it facilitates in conduction process and relaxation frequency increases.

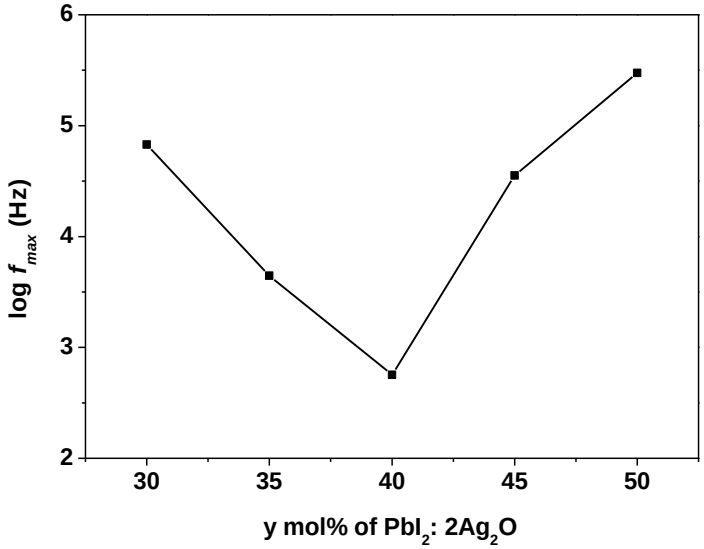

Fig. 5.65. Variation of peak frequency (at 30 ˚C) with increasing *y* mole% of PbI_2:Ag_2O content.

However, the stretched exponential constant, β, shows no systematic dependence on temperature for any of the compositions. Though a close inspection reveals that for *z* = 30, 35 and 45 mole% compositions, β increase weakly with temperature and for 40 and 45 mole% decrease weakly, albeit, not in a systematic manner (Fig. 5.66). The β values are found to be in the range of 0.4-0.6, suggesting that the conductivity relaxation also from the ideal Debye. Ngai *et al.* [130] reported

, an increase in β value with decrease in mobile ion concentration and vice versa and it is almost unity at very low ion concentrations [131-133].

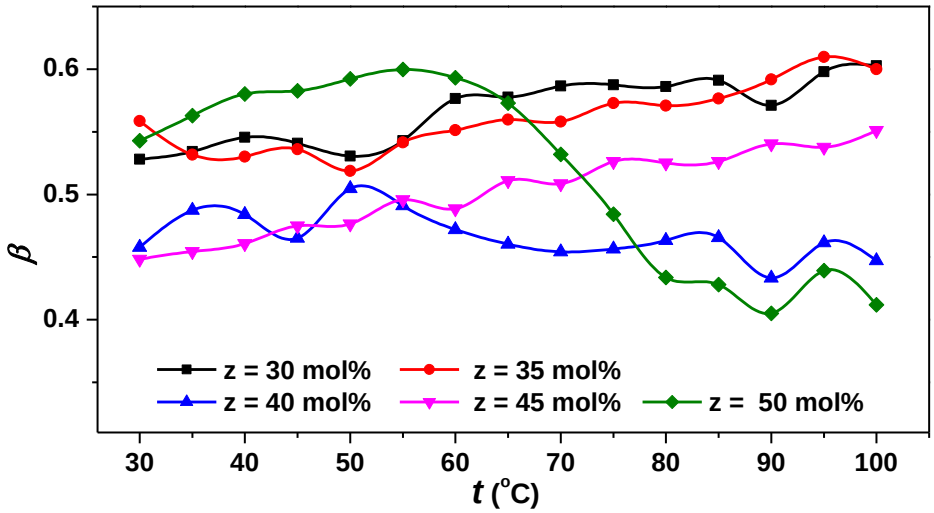

Fig. 5.66. Stretched exponential constant, β, as a function of temperature for all glass compositions of glass series (c). (*Solid lines are as a guide for eyes*)

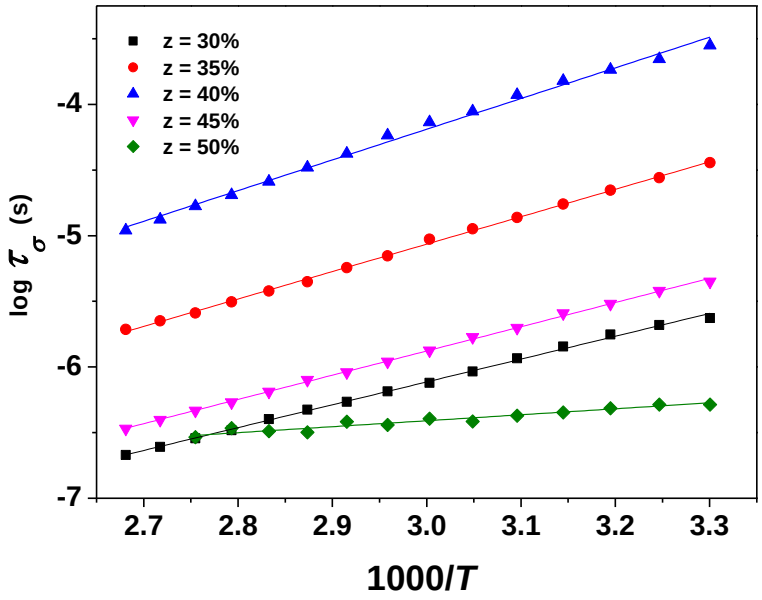

Fig. 5.67. Arrhenius temperature dependent plots of relaxation time for all compositions of glass series (c).

The relaxation time τ_σ plotted with inverse temperature for glass samples of glass series (c) exhibit similar variation as observed for other samples in which V2O5 has been varied. is shown in Fig. 5.67. The solid lines are the best fits to the

Arrhenius equation 5.36. Fig. 5.68 shows σ_{DC} and τ_σ as a function of composition at 30 ˚C. It is inferred that the relaxation time of Ag^+ ions is correlated with ionic conductivity.

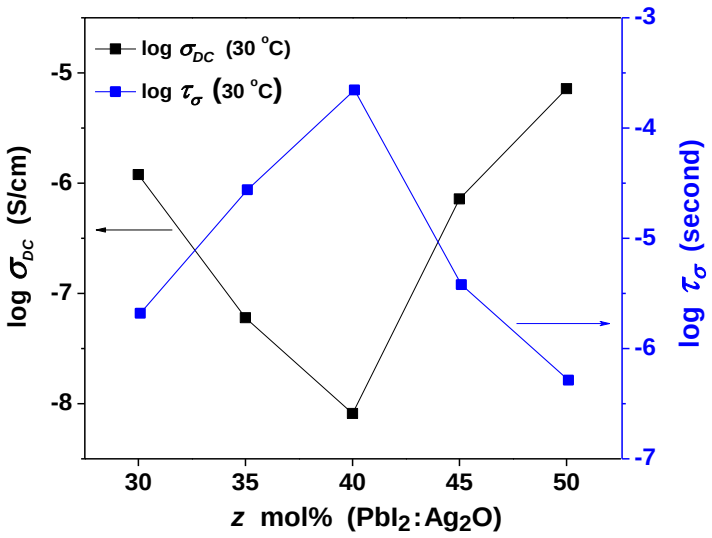

Fig. 5.68. Variation of relaxation time, τ_σ and conductivity σ_{DC} (30 ˚C) with *z* = PbI_2: $2Ag_2O$ content. (*solid line is a guide for eyes*)

The activation energy, E_τ, is calculated from fitting of the relaxation time curves and is found to decrease with increasing V_2O_5 content. Conductivity activation energy, E_σ and conductivity relaxation energy, E_τ, values are comparable (Table 5.6) suggesting that the mobile Ag^+ ions face similar energy barriers while conducting as well as while relaxing even with change of glass former in the present glass system.

Table 5.6: E_σ and E_τ as a function of *z* mole% of PbI_2:Ag_2O content for glass series (c)

z mol% of PbI_2:Ag_2O	E_σ (eV)	E_τ (eV)
30	0.38	0.35
35	0.43	0.41
40	0.49	0.46
45	0.43	0.37
50	0.19	0.09

Scaling of *M″* spectra

Moynihan [134], Ngai [130], Patel [133] and others [89, 135, 136] have extensively used the modulus formalism for understanding the ion relaxation process in glasses and other solids. And the widespread conclusion is that for a given solid system, the *M″* spectra do not change in shape with change in temperature. And hence an appropriate scaling of *M″* spectra results into a master curve, suggesting that the ionic relaxation mechanism is temperature independent or a Time Temperature Superposition (TTS) holds. In addition to this, it is widely studied that the shape of *M″* spectra is sensitive to changes in the glass composition, and generally they become narrower with decreasing ion concentration and it leads to a conclusion that the ion relaxation mechanism must be dependent on the total ionic (mobile charge carrier) concentration in glass.

Scaling of *M″* spectra is generally carried out by selecting the M''_{max} (peak) and its corresponding frequency f_{max}. Fig. 5.69, 5.70 & 5.71 present the scaling of the *M″* curves ($M''/M''_{max} \rightarrow log(f/f_{max})$) at different temperatures for all compositions of glass series (a), series (b) and series (c) respectively.

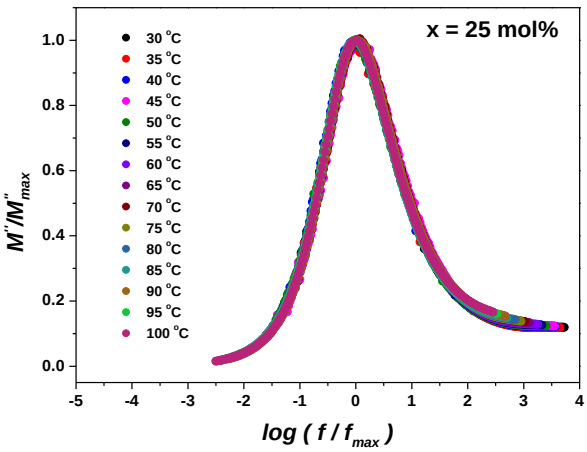

Fig. 5.69. Scaling of *M″* spectra for glass series (a).

As observed from the Fig. 5.69, 5.70 and 5.71, the *M''* spectra for different temperatures are found to merge perfectly onto a single master curve.

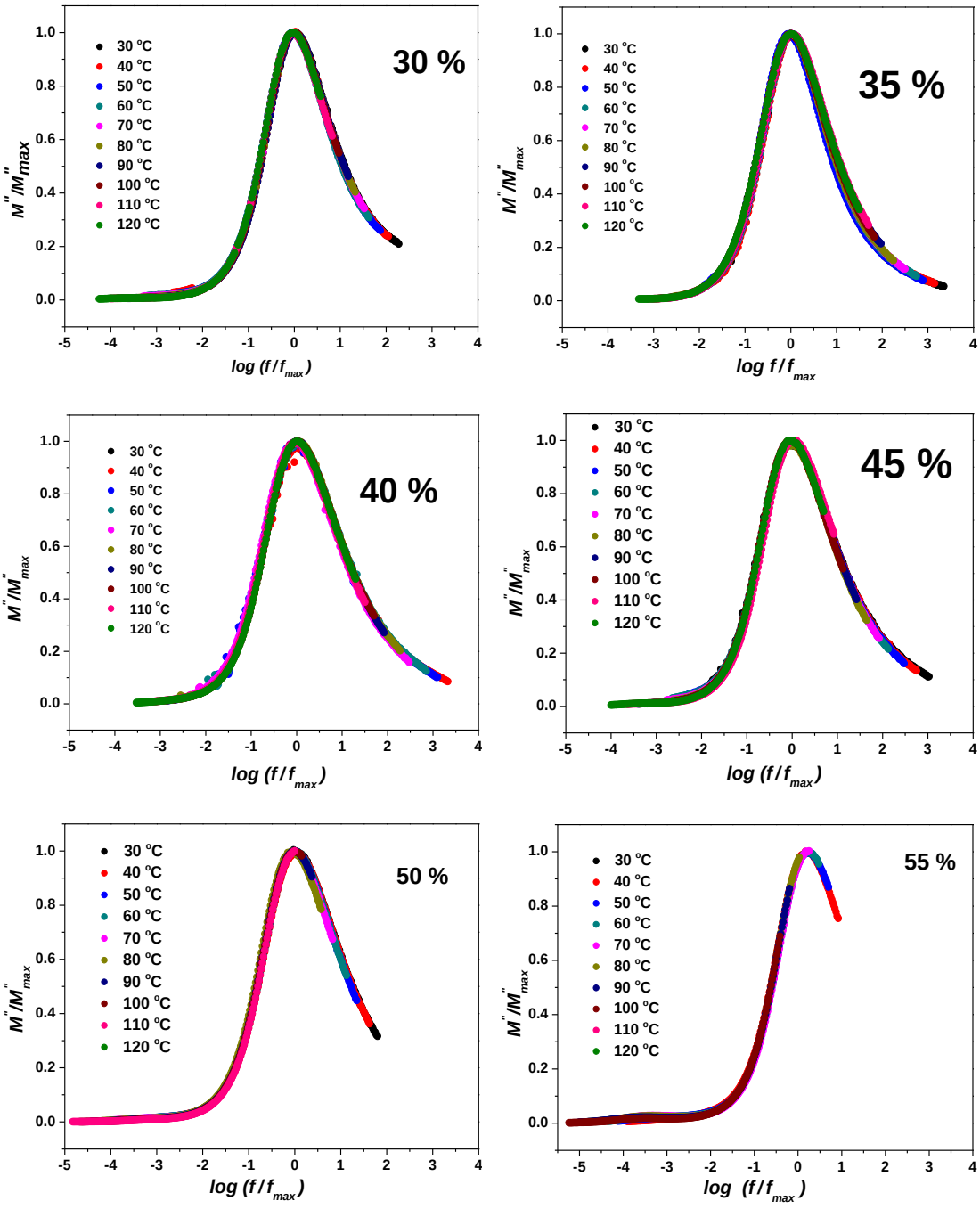

Fig. 5.70. Scaling of *M''* spectra for glass series (b).

It suggests that all the dynamic processes occurring at different time scales exhibit the same activation energy and the distribution of relaxation times is independent of temperature. However, no such scaling of *M″* at any particular temperature for all compositions could not be observed to result into single master curve, which implies that the relaxation mechanism is affected by the changes occurring in the glass electrolyte with composition.

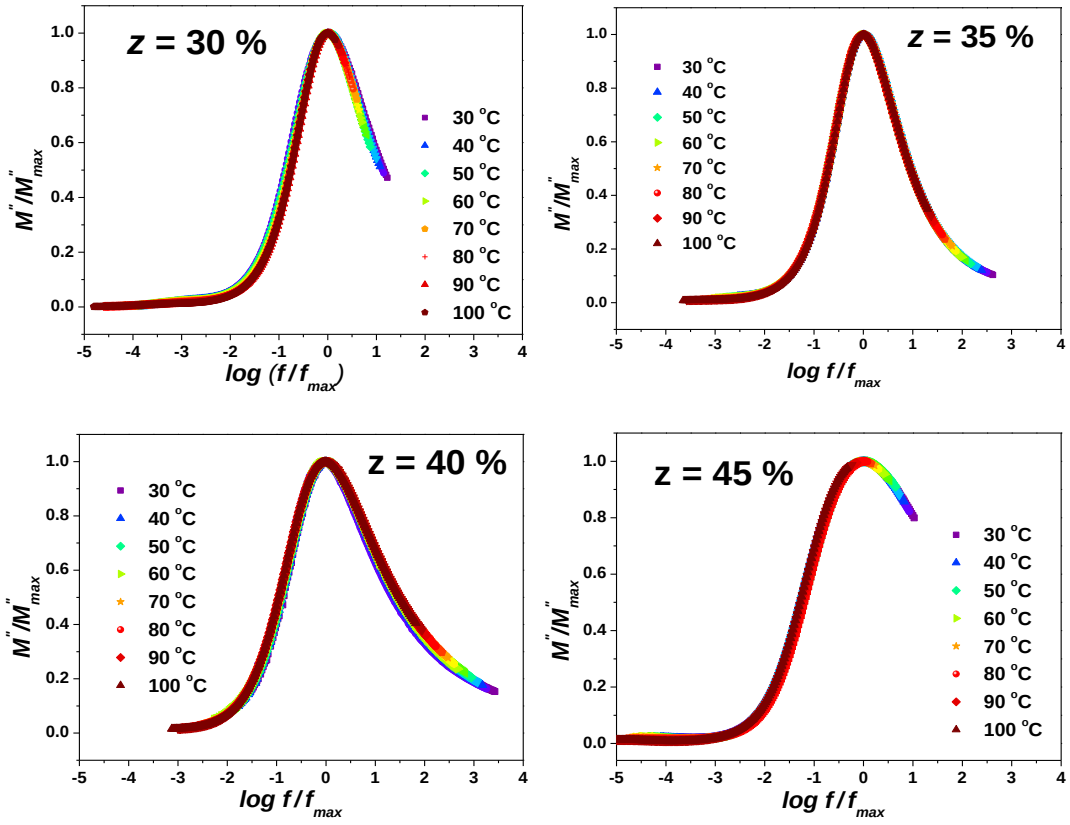

Fig. 5.71. Scaling of *M″* spectra for glass series (c).

References

1. R.J. Grant, M.D. Ingram, L.D.S. Turner, C.A. Vincent, J. Phys. Chem. 82 (1978) 2838.
2. J. Kawamura. M. Shimoji, J. Non-Cryst. Solids 79 (1986) 367.
3. G. Chiodelli, A. Magistris, Mater. Res. Bull. 17 (1982) 1.
4. M.C.R. Shastry, K.J Rao, Solid State Ionics 44 (1991) 187.
5. K. Pathmanathan, S.R. Hope, G.P. Johari, J. Non-Cryst. Solids 94 (1987) 186.
6. K. Sebastian, G.H. Frischat, Phys. Chem. Glasses 33 (1992) 199.
7. K. Hariharan, R. Kaushik, J. Mate. Sci. 22(1987) 3335.
8. K. Singh, G. Chiodelli, A. Magistris, J. Power Sources 58 (1996) 103.
9. A.K. Arof, J. Power Sources 52 (1994) 129.
10. J.P. Malugani, R. Mercier, M. Tachez, Solid State Ionics 21 (1986) 131.
11. K. Hariharan, R. Suresh Kumar, in: Solid State Ionics: Materials and Applications, B.V.R. Chowdari *et al.* (Eds.), World Scientific, Singapore, 1992, p. 533.
12. V.G. Chandrasekhar, S.A. Suthanthiraraj, Solid State Ionics 62 (1993) 61.
13. K. Hariharan, R. Suresh Kumar, Solid State Ionics 104 (1997) 227.
14. K. Padmasree, D.K. Kanchan, Mat. Chem. Phys. (2005) 551.
15. S. Machida, M. Tatsumisago, T. Minami, Proc. 13th Solid State Ion. Conf., Japan (1986) p. 23.
16. V.K. Deshpande, A. Pradel, M. Ribes, Mater. Res. Bull. 23 (1988) 379.
17. P.S.S. Prasad, A.N. Durga Rani, S. Radhakrishna, Mat. Chem. Phys. 25 (1990) 487.
18. A. Costantini, A. Buri, F. Branda, Solid State Ionics 67 (1994) 175.
19. D. Coppo, M.J. Duclot, J.L. Souquet, Solid State Ionics 90 (1996) 111.
20. D. Larink, H. Eckert, M. Reichert, S. W. Martin, J. Phys. Chem. C 116 (2012) 26162.
21. B. Raguenet, G. Tricot, G. Silly, M. Ribes, A. Pradel, J. Mater. Chem. 21 (2011) 17693.
22. K.P. Padmasree, D.K. Kanchan, J. Non-Cryst. Solids 352 (2006) 3841.
23. S. Murugesan, A. Wijayasinghe, B. Bergman, J. Non-Cryst. Solids 354(2008) 1066.
24. K.P. Padmasree, D.K. Kanchan, J. Non-Cryst. Solids 352 (2006) 3841.
25. M. Cutroni, M. Federico, A. Mandanica, P. Mustarelli, C. Tomasi, Solid State Ionics 113–115 (1998) 681.
26. H. Takahashi, K. Shishitsuk, T. Sakuma, Y. Shimojo, Y. Ishii, Solid State Ionics 113–115 (1998) 685.
27. A. Doi, J. Non-Cryst. Solids 246 (1999) 158.
28. P. Machowski, J.E. Garbarczyk, M. Wasiucionek, Solid State Ionics 157 (2003) 281.
29. J.R. Macdonald, Solid State Ionics 176 (2005) 1961.
30. J.R. Macdonald, L.D. Potter Jr., Solid State Ionics 23 (1987) 61.
31. J.R. Macdonald, J. Computational Phys. 157 (2000) 280.
32. M.S. Jayswal, D.K. Kanchan, P. Sharma, M. Pant, Solid State Ionics 186 (2011) 7.
33. S. Adams, J. Maier, Solid State Ionics 105 (1998) 67.
34. M.D. Ingram, M.A. Mackenzie, W. Muller, M. Torge, Solid State Ionics 28-30 (1980) 677.

35. M. Ganguli, K.J. Rao, J. Solid State Chem. 145 (1999) 65.
36. J.D. Wicks, L. Borjesson, G.B. Wye, W.S. Howells, R.L. McGreevy, Phys. Rev. Lett. 74 (1995) 726.
37. J. Swenson, L. Borjesson, Phys. Rev. Lett. 77 (1996) 3569.
38. G. El-Damrawi, A.K. Hasan, H. Doweidar, Physica B 291 (2000) 34.
39. S.R. Elliott, Solid State Ionics 27 (1988) 131.
40. C.A. Angell, Annu. Rev. Phys. Chem. 43 (1992) 693.
41. J. Kawamura, M. Shimoji, J. Non-Cryst. Solids 88 (1986) 281.
42. S. Bhattacharya, A. Ghosh, Solid State Ionics 161 (2003) 61.
43. J.P. Malugani, R. Mercier, M. Tachez, Solid State Ionics 21 (1986) 131.
44. A. Sanson, F. Rocca, C. Armellini, G. Dalba, P. Fornasini, R. Grisenti, Phys. Rev. Lett. 101 (2008) 155901.
45. R.G. Pearson, J. Chem. Educ. 45(1968) 581.
46. P.B. Macedo, C.T. Moynihan, R. Bose, Phys. Chem. Glass. 13 (1972) 171.
47. M. Ganguli, M.H. Bhat, K.J. Rao, Mater. Res. Bul. 34 (1999) 1757.
48. A.K. Jonscher, Nature 267 (1977) 673.
49. A.K. Jonscher, J. Phys. C: Solid State Phys. 6 (1973) L235.
50. D.P. Almond, A.R. West, Solid State comm. 44 (1982) 1277.
51. D.P. Almond, A.R. West, Solid State Ionics 8 (1983) 159.
52. D.P. Almond, A.R. West, Solid State Ionics 9-10 (1983) 277.
53. D.P. Almond, A.R. West, Solid State Ionics 11 (1983) 57-64.
54. A.K. Jonscher, Dielectric Relaxation in Solids, Chelsea Dielectric Pres, 1983, London.
55. K. Funke, Solid State Ionics 18–19 (1986) 183.
56. K. Funke, Prog. Solid State Chem. 22 (1992) 111-195.
57. D.P.Almond, A.R. West, J. Electroanal. Chem. 193 (1985) 49.
58. H. Kahnt, Ber. Bensen-Ges. Phys. Chem. 95 (1991) 1021.
59. A. Pan, A. Ghosh, Phys. Rev. B 59 (1999) 899.
60. A.R. Kulkarni, P. Lunkenheimer, A. Loidl, Solid State Ionics 112 (1998) 69.
61. A.W. Imre, S. Voss, H. Mehrer, Phys. Chem. Chem. Phys. 4 (2002) 3219.
62. S. Summerfield, Phil. Mag. B 52 (1985) 9.
63. B. Roling, A. Happe, K. Funke, M.D. Ingram, Phys. Rev. Lett. 78 (1997) 2160.
64. S. Ghosh, A. Pan, Phys. Rev. Lett. 84 (2000) 2188.
65. B. Roling, A. Happe, K. Funke, M.D. Ingram, Phys. Rev. Lett. 78 (1997) 2160.
66. D.L. Sidebottom, Rev. Mod. Phy. 81 (2009) 999.
67. J.C. Dyre, P. Maass, B. Roling, D.L. Sidebottom, Rep. Prog. Phys. 72 (2009) 046501.
68. M. Bettman, C.R. Peters J. Phys. Chem. 73 (1969) 1774.
69. K. Funke, H.J. Schneider, Solid State Ionics 13 (1984) 335.
70. K. Funke, R.D. Banhatti, D. Wilmer, R. Dinnebier, A. Fitch, M. Jansen, J. Phys. Chem. A 110 (2006) 3010.

71. I. Svare, Solid State Ionics 125 (1999) 47.
72. M. Vogel, C. Brinkmann, H. Eckert, A. Heuer, Phys. Rev. B 69 (2004) 094302.
73. B. Roling, Solid State Ionics 105 (1998) 185.
74. N. Kuwata, T. Saito, M. Tatsumisago, T. Minami, J. Kawamura, Solid State Ionics 175 (2004) 679.
75. N.K. Karan, B. Natesan, R.S. Katiyar, Solid State Ionics 177 (2006) 1429.
76. W. Buchelli, R. Jimenez, J. Sanz, A. Varez, Solid State Ionics 227 (2012) 113.
77. M. Dubiel, B. Roling, M. Futing, J. Non-Cryst. Solids 331 (2003) 11.
78. U. Strom, K.L. Ngai, Solid State Ionics 5 (1981) 167.
79. W.K. Lee, B.S. Lim, J.F. Liu, A.S. Nowick, Solid State Ionics 53-56 (1992) 831.
80. D. Dutta, A. Ghosh, Phys. Rev. B 72 (2005) 024201.
81. S.R. Elliott, Solid State lonics 27 (1988) 131.
82. H. Jain, J.N. Mundy J. Non-Cryst. Solids 91 (1987) 315.
83. K.J. Rao, C. Estournes, M. Menetries, A. Levasseur, Philos. Mag. B 70 (1994) 809.
84. S.R. Elliott, F.E.G. Henn, J. Non-Cryst. Solids 116 (1990) 179.
85. S.R. Elliott, A.P. Owens, Philos. Mag. B 60 (1989) 777.
86. A. Ghosh, A. Pan, Phys. Rev. Lett. 84 (2000) 2188.
87. A. Pan, A. Ghosh, Phys. Rev. B 66 (2002) 012301.
88. K.S. Cole, R.H. Cole, J. Chem. Phys. 9 (1941) 341.
89. D.L. Sidebottom, B. Roling and K. Funke, Phys. Rev. B 63 (2000) 024301.
90. J. Świergiel, J. Jadżyn, J. Phys. Chem. B 116 (2012) 3789.
91. H. Froehlich, Theory of Dielectrics, Oxford University Press, Clarendon Press, London, 1949.
92. J.C. Dyre, T.B. Shrøder, Rev. Mod. Phys. 72 (2000) 873.
93. D.L. Sidebottom, Phys. Rev. Lett. 82 (1999) 3653.
94. D.L. Sidebottom, Rev. Mod. Phys. 81 (2009) 999.
95. B. Singh, P.S. Tarsikka, L. Singh, Pramana 59 (2002) 653.
96. F.A. Wahab, M.S. Aziz, A.G. Mostafa, E.M. Ahmed, Mater. Sci. Eng. B 134 (2006) 1.
97. L.C. Costa, F. Henry, J. Non-Cryst. Solids 353 (2007) 4380.
98. M. Hanaya, K. Echigo, M. Oguni, J. Phys.: Condens. Matter 17 (2005) 2281.
99. T. Yano, T. Nagano, J. Lee, S. Shibata, M. Yamane, Solid State Ionics 150 (2002) 281.
100. K.L. Ngai, R. W. Rendell, Phys. Rev. B 61 (2000) 9394.
101. M.M. Ahmad, K. Yamada, T. Okuda, Solid State Ionics 167 (2004) 285.
102. D.L. Sidebottom, Phys. Rev. Lett. 18 (1999) 3653.
103. J.L. Barton, Verres Refr. 20 (1966) 328.
104. T. Nakajima, in: 1971 Annual Report, Conference on Electric Insulation and Dielectric Phenomena (National Academy of Sciences, Washington, DC, (1972) p. 168.
105. H. Namikawa, J. Non-Cryst. Solids 18 (1975) 173.
106. D.L. Sidebottom, J. Zhang, Phys. Rev. B 62 (2000) 5503.

107. M.S. Jayswal, D.K. Kanchan, P. Sharma, N. Gondaliya, Mater. Sci. Eng. B 178 (2013) 775.
108. J.R. Dygas, Solid State Ionics 176 (2005) 2065.
109. J.R. Dygas, in Proceedings of the 1st International Discussion Meeting on Superionic Conductor Physics, J. Kawamura *et al.* (Ed.), World Scientific, Singapore, 2003.
110. K. Hariharan, R. Kaushik, J. Mater. Sci. 22(1987) 3335.
111. B.V.R. Chowdari, K. Radhakrishnan, J. Non-Cryst. Solids 110 (1989) 101.
112. B.V.R. Chowdari, R. Gopalakrishnan, Solid State Ionics 18-19 (1986) 483.
113. S.A. Chen, C.S. Liao, Macromolecules 26 (1993) 2810.
114. G.M. Tsangaris, G.C. Psarras, N. Kouloumbi, J. Mater. Sci. 33 (1998) 2027.
115. A.S. Nowick, B.S. Lim, J. Non-Cryst. Solids 172 (1994) 1389.
116. J.M. Bose, J. M. Reau, J. Senegas, M.Poulain, Solid State Ionics 82 (1995) 39.
117. I.M. Hodge, M.D. Ingram, A.R. West, J. Electroanal. Chem. 74 (1976) 125.
118. M. Pant, D.K. Kanchan, P. Sharma, M.S. Jayswal, Mat. Sci. Engg. B 149 (2008) 18.
119. S. Szu, Fu-S. Chang, Solid State Ionics 176 (2005) 2695.
120. S. Bhattacharya, A. Ghosh, Solid State Ionics 161 (2003) 61.
121. A. Dutta, A. Ghosh, J. Non-Cryst. Solids 351 (2005) 203.
122. G. Williams, D.C. Watts, Trans. Faraday Soc. 66 (1970) 8
123. R. Kohlrausch, Ann. Phys. 12 (1847) 39
124. C.T. Moynihan, L.P. Boesch, N.L. Laberge, Phys. Chem. Glasses 14 (1973) 12
125. I.M. Hodge, K.L. Ngai, C.T. Moynihan, J. Non-Cryst. Solids 351 (2005) 104.
126. A.K. Jonscher, J. Mater. Sci. 16 (1981) 2037.
127. S.R. Elliott, Solid State Ionics 70-7 1 (1994) 27.
128. K.L. Ngai, Comm. Solid State Phys. 9 (1979) 127.
129. C.A. Angell, Solid State Ionics 9&10 (1983) 3.
130. K.L. Ngai, R.W. Rendell, Phys. Rev. B, 61 (2000) 9393.
131. K.L. Ngai, J.N. Mundy, H. Jain, Phys. Rev. B, 40 (1989) 6169.
132. C.A. Angell, Chem. Rev. 90 (1990) 523.
133. H.K. Patel, S.W. Martin, Phys. Rev. B, 45 (1992) 10292.
134. K.L. Ngai, G.N. Greaves, C.T. Moynihan, Phys. Rev. Lett. 80 (1998) 1018.
135. J.M. Bose, J. M. Reau, J. Senegas, M. Poulain, Solid State Ionics 82 (1995) 39.
136. A.S. Nowick, B.S. Lim, J. Non-Cryst. Solids 172 (1994) 1389.